CHIRAL SYMMETRY IN NUCLEONS

A thesis submitted to the University of Manchester
for the degree of Doctor of Philosophy
in the Faculty of Engineering and Physical Sciences

2015

Paul Joseph Hewson
School of Physics and Astronomy

Contents

Word count 34500

List of Tables

List of Figures

The University of Manchester

Paul Joseph Hewson
Doctor of Philosophy
Chiral symmetry in nucleons
April 23, 2015

Chiral perturbation theory allows us to probe the low energy properties of hadrons. In this thesis we have looked at the axial coupling constant (see chapter 4) and baryon number violation (see chapter 5).

We calculated the axial coupling constant up to $\mathcal{O}(p^4)$ using the extended on mass shell renormalisation scheme in chiral perturbation theory. We also included the decuplet as an explicit degree of freedom. To fit the free parameters in our expression we used a combination of lattice and experimental data.

We found that the fourth order corrections were quite large, and we struggled to produce an acceptable fit to the data. We also saw that the running of g_A^{pn} with M_π predicted by lattice QCD and ChPT at $\mathcal{O}(p^4)$ do not agree well. This is likely due to a combination of finite size effects impacting the low pion mass lattice data and the chiral perturbative series converging slowly.

For our work on baryon number violation we looked at determining the values of two low-energy constants that appear in the baryon violating chiral Lagrangian. To do this, we matched our expression to lattice data. Previous determinations of the parameters had been done without calculating the effect of loops, ours was the first investigation to see what impact the loop diagrams would have. We found that our determinations of the parameters were in agreement with previous results, suggesting the effect of the loops is small. We also performed a chiral extrapolation, and found that our results were in agreement with previous results that did not account for loop corrections. This suggests that the impact of higher-order corrections is not significant for this baryon-number-violating process.

Declaration

No portion of the work referred to in the thesis has been submitted in support of an application for another degree or qualification of this or any other university or other institute of learning.

Copyright Statement

i. The author of this thesis (including any appendices and/or schedules to this thesis) owns certain copyright or related rights in it (the "Copyright") and s/he has given The University of Manchester certain rights to use such Copyright, including for administrative purposes.

ii. Copies of this thesis, either in full or in extracts and whether in hard or electronic copy, may be made **only** in accordance with the Copyright, Designs and Patents Act 1988 (as amended) and regulations issued under it or, where appropriate, in accordance with licensing agreements which the University has from time to time. This page must form part of any such copies made.

iii. The ownership of certain Copyright, patents, designs, trade marks and other intellectual property (the "Intellectual Property") and any reproductions of copyright works in the thesis, for example graphs and tables ("Reproductions"), which may be described in this thesis, may not be owned by the author and may be owned by third parties. Such Intellectual Property and Reproductions cannot and must not be made available for use without the prior written permission of the owner(s) of the relevant Intellectual Property and/or Reproductions.

iv. Further information on the conditions under which disclosure, publication and commercialisation of this thesis, the Copyright and any Intellectual Property

Acknowledgements

I would like to thank my supervisor Judith McGovern for her considerable help during my time at Manchester. In particular for providing valuable insights into how to improve both the work I have done, and the thesis I have presented it in.

I would also like to thank Vadim Lensky for teaching me to use FORM, which proved to be an invaluable tool, and for happily answering any questions I had during the start of my PhD.

Chapter 1

Introduction

Since their discovery many years ago the proton and neutron have been studied in great detail. They were originally thought to be fundamental, and this was believed until scattering experiments in the 1960s showed that they were composite particles. We now think of protons and neutrons as being composed of quarks and gluons, and it is these particles that are, in the standard model, assumed to be fundamental.

Protons and neutrons, along with all other particles made of quarks, are collectively known as hadrons. This family of particles can be further divided into particles with three valence quarks known as baryons, and particles with two valence quarks known as mesons. Physicists have done much more than simply classify particles, their masses, decay modes, and many other observables have been measured and studied.

For this thesis the axial coupling constant of the lightest baryons, known as the baryon octet, and the lifetime of the proton, have been studied using an effective theory known as chiral perturbation theory. We have also used a large amount of lattice data to study how these observables vary with the pion mass. Chiral

perturbation theory is a theory based on the symmetries of quantum chromo dynamics, which is currently the best theory we have to describe the interactions of quarks and gluons. In the rest of this chapter we will discuss some details of QCD and mention some other methods that have been developed for studying hadrons and introduce the concept of an effective field theory.

In chapter 2 we will introduce chiral perturbation theory. As there has been a lot of lattice data used in this work, in chapter 3 we shall give a brief introduction to some of the key features of a lattice calculation.

In chapter 4 we discuss our work on the axial coupling constant and chapter 5 shows our work on proton decay and baryon number violation. Chapter 6 contains our conclusions.

1.1 QCD

It is accepted that the strong force is well described in terms of quarks and gluons by QCD. The Lagrangian for QCD can be written in a very compact form

$$\mathcal{L} = \bar{q}_f(i\not{D} - m_f)q_f - \frac{1}{4}\mathcal{G}_{\mu\nu}\mathcal{G}^{\mu\nu} \tag{1.1}$$

where the covariant derivative D_μ and the field strength tensor $\mathcal{G}_{\mu\nu}$ are given by

$$D_\mu = \partial_\mu - igA^a_\mu t^a \tag{1.2}$$

$$\mathcal{G}_{\mu\nu} = \partial_\mu A^a_\nu - \partial_\nu A^a_\mu + gf^{abc}A^b_\mu A^c_\nu. \tag{1.3}$$

The Roman superscripts a, b, c run from 1 to 8, the t^a are the 8 Gell-Mann matrices and f^{abc} are the antisymmetric structure constants of SU(3). The subscript f in eq. (1.1) refers to the flavour of the quark. There are six flavours of quarks with a

wide range of masses (given in GeV) [1]

$$\begin{array}{lll} m_u = 0.0023^{+0.007}_{-0.005} & & m_c = 1.275(25) \\ m_d = 0.0048^{+0.005}_{-0.003} & < 1 < & m_b = 4.18(3) \\ m_s = 0.095(5) & & m_t = 173.21(51)(71) \end{array} \tag{1.4}$$

and eight massless gluons. The gluons interact indiscriminately with the different quarks meaning QCD has an approximate flavour symmetry which is broken by the differing quark masses.

Although the Lagrangian looks similar to the Lagrangian for QED, there are important differences. The symmetry group for QCD is SU(3), whose elements are matrices which generally do not commute. Groups with non commuting elements are known as non-Abelian groups, and QCD is a non-Abelian gauge theory. One consequence of this is that we see terms in the Lagrangian that allow for three- and four-gluon interaction vertices. There are three notable features of QCD that we shall introduce in this section: asymptotic freedom, colour confinement and approximate chiral symmetry.

It was shown in 1973 by Gross & Wilczek and Politzer [2, 3] that non-Abelian gauge theories can exhibit asymptotic freedom. This means the strength of the coupling between quarks and gluons decreases at high energies. The physical explanation for this is screening caused by the vacuum. In the presence of a colour charge, $\bar{q}q$ pairs formed in the vacuum will align themselves with the field. In the case of QED, this effect, known as vacuum polarization, screens the charge of the electron at large distances and makes the apparent charge smaller than the bare charge. In QCD we have a similar picture, with quarks instead of electrons and colour charge instead of electromagnetic charge. However, we also have anti-screening from gluons which acts in the opposite way to the screening from quarks. As long as the number of quarks is less than 16, the effect of the gluons is greater

than that of the quarks. At high energies (i.e. short distances), the effect of screening is reduced and we see a lower effective colour charge. At high energy the QCD coupling becomes small, and the theory becomes asymptotically free. A consequence of asymptotic freedom is that we expect to see scaling behaviour in deep inelastic experiments at high energies. Bjorken [4] showed that the structure functions describing lepton nucleon scattering should approach a fixed limit for very large momentum transfers Q^2. When scattering a lepton off a particle with finite size (e.g. a proton), the cross section is expected to fall rapidly with increasing Q^2. Conversely, when scattering a lepton off a point source, the cross section is expected to show little dependence on Q^2 as $Q^2 \to \infty$. The SLAC-MIT experiment showed strong evidence of scaling, and subsequent experiments have demonstrated the point like nature of quarks. Any potential quark structure is inaccessible at current experimental energies.

At high energies, the QCD coupling is weak, and a perturbative treatment should converge well. At low energies however, we observe colour confinement, that is, all observable states are colour singlet states. Although asymptotic freedom can be proved to be true, and we can create a physically realistic interpretation of how this happens via screening, there is currently no proof that QCD exhibits confinement. There is a large body of evidence supporting the theory, in that a lone quark or gluon has never been observed.

The Lagrangian of QCD is invariant under colour SU(3). In the limit $m_q \to 0$ there are no interactions between left and right handed quarks. In this limit the Lagrangian is invariant under independent $\mathrm{SU}(N_f)_L$ and $\mathrm{SU}(N_f)_R$ transformations where N_f is the number of quark flavours. Another way of saying this is that the Lagrangian has an approximate chiral symmetry that becomes exact as the quark mass tends to zero, with the limit $m_q \to 0$ known as the chiral limit. For hadrons that just contain light valence quarks, this symmetry is realised fairly well, and

the symmetry is broken badly by the heavier quarks.

The up, down and strange quarks have masses much less then 1 GeV, while the charm, bottom and top quarks have masses greater than 1 GeV. This suggests that if we consider only the three lightest quarks we would expect flavour SU(3) to be a fairly good symmetry of the Lagrangian. We can also see that within the three light quarks there is a notable separation of scales between the lighter up and down quarks and the heavier strange quark, suggesting that flavour SU(2) should also be quite a good symmetry.

There are consequences of these symmetries that should be evident in nature. The linear combinations of the $\mathrm{SU}(3)_L$ and $\mathrm{SU}(3)_R$ generators, $V = R + L$ and $A = R - L$ both commute with the QCD Hamiltonian and have opposite parity. We could therefore reasonably assume that the hadron spectrum exhibited parity doubling i.e. particles of opposite parity and equal mass. This is not observed in nature. If we assume instead that the combinations of $R+L$ generators annihilate the ground state, but the combinations $R - L$ do not, then we might expect to see a light Goldstone boson for each generator that does not annihilate the ground state. For flavour $\mathrm{SU}(2)_L \otimes \mathrm{SU}(2)_R$ there are $2(2^2 - 1) = 6$ generators, half of which leave the ground state invariant, so we would expect to see 3 massless spin 0 particles with negative parity. These particles are taken to be the three light 0^- pions, as their mass is much lower than the typical hadronic mass scale, e.g. $M_\rho \sim 0.77$ GeV. Their small mass is due to the explicit symmetry breaking caused by the small but finite up and down quark masses. For three flavours we have 8 Goldstone bosons, assumed to be the meson octet consisting of (π, K, η). The larger mass of the K and η is due to the larger mass of the strange quark breaking chiral symmetry.

We have mentioned three interesting aspects of QCD: asymptotic freedom,

confinement and chiral symmetry. The reason QCD is hard to study in the low-energy regime is because the fundamental degrees of freedom form bound states that are colour singlets. This also makes it very interesting. Conventional perturbative techniques do not uniformly converge for low-energy QCD, and so to study hadronic physics, many models have been implemented that capture some of the unique aspects of QCD. We shall discuss some of these models in section 1.3, however the method we have used is an effective field theory based on chiral symmetry that reproduces all the symmetries of QCD.

1.2 SU(N)

The special unitary group is the mathematical group whose elements are $N \times N$ unitary matrices with determinant $\det = 1$. The elements of the matrices may be complex. For example, an arbitrary element of SU(2) can be written as [5]

$$\begin{pmatrix} a & b \\ -b^* & a^* \end{pmatrix} \tag{1.5}$$

with a and b are complex numbers and $a^*a + b^*b = 1$. As the values of a and b are continuous, the elements of SU(N) form a continuous group. An important feature of Lie groups is that we can generate elements of the group using a finite number of matrices known as generators; we can also express an arbitrary SU(N) element as

$$\exp\left(i\alpha_i S_i\right) \tag{1.6}$$

where S_i is known as a generator and α_i is a real parameter and the exponential function is defined in terms of the power series

$$\exp(A) = \sum_{n=0}^{\infty} \frac{A^n}{n!}. \tag{1.7}$$

It is important to distinguish between the Lie group and the Lie algebra; a generator is an element of the Lie algebra, and the Lie group is generated using the generators and the exponential map. For instance, if we have a Lie group SU(N) and a Lie algebra $\mathbf{su}(N)$ and generators S_i then we have

$$\exp(-i\alpha_i S_i) \in \mathrm{SU}(N) \qquad\qquad S_i \in \mathbf{su}(N). \tag{1.8}$$

The elements of the Lie algebra (i.e. the generators) satisfy the following commutation relationship

$$[S_i, S_j] = i a_{ijk} S_k \tag{1.9}$$

where a_{ijk} are known as structure constants and the indices are from 1 to $N^2 - 1$, i.e. for SU(N) there are $N^2 - 1$ generators. For SU(2) the structure constants are given by the antisymmetric Levi Civita tensor ε_{ijk}, and the SU(3) structure constants are given by

$$\begin{aligned} &f_{123} = 1 \\ &f_{147} = f_{165} = f_{246} = f_{257} = f_{345} = f_{376} = \tfrac{1}{2} \\ &f_{458} = f_{678} = \tfrac{\sqrt{3}}{2}. \end{aligned} \tag{1.10}$$

The generators of SU(2) are related to the three Pauli matrices

$$\sigma_1 = \begin{pmatrix} 0 & 1 \\ 1 & 0 \end{pmatrix} \quad \sigma_2 = \begin{pmatrix} 0 & -i \\ i & 0 \end{pmatrix} \quad \sigma_3 = \begin{pmatrix} 1 & 0 \\ 0 & -1 \end{pmatrix} \tag{1.11}$$

with the generators given by $S_i = \sigma_i/2$. The generators of SU(3) are commonly taken to be the Gell-Mann matrices

$$\lambda_1 = \begin{pmatrix} 0 & 1 & 0 \\ 1 & 0 & 0 \\ 0 & 0 & 0 \end{pmatrix} \quad \lambda_2 = \begin{pmatrix} 0 & -i & 0 \\ i & 0 & 0 \\ 0 & 0 & 0 \end{pmatrix} \quad \lambda_3 = \begin{pmatrix} 1 & 0 & 0 \\ 0 & -1 & 0 \\ 0 & 0 & 0 \end{pmatrix}$$
$$\lambda_4 = \begin{pmatrix} 0 & 0 & 1 \\ 0 & 0 & 0 \\ 1 & 0 & 0 \end{pmatrix} \quad \lambda_5 = \begin{pmatrix} 0 & 0 & -i \\ 0 & 0 & 0 \\ i & 0 & 0 \end{pmatrix} \quad \lambda_6 = \begin{pmatrix} 0 & 0 & 0 \\ 0 & 0 & 1 \\ 0 & 1 & 0 \end{pmatrix} \tag{1.12}$$
$$\lambda_7 = \begin{pmatrix} 0 & 0 & 0 \\ 0 & 0 & -i \\ 0 & i & 0 \end{pmatrix} \quad \lambda_8 = \tfrac{1}{\sqrt{3}} \begin{pmatrix} 1 & 0 & 0 \\ 0 & 1 & 0 \\ 0 & 0 & -2 \end{pmatrix}.$$

For any Lie group, the Lie algebra contains a sub-algebra of members that commute with each other, but not with the other members of the algebra [5]. This sub-algebra is known as the Cartan sub-algebra, and its members are diagonal matrices. The number of Cartan matrices in a Lie algebra defines the rank of the Lie group. The reason the Cartan sub-algebra is important to physicists is that we can relate gauge bosons that do not alter charges (e.g. photon and Z^0) to the Cartan sub-algebra, and gauge bosons that do alter charge (e.g. $W^{\pm}$) to the non Cartan sub-algebra. Particles that interact with the gauge bosons are described by the eigenvectors of the Cartan sub-algebra, with the eigenvalues denoting the charges [5].

Although we have said that the group SU(N) is the set of $N \times N$ unitary matrices with a determinant of 1, this is actually only one of an infinite number of representations of the group. Any set of square matrices with dimension $n > N$ that satisfies eq. (1.9) will give an n dimensional representation of SU(N) (this is

not possible for all n, for instance there is no four or five dimensional representation of SU(3)). The smallest possible representation of SU(N) has dimension N and is known as the fundamental representation. It is possible to build a picture of the hadron spectrum by taking direct products of quarks living in the fundamental representation of SU(N). This was noted by Gell-Mann, who pointed out that combining quarks living in flavour SU(3) can reproduce representations observed in nature [6].

1.2.1 Irreducible representations

If we consider only the two lightest quarks, they live in the fundamental representation of flavour SU(2) (this would be exactly true if they were massless, their small mass dynamically breaks SU(2) by a small amount). The irreducible dimensions of the direct product of a quark and anti quark are

$$\mathbf{2} \otimes \bar{\mathbf{2}} = \mathbf{1} \oplus \mathbf{3}. \tag{1.13}$$

This tells us that we would expect to see a triplet with similar masses and a singlet, both consisting of up and down quarks. The triplet are the three pions with masses close to 140 MeV and the singlet is the η'. Including the strange quark, we would have

$$\mathbf{3} \otimes \bar{\mathbf{3}} = \mathbf{1} \oplus \mathbf{8} \tag{1.14}$$

with the octet consisting of (π, K, η) and the singlet being the η'. The masses of the K and η are larger than the π due to the larger mass of the strange quark.

We can repeat the process for baryons. If we take three quarks in the fundamental representation and combine them using the direct product we see that

$$\mathbf{2} \otimes \mathbf{2} \otimes \mathbf{2} = \mathbf{2} \oplus \mathbf{2} \oplus \mathbf{4}. \tag{1.15}$$

We would expect to see the nucleon doublet and the Δ quartet. The **4** can be taken to be the Δ multiplet. To explain the fact that there are 2 **2** representations we need to consider the symmetry of the wavefunction [7]. The nucleons are spin 1/2, and so have a completely antisymmetric wavefunction consisting of the direct product of colour, flavour, spin and position. The colour part must be antisymmetric, as a colour neutral particle must be a colour singlet which is antisymmetric. The space part must be symmetric, and so the combination of spin and flavour must be symmetric. There is no completely symmetric or antisymmetric way to write a spin half wavefunction from three spin half quarks, but we can have mixed symmetric and mixed anti symmetric states which are symmetric or anti symmetric under exchange of the first and second particles. There is also no way to combine two up (down) quarks and a down (up) quark for a proton (neutron) in a completely symmetric or anti symmetric states. The mixed spin and flavour wavefunctions can be combined to make a symmetric wavefunction, so we need two **2** representations to describe the nucleon.

1.3 Hadronic physics

We have mentioned that QCD exhibits several interesting features: quark confinement, asymptotic freedom and approximate chiral symmetry (which is exact when we have massless quarks). Asymptotic freedom immediately restricts the use of perturbative techniques to high momentum scales, and so to study the properties of hadrons, two possible paths are to pursue non-perturbative methods or construct QCD-inspired models that can be solved at low energies. In this section we will briefly discuss some existing approaches to studying QCD, particularly at low energies. As they play a large role in this thesis, we will not mention chiral perturbation theory or lattice QCD in this chapter, but instead discuss them in

chapters 2 and 3 respectively.

1.3.1 Non-relativistic quark model

The non-relativistic quark model (NRQM) assumes that the quarks inside a hadron are heavy, slow and interact through an empirical potential [8]. The potential is modelled to have a confining part that grows with distance, r, and a short range part that is less singular than $1/r$ [8]. A simple example for mesons used initially to study the charm anti-charm bound states, is the Cornell or funnel potential [9] given by

$$V(r) = -\frac{a}{r} + b\,r + c \tag{1.16}$$

where a, b and c are inputs that can be tuned to match experimental data.

With the quarks alone accounting for the mass of the hadrons we have, for the light up and down quarks (assuming isospin symmetry) $m_N \sim 3m_q$ suggesting $m_q \sim 300$ MeV. Clearly, this does not provide a good description of the pion mass ($M_\pi \sim 140$ MeV), but for states containing heavier quarks, the NRQM has been shown to have some predictive power.

Baryon properties in the NRQM are complicated by the presence of a third quark making calculations involving a quark potential rather more involved than is the case for mesons. However, just based on the symmetries of the baryon wavefunction it is possible to make some predictions. For instance, the axial coupling constant of the proton can be shown to be g_A=5/3 [10], which is not substantially far from the experimental value $g_A = 1.2723(23)$ [1].

1.3.2 MIT bag model

The MIT bag model was introduced by Chodos et al. [11] as a method of modelling the observed confinement of quarks. In the model quarks are confined to a finite

region of space. Outside this region, their wavefunction is set to zero and the quark flux through the boundary is also zero. Inside the bag, the quarks are modelled as weakly coupled to gluon fields, which are also confined to the bag. The confinement is achieved by assuming the bag has a constant, positive energy per unit volume B, which is a free parameter that can be fixed using experimental data. The model is constructed so that hadrons are described by colour-singlet combinations of quarks. A colour neutral hadron cannot fission into its constituent quarks in the model, as to do this there would have to be a region in the bag where the cross section $A \to 0$. As this happens, the colour flux through this region of the bag would have to diverge, meaning an infinite amount of energy would be required to ionize the hadron [11].

Chodos et al. [12] showed that, by setting B so the model fits the average mass of the $N - \Delta$ system (~ 1.1 MeV), they could predict the magnetic moment, axial vector charge and charge radius of the proton to be

$$\begin{array}{ccc} g_p = 5.2 & g_A = 1.09 & r_c = 1.0 \text{ fm} \\ g_p^{\text{expt}} = 5.585694713(46) & g_A^{\text{expt}} = 1.2723(23) & r_c^{\text{expt}} = 0.8775(51) \text{ fm} \end{array} \tag{1.17}$$

where we have included modern experimental results as well [1].

The advantages of the bag model are that it is conceptually simple to understand, and can predict some fundamental hadronic properties. However, it cannot explain the N Δ mass difference without further extensions. It cannot explain the light mass of the pion either, and makes no attempt to model chiral symmetry. Indeed, taking the Lagrangian for the bag model to be [13]

$$\mathcal{L}_{\text{MIT}} = \frac{i}{2}\bar{\psi}(\overleftarrow{\partial\!\!\!/} - \overrightarrow{\partial\!\!\!/})\psi\theta(R-r) - \frac{1}{2}\bar{\psi}\psi\delta(r-R) \tag{1.18}$$

we can see that chiral symmetry is explicitly broken. It can also be said that the

model does not actually seek to model QCD, just some aspects of it. There is no guarantee that an advanced bag model that tried to account for as many QCD features as possible would actually be a good model of QCD [14].

An extension to the MIT bag model that accounts for chiral symmetry is known as the cloudy bag model [15, 16, 17]. In this model pions can interact with the surface of the bag, and it can be thought of conceptually as bag of quarks surrounded by a cloud of pions.

1.3.3 NJL model

Whereas the MIT bag model emulates the confining aspects of QCD but not chiral symmetry (in the original form of the model), the NJL model is fundamentally chirally symmetric, but does not model confinement. The NJL model was presented in two papers by Nambu and Jona-Lasinio [18, 19] with a Lagrangian given by

$$\mathcal{L} = i\bar{\psi}\partial\!\!\!/\psi + g_0(\bar{\psi}\psi\,\bar{\psi}\psi - \bar{\psi}\gamma_5\tau_i\psi\,\bar{\psi}\gamma_5\tau_i\psi). \tag{1.19}$$

The states ψ and $\bar{\psi}$ were initially referred to as nucleon states by Nambu and Jona-Lasinio. As this model was introduced before the concept of quarks (the quark model was first published by Gell-Mann in 1964 [6], three years after the NJL model) it was not proposed as a QCD model; rather, it was proposed to describe the low-energy hadron spectrum which it did fairly well.

Because of the relative simplicity of the NJL Lagrangian, and the fact that it has chiral symmetry, it can be used to study interesting effects such as dynamical quark mass generation and the role of pions as Goldstone bosons [20]. In its simplest form the NJL model is a rather simple non confining toy model, however there have been extensions to the model that can account for some of its shortcomings [21, 22]. Recently, Carrillo-Serrano et al. [23] have used the NJL model

to study the baryon masses and axial couplings, however they were only able to calculate the strangeness conserving axial couplings.

1.3.4 Large N_c QCD

Experimental evidence strongly suggests that the number of colours in QCD is 3, however there exists a large amount of work studying the limit as the number of colours $N_c \to \infty$. The first paper on this topic was by t'Hooft [24] where he discussed the idea of having an infinite number of colours whilst keeping the quantity $\lambda = g^2 N_c$, where g is the coupling constant fixed.

In large N_c QCD, there are $N_c^2 - 1 \sim \mathcal{O}(N_c^2)$ gluons, as the gluons live in the adjoint representation, and quarks, which live in the fundamental representation, have $\mathcal{O}(N_c)$ colour components [25]. To reflect this, large N_c diagrams have a single line for a fermion propagator and a double line for a gluon propagator [26]. Drawing a Feynman diagram with a double line for a gluon propagator and a single line for a quark propagator and including a factor of g for every vertex it is possible to determine to what order in N_c a diagram will contribute [26]. For any process, the type of diagram that contributes the largest power of N_c, and is therefore the most important as $N_c \to \infty$, is a planar diagram with no internal quark propagators. Diagrams with internal quark propagators are suppressed by one or more powers of $1/N_c$ and diagrams that contain crossing propagators are suppressed by two or more powers of $1/N_c$ [26]. In the large N_c limit, only a subset of diagrams (planar diagrams with gluon propagators) contribute, however a method of exactly resumming this partial series has yet to be found [26].

Studies of mesons using large N_c show that they are stable particles with mass $\sim \mathcal{O}(1)$, and they weakly couple to each other as $N_c \to \infty$. It can be shown that the baryon mass goes as $\sim \mathcal{O}(N_c)$, so they are infinitely heavy as $N_c \to \infty$.

The expansion parameter for SU(N_c) is $1/N_c$. As the number of colours is 3,

it seems that first order corrections could potentially be quite large, however some observables have the first correction at $1/N_c^2$, in which case the corrections will be fairly small, around 10% [10].

1.4 Effective field theories

We shall discuss in the next chapter an alternative method of studying QCD that does not rely on model building: chiral perturbation theory. This is an effective theory based on the symmetries of QCD. To finish this chapter, we shall briefly mention some key points about effective field theories in general.

There exists a huge range of interesting phenomena over a huge range of energy scales. The degrees of freedom that are relevant at different energy scales are not necessarily the same, and can be completely independent of each other. A good example is the Fermi theory of weak decay. We know that the weak decay of a neutron $n \to p + e^- + \bar{\nu}_e$ is mediated by the massive W boson ($M_W = 80.385(15)$ GeV), however at low energy this process can be described quite accurately using a simple four point vertex. The reason the four point vertex works well at low energy is because there is a large separation of scales between the centre of mass energy, E and the W boson mass M_W. We can also tell at what energies the approximation is valid; with $E \ll M_W$ the approximation will be a good one, and when $E \sim M_W$ we expect to see substantial differences between experiment and theory.

To discuss the concepts of an EFT more clearly, we can consider a theory with two interacting real scalar fields ϕ and χ with a Lagrangian given by [27]

$$\mathcal{L} = \frac{1}{2}\partial^\mu \chi \partial_\mu \chi - M_\chi^2 \chi^2 + \frac{1}{2}\partial^\mu \phi \partial_\mu \phi - m_\phi^2 \phi^2 + \lambda \phi \phi \chi. \tag{1.20}$$

This theory is not particularly realistic as the energy is unbounded from below, but as a toy model it is quite useful. If we consider the s channel diagram in the

process $\phi\phi \to \phi\phi$ this will give us the amplitude

$\mathcal{M} =$ 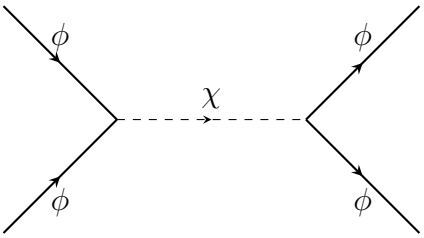

$= \dfrac{i\lambda^2}{k^2 - M_\chi^2}.$ (1.21)

If the ϕ field is much lighter than the χ field and the momentum k^2 is much less than M_χ^2 then we can approximate eq. (1.21) with a Taylor series

$$\mathcal{M} = \frac{-i\lambda^2}{M_\chi^2}\left(1 + \frac{k^2}{M_\chi^2} + \mathcal{O}(k^4)\right). \tag{1.22}$$

We can produce the same series using an effective Lagrangian with no heavy χ fields

$$\mathcal{L}_{\text{eff}} = \frac{1}{2}\partial^\mu\phi\partial_\mu\phi - m_\phi^2\phi^2 + \tilde{\lambda}_1\phi^4 + \tilde{\lambda}_2\phi^2\partial^\mu\phi\partial_\mu\phi + \ldots \tag{1.23}$$

where we have two new constants $\tilde{\lambda}_1$ and $\tilde{\lambda}_2$ given by

$$\tilde{\lambda}_1 = \frac{\lambda^2}{M_\chi^2}, \qquad \tilde{\lambda}_2 = \frac{\lambda^2}{M_\chi^4}. \tag{1.24}$$

Higher order terms in eq. (1.22) can be generated by terms in eq. (1.23) with more derivatives. The effective Lagrangian contains an infinite number of terms which can be grouped according to how many powers of the momentum k^2 they will contribute. This is a very simple form of power counting. We also know at what energy scales the effective Lagrangian is actually effective. For a Taylor series in k^2/M_χ^2 up to order n, the error will be of the order $\mathcal{O}(k^{2n}/M_\chi^{2n})$.

For this simple example it is possible to determine the parameters $\tilde{\lambda}_1$ and $\tilde{\lambda}_2$ in terms of parameters in the original Lagrangian. With a more complicated theory it is usually not possible to express the EFT parameters in terms of parameters

from the original theory. If this is the case, the parameters are commonly deduced by matching theory with experiment.

We can formulate the concept of an EFT more concretely by looking at the generating functional

$$\mathcal{Z} = \int \mathcal{D}\phi \mathcal{D}\chi \exp(-iS) \tag{1.25}$$

where S is the action associated with the Lagrangian 1.20. If we are not interested in the heavy degrees of freedom, we can explicitly integrate over them to leave an expression in terms of the light degrees of freedom

$$\mathcal{Z} = \int \mathcal{D}\phi \exp(-iS_{\text{eff}}) \tag{1.26}$$

where S_{eff} contains only the light fields ϕ. Unfortunately, it is normally not possible to perform the integration, and so the effective Lagrangian must be constructed based on the symmetries of the original Lagrangian.

We shall discuss how it is possible to use the language of an EFT to describe the low energy nature of QCD. The resulting theory is known as chiral perturbation theory (ChPT). The relevant degrees of freedom at low energies are not quarks and gluons, but hadrons. With the use of ChPT it has been possible to investigate many interesting properties of the low mass hadrons.

Chapter 2

Chiral perturbation theory

QCD has an approximate chiral symmetry that becomes exact as the quark mass $m_q \to 0$. For N_f massless quarks the QCD Lagrangian is invariant under global $\mathrm{SU}(N_f)_L \otimes \mathrm{SU}(N_f)_R$ transformations. It is useful to define the combinations $V = R + L$ and $A = R - L$. We mentioned in chapter 1 that the presence of 8 light pseudoscalar mesons (see table 2.1) suggests the vacuum is annihilated by V and not A. These mesons are lighter than would be expected from a simple quark model, and within the 8 Goldstone bosons the pions are particularly light, reflecting the fact that the up and down quarks are much lighter than the strange quark. The average pseudoscalar meson mass, $\bar{M}_\phi = 368.2$ MeV is much lighter than a typical hadronic scale (e.g. $M_\rho = 775.26(25)$ MeV).

With the baryon octet (see table 2.2) and decuplet (table 2.3) we can again see the effect of the heavier strange quark in their masses. Particles of equal strangeness have almost identical masses, and increasing the magnitude of the strangeness gives an increase in mass of approximately 200 MeV.

Chiral perturbation theory (ChPT) is an effective field theory, based on the symmetries of QCD, that describes the interactions of these hadrons at low energies (ChPT deals with only mesons, and baryon ChPT also includes interactions

Particle	Mass (MeV)	Lifetime (s)	Main decay	Branching ratio	S
π^+	139.57018(35)	$2.6033(5) \times 10^{-8}$	$\pi^+ \to \mu^+\nu_\mu$	0.9998770(4)	0
π^-	139.57018(35)	$2.6033(5) \times 10^{-8}$	$\pi^- \to \mu^-\bar{\nu}_\mu$	0.9998770(4)	0
π^0	134.9766(6)	$8.52(18) \times 10^{-17}$	$\pi^0 \to \gamma\,\gamma$	0.98823(34)	0
η	547.862(18)	$5.0(2) \times 10^{-19}$	$\eta \to \gamma\gamma$	0.3941(21)	0
K^+	493.677(16)	$1.2380(21) \times 10^{-8}$	$K^+ \to \mu^+\nu_\mu$	0.6355(11)	1
K^-	493.677(16)	$1.2380(21) \times 10^{-8}$	$K^- \to \mu^-\bar{\nu}_\mu$	0.6355(11)	-1
K^0	497.614(24)	–	–	–	1
$\bar{K}^0$	497.614(24)	–	–	–	-1

Table 2.1: Masses, widths, main decay modes and strangeness of the meson octet.

Particle	Mass (MeV)	Lifetime (s)	Main decay	Branching ratio	S
p	938.272046(21)	$> 6.6 \times 10^{36}$	–	–	0
n	939.565379(21)	$8.803(11) \times 10^{2}$	$n \to pe^-\bar{\nu}_e$	~ 1	0
Λ	1115.683(6)	$2.632(20) \times 10^{-10}$	$\Lambda \to p\pi^-$	0.639(5)	-1
Σ^+	1189.37(7)	$8.018(26) \times 10^{-11}$	$\Sigma^+ \to p\pi^0$	0.5159(30)	-1
Σ^0	1192.642(24)	$0.074(7) \times 10^{-18}$	$\Sigma^0 \to \Lambda\gamma$	~ 1	-1
Σ^-	1197.449(30)	$1.479(11) \times 10^{-10}$	$\Sigma^- \to n\pi^-$	0.99848(5)	-2
Ξ^0	1314.86(20)	$2.90(9) \times 10^{-10}$	$\Xi^0 \to \Lambda\pi^0$	0.99524(12)	-2
Ξ^-	1321.71(7)	$1.639(15) \times 10^{-10}$	$\Xi^- \to \Lambda\pi^-$	0.99887(35)	-2

Table 2.2: Masses, widths, main decay modes and strangeness of the baryon octet.

Resonance	Mass (MeV)	Width (MeV)	Main decay	Branching ratio	S
Δ^{++}	$1230 - 1232$	114-117	$\Delta \to N\pi$	~ 1	0
Δ^+					
Δ^0					
Δ^-					
Σ^{*+}	1382.80(35)	36.0(7)	$\Sigma^* \to \Lambda\pi$	0.870(15)	-1
Σ^{*0}	1383.7(1.0)	36(5)			
Σ^{*-}	1387.2(5)	39.4(2.1)			
Ξ^{*0}	1531.80(32)	9.1(5)	$\Xi^* \to \Xi\pi$	~ 1	-2
Ξ^{*-}	1535.0(6)	$9.9^{+1.7}_{-1.9}$			
Ω^-	1672.45(29)	$8.019(60) \times 10^{-12}$	$\Omega^- \to \Lambda K^-$	0.678(7)	-3

Table 2.3: Masses, widths, main decay modes and strangeness of the baryon decuplet.

between hadrons and mesons). The advantage of ChPT lies in the fact that it is not a model, but a theory that obeys all of the same symmetries of QCD. It allows us to study the important effects that Goldstone bosons have on low-energy baryon properties.

There are two important features of ChPT: there is a separation of scales, and the interactions between Goldstone Bosons are weak.

The separation of scales refers to the difference between a typical chiral scale, q^2 (for instance M_ϕ^2 for on shell Goldstone Bosons), and the chiral symmetry-breaking scale, Λ_χ. The chiral symmetry-breaking scale can be taken to be the mass of the lightest excitations that have been integrated out, for instance the the vector meson mass m_ρ or the nucleon mass m_N. Because $\Lambda_\chi^2 \gg q^2$ we expect a perturbative expansion in the ratio q^2/Λ_χ^2 to converge well.

Of equal importance is the fact that interactions between Goldstone Bosons are weak. In the limit of massless quarks, the Goldstone Boson do not interact with each other. The three lightest quarks are light when compared to Λ_χ, and so in the real world, where chiral symmetry is not exact, we can still expect the interactions between Goldstone Bosons to be weak at low energy. If the interactions were strong, it would not be possible to construct a useful perturbative expansion.

In this chapter we will introduce the leading order Lagrangians used in mesonic ChPT and baryonic ChPT. We will mention the importance of power counting and some of the problems involved with including baryons in ChPT, and how the heavy-baryon and extended on mass shell formulations avoid the problems. We shall also discuss how the decuplet can be included as an explicit degree of freedom.

2.1 ChPT with mesons

Phenomenological Lagrangians were in use before the advent of ChPT, and were generally used to simplify calculations based on current algebra. It was Weinberg who advanced the idea of using a phenomenological Lagrangian [28], and his ideas led to the development of ChPT. Weinberg mentions that the most general Lagrangian that is analytic, unitary, and assumes some symmetry principles should result in the most general matrix elements that obey the same symmetry principles [28]. Weinberg also demonstrated that it is possible to establish a power counting hierarchy that allows for the systematic inclusion of loop diagrams, as we shall see later.

An effective field theory relies on the presence of a small parameter that will allow the construction of a sensible perturbative series. For ChPT with mesons, the mass of the meson octet is small compared to the typical hadronic scale, and interactions between pions scale with their momentum; they become non-interacting in the limit of zero momentum. Their mass also tends to zero in the chiral limit. These parameters (mass or momentum) are small, and so are ideal for a perturbative expansion.

ChPT was extended by Gasser and Leutwyler [29]. They calculated higher-order terms in the chiral Lagrangian and showed how loop diagrams and divergences could be dealt with. The advantage of ChPT over previous soft-pion theorems was that ChPT could be used to calculate non-analytic corrections to soft-pion results (using tree-level ChPT we recover exactly results using soft-pion theorems). In some cases, these corrections were surprisingly large, for example the S wave $\pi\pi$ scattering length was calculated by Gasser and Leutwyler [30] up to $\mathcal{O}(M_\pi^2)$ and the chiral logarithm gives a correction of $\sim 25\%$.

If we consider the three lightest quarks as massless, then the QCD Lagrangian will be invariant under flavour $\mathrm{SU}(3)_L \otimes \mathrm{SU}(3)_R$, and also invariant under discrete

charge and parity transformations. We can construct an SU(3) matrix using as follows

$$U = \exp\left(\frac{\lambda_i \phi_i}{F_\pi}\right) = 1 + \frac{\lambda_i \phi_i}{F_\pi} + \cdots \tag{2.1}$$

where λ_i are the SU(3) Gell-Mann matrices and ϕ_i are field operators. The parameter F_π is known as the pion decay constant, and is a low-energy constant (LEC) that is determined via matching to experimental or lattice data. We can collect the light pseudoscalar mesons into the matrix $\lambda_i \phi_i$

$$\phi \equiv \lambda_i \phi_i = \begin{pmatrix} \pi^0 + \frac{\eta}{\sqrt{3}} & \sqrt{2}\pi^+ & \sqrt{2}K^+ \\ \sqrt{2}\pi^- & -\pi^0 + \frac{\eta}{\sqrt{3}} & \sqrt{2}K^0 \\ \sqrt{2}K^- & \sqrt{2}\bar{K}^0 & -\frac{2\eta}{\sqrt{3}} \end{pmatrix}. \tag{2.2}$$

Under $\mathrm{SU}(3)_L \otimes \mathrm{SU}(3)_R$ transformations, U and $U^\dagger$ will transform as

$$U \to U' = RUL^\dagger \tag{2.3}$$

$$U^\dagger \to U^{\dagger\prime} = LU^{\dagger\prime}R^\dagger. \tag{2.4}$$

The chiral Lagrangian must couple to external vector, axial vector, scalar and pseudoscalar fields (v_μ, a_μ, s and p) in a manner consistent with QCD. We introduce these via the covariant derivative and the field χ

$$D_\mu U = \partial_\mu U - i r_\mu U + i U l_\mu \tag{2.5}$$

$$\chi = 2B_0(s + ip) \tag{2.6}$$

where we have $r_\mu = v_\mu + a_\mu$ and $l_\mu = v_\mu - a_\mu$ and B_0 is an LEC related to the

chiral quark condensate. In the absence of external pseudoscalar fields, we have

$$\chi = 2B_0 \begin{pmatrix} m_u & 0 & 0 \\ 0 & m_d & 0 \\ 0 & 0 & m_s \end{pmatrix}. \tag{2.7}$$

The product $D_\mu U$ has the same transformation properties under $\mathrm{SU}(3)_L \otimes \mathrm{SU}(3)_R$ as U. We can write the leading order mesonic ChPT Lagrangian as

$$\mathcal{L}_\phi^2 = \frac{F_\pi^2}{4}\mathrm{Tr}(D^\mu U (D_\mu U)^\dagger) + \frac{F_\pi^2}{4}\mathrm{Tr}(\chi U^\dagger + U\chi^\dagger) \tag{2.8}$$

$$= \frac{1}{2}\partial_\mu\phi\partial^\mu\phi - \frac{1}{2}M_\phi^2\phi^2 + \cdots . \tag{2.9}$$

all interaction terms would either have two derivatives acting on them, or would be multiplied by $B_0(s + ip) = B_0 \mathrm{diag}\,(m_u, m_d, m_s)$. That is, every vertex using the Lagrangian in eq. (2.8) is multiplied by a momentum squared term or a quark mass term and is of chiral order $\mathcal{O}(q^2)$.

Higher-order terms in the Lagrangian will contain new LECs. The LECs cannot be determined using symmetry arguments and their values are often determined by fitting to data. They could, in principle, be calculated directly from QCD, and in practice, can be determined via lattice QCD.

We mentioned earlier how power counting plays an important role in ChPT. It allows us to relate a given diagram to a given order in ChPT without having to calculate the diagram first. This allows us to write down all the diagrams that contribute up to a given order. To do this, it is important to know the chiral order

of the structures in eq. (2.8), they are [31]

$$\begin{aligned} &U = \mathcal{O}(q^0) \quad D_\mu U = \mathcal{O}(q) \\ &r_\mu = \mathcal{O}(q) \qquad l_\mu = \mathcal{O}(q) \\ &\chi = \mathcal{O}(q^2). \end{aligned} \tag{2.10}$$

The lowest order mesonic ChPT Lagrangian is of chiral order $\mathcal{O}(q^2)$. The order, D, to which a given diagram will contribute in ChPT can be calculated using

$$D = 2 + 2N_L + \sum_{n=1}^{\infty} N_{2n}(2n-2) \tag{2.11}$$

where N_L is the number of loops and N_{2n} is the number of vertices from the Lagrangian of order $2n$. The importance of this result is that diagrams from a Lagrangian of order n with loops contribute at a higher chiral order than those without loops. This power counting allows us to systematically calculate a uniformly converging perturbative series and is a key feature of ChPT.

As ChPT is an effective field theory it is non-renormalisable. However, it can be renormalised order by order. Loop diagrams with vertices from $\mathcal{L}_2^\phi$ will be renormalised by tree-level diagrams with vertices from $\mathcal{L}_2^\phi$. It is possible to construct higher-order Lagrangians, but the number of terms, and the number of undetermined LECs, increases at each order. For example, the fourth order mesonic Lagrangian calculated by Gasser and Leutwyler [32] contains 12 LECs. The LECs are mostly scale dependent, but when they are included in observables, the total expression will be scale independent.

2.2 ChPT with baryons

The extension of ChPT to include baryons is complicated by the fact that the baryon mass is not a chiral parameter, meaning it does not vanish in the chiral limit. It was noted by Gasser et al. [33] that the power counting of ChPT, that relates a Feynman diagram to a particular order in a perturbative series, is broken by the presence of the nucleon mass.

When performing loop calculations involving baryons, we obtain terms both of a lower and higher chiral order than would be expected from power counting. This was first pointed out by Gasser et al. [33]. The presence of the non-chiral scale destroys power counting.

Fortunately, there is a solution to this problem (there are in fact several solutions). In this section we shall introduce the tree-level Lagrangian for two and three-flavour ChPT and show two methods used to restore power counting. The first method we shall discuss is known as heavy-baryon ChPT (HBChPT), and the basic idea is to use the fact that the baryon mass is of the same order as Λ_χ so we can simultaneously form a power series in q^2/Λ_χ^2 and q^2/m_N^2, with q^2 being a chiral parameter.

The second method we shall discuss is known as extended on-mass-shell ChPT (EOMS ChPT). With this method, the terms that violate power counting are subtracted using counter-terms from higher-order Lagrangians. As the Lagrangian is assumed to be the most general Lagrangian that obeys all relevant symmetries, it can be assumed that it contains terms that exactly cancel power-counting-violating terms.

2.2.1 Two-flavour baryon ChPT

For SU(2) ChPT we are interested in the interactions between the nucleon doublet (p, n) and the pion triplet (π^+, π^-, π^0). The lowest order Lagrangian can be written

$$\mathcal{L}^0_{\pi N} = \bar{\psi}\left(i\not{D} - m_N - \frac{g_A}{2}\gamma^\mu\gamma_5 u_\mu\right)\psi \tag{2.12}$$

where there are two LECs, the nucleon mass m_N and the axial coupling constant g_A. These parameters are both bare parameters in the leading order Lagrangian. Defining

$$u_\mu = i\left(u^\dagger(\partial_\mu - ir_\mu)u - u(\partial_\mu - il_\mu)u^\dagger\right), \tag{2.13}$$

$$\Gamma_\mu = \frac{1}{2}\left(u^\dagger(\partial_\mu - ir_\mu)u + u(\partial_\mu - il_\mu)u^\dagger\right) \tag{2.14}$$

with u defined as $u^2 = U$ (see eq. 2.1) we can write the covariant derivative as

$$D_\mu\psi = (\partial_\mu + \Gamma_\mu)\,\psi. \tag{2.15}$$

The problem with using this Lagrangian is that the presence of the nucleon mass spoils power counting. As an illustrative example, we shall look at the loop contribution to the nucleon mass which should be of order $\mathcal{O}(q^3)$

$$= \int \frac{d^dk}{(2\pi)^d} g_A \not{k}\gamma_5 \frac{i(\not{p} - \not{k} + m_N)}{(p-k)^2 - m_N^2} g_A \not{k}\gamma_5 \frac{i}{k^2 - M_\pi^2} \tag{2.16}$$

$$= g_A^2\left(2m_N(1-d)I_2^1 - m_N(2+d)I_3^1 - m_N^3 I_3^2\right) \tag{2.17}$$

$$\overset{d\to 4}{=} \frac{g_A^2}{(4\pi F)^2}\Big(2m_N^3(n-1) + 2M_\pi^2 m_N n$$
$$- 2M_\pi^3\sqrt{4 - \frac{M_\pi^2}{m_N^2}}\arccos\left(\frac{M_\pi}{2m_N}\right) - \frac{M_\pi^4}{m_N}\log\left(\frac{M_\pi^2}{m_N^2}\right)\Big) \tag{2.18}$$

with the expressions for I_i^j, regularised using dimensional regularisation, shown in appendix A. The parameter n defines our renormalisation scheme which is used to remove divergences that appear when calculating loop integrals. The minimal subtraction scheme, MS, removes only the divergent parts, and the modified minimal subtraction ($\overline{\text{MS}}$ corresponding to $n = 2$) removes divergent parts plus additional constant terms. We have used the $\overline{\text{MS}}$ scheme throughout this thesis.

In eq. (2.18) we see that we actually have a $\mathcal{O}(q^0)$ term and a $\mathcal{O}(q^2)$ term where would expect to have only terms of order $\mathcal{O}(q^3)$. There are also terms of order $\mathcal{O}(q^4)$ and higher. In other words, we have an order $\mathcal{O}(q^3)$ diagram giving contributions of order $\mathcal{O}(q^0)$ and $\mathcal{O}(q^2)$, and also $\mathcal{O}(q^4)$ and higher. This means that all orders of the perturbative series are potentially equally important and we have no way of assigning a power counting method as we did in the mesonic case.

2.2.2 Heavy-baryon formalism

The first method that was devised to restore power counting is known as heavy-baryon ChPT (HBChPT). It was first introduced by Jenkins and Manohar [34] and formalised by Bernard et al. [35]. In the heavy-baryon scheme, the momentum of the baryon is split into a large and a small part

$$p_\mu = m_N v_\mu + k_\mu \tag{2.19}$$

where v_μ is known as the four velocity and constructed such that $v^2 = 1$ and $v_0 \geqslant 1$ and k_μ is taken to be small (of chiral order). The idea to separate the momentum in this fashion was first developed by Georgi [36] to deal with heavy quarks at low energies. For the case of baryons, we can define new fields that depend on v_μ

$$\mathcal{N} = \exp(im_N v \cdot x) P_{v+} \psi \tag{2.20}$$

$$\mathcal{H} = \exp(im_N v \cdot x) P_{v-} \psi \tag{2.21}$$

with the projection operators

$$P_{v\pm} = \frac{1 \pm \not{v}}{2}. \tag{2.22}$$

In the appendix of their paper, Bernard et al. [35] used the path integral formalism to write the ChPT Lagrangian in terms of light ($\mathcal{N}$) and heavy ($\mathcal{H}$) fields and explicitly integrate out the heavy degrees of freedom. The resulting Lagrangian contained an infinite string of terms, with higher-order terms suppressed by powers of $1/m_N$. The lowest order Lagrangian is

$$\mathcal{L}^{(1)}_{\pi N} = \bar{\mathcal{N}} \left(iv \cdot D + g_A S \cdot u \right) \mathcal{N} \tag{2.23}$$

where S^μ is defined as

$$S^\mu = \frac{i}{2} \gamma_5 \sigma^{\mu\nu} v_\nu, \quad S^{\mu\dagger} = \gamma_0 S^\mu \gamma_0 \tag{2.24}$$

and so carries the spin information of the nucleon. The parameter m_N does not appear in the leading order Lagrangian, so we will not receive unexpected lower order contributions from higher-order calculations. As with the mesonic case, the loop diagrams will not break the power counting scheme and a diagram at order $\mathcal{O}(q^n)$ will only give contributions of order $\mathcal{O}(q^n)$. The divergences caused by loop diagrams must be removed using counter terms. There are more LECs in HBChPT than there are in mesonic ChPT, and through considerable theoretical input many of the LECs have been fit to data (see, for instance, Bernard [37]).

The heavy-baryon formulation of ChPT (HBChPT) is a non relativistic reduction, where relativistic invariance is restored as higher-order terms are included in calculations. It yields a power series in the small chiral parameter q^2/Λ^2 and in

the inverse nucleon mass q^2/m_N^2. It has been used with great success in a variety of situations, however there can be issues relating to analyticity under certain kinematics [27]. For instance, the invariant amplitudes for pion-nucleon scattering should have poles at $s = m_N^2$ and $u = m_N^2$. However, the heavy-baryon approach has no pole at $u = m_N^2$. This region of parameter space is not physically realistic, but analyticity requires the presence of the pole, and the heavy-baryon approach can only achieve this by summing an infinite number of diagrams [27].

2.2.3 Extended on-mass-shell formalism

Since the application of ChPT to the baryon sector, there have been attempts to formulate a fully relativistic baryon ChPT that obeys power counting. Currently, the most widely used is known as extended on mass shell ChPT (EOMS ChPT) developed by Fuchs et al. [38]. Fuchs et al. note that terms that violate power counting are analytic in the quark mass (or equivalently, have even powers of M_ϕ). This means that it is possible to subtract the power-counting-violating terms using counter-terms.

The heavy-baryon formalism removes large (non-chiral) terms from the Lagrangian. However, in certain circumstances, the resulting perturbative series converges in only part of the low-energy region [39]. The EOMS formalism leaves non-chiral terms in the Lagrangian and removes them once the calculation is complete.

Returning to our example of the self energy calculation in eq. 2.18, the terms that violated power counting were multiplied by an even power of the pion mass (in this case the powers were 0 and 2), in other words the terms are analytic in the quark mass. This means they can be compensated for by counter-terms. For every loop diagram that could potentially violate power counting, there must be a counter term that can restore power counting. Fortunately, an effective theory

contains an infinite number of terms, and in fact contains all terms that are allowed under symmetry and conservation laws.

The specific counter-terms that are required for a particular calculation are not known beforehand, unlike in the heavy-baryon sector where the counter-terms will remove all divergences if included correctly. If an EOMS diagram can be calculated in closed form, an expansion of the result in powers of a chiral scale (usually the meson octet mass) will identify the terms that violate power-counting. These terms can then be subtracted from the final result. If the diagram can only be solved numerically, then the integrand must be expanded first in inverse powers of the small chiral scales and then solved. This will also reveal the terms violating power-counting. All of the integrals encountered in this thesis could be solved without using numerical methods, so we did not have to expand out the integrals to determine the power-counting-violating terms.

The counter terms required are quite general, we do not require an infinite number of terms at any given order to restore power counting. For instance, any process calculated up to order $\mathcal{O}(p^3)$ will need renormalising, but the relevant terms in the Lagrangian will be from $\mathcal{L}^{(1)}$, $\mathcal{L}^{(2)}$ and $\mathcal{L}^{(3)}$. Although the total number of counter terms is infinite, at any given order they are finite.

If we contrast this with the heavy-baryon sector, in both cases we require higher-order terms to renormalise infinities produced by loop diagrams. The key difference is that in the heavy-baryon scheme, power counting is obeyed naturally, and in the EOMS scheme we require the counter terms to also restore power-counting. The EOMS scheme also includes a partial summation of higher-order terms.

If we take an EOMS expression and perform a series expansion in powers of the inverse nucleon mass, the resulting series will have the same non-analytic terms as a heavy-baryon calculation.

2.2.4 Three-flavour EOMS ChPT

If we collect the baryon octet fields into the matrix B

$$B = \begin{pmatrix} \frac{\Sigma^0}{\sqrt{2}} + \frac{\Lambda}{\sqrt{6}} & \Sigma^+ & p \\ \Sigma^- & -\frac{\Sigma^0}{\sqrt{2}} + \frac{\Lambda}{\sqrt{6}} & n \\ \Xi^- & \Xi^0 & -\frac{2\Lambda}{\sqrt{3}} \end{pmatrix} \tag{2.25}$$

the interactions of the meson and baryon octet can be studied using the three-flavour Lagrangian

$$\mathcal{L} = \mathrm{Tr}\left(\bar{B}(i\not{D} - m_B)B\right) - \frac{D_0}{2}\mathrm{Tr}\left(\bar{B}\gamma^\mu\gamma_5\{u_\mu, B\}\right) - \frac{F_0}{2}\mathrm{Tr}\left(\bar{B}\gamma^\mu\gamma_5[u_\mu, B]\right). \tag{2.26}$$

The SU(3) lowest order Lagrangian contains three free parameters, the baryon mass m_B and the two Clebsch Gordan coefficients D_0 and F_0. For the SU(2) Lagrangian there are only two parameters, m_N and g_A, however in the SU(3) theory there are two independent ways to combine two octet baryon fields and one octet meson field and so we have one extra parameter at leading order.

The three-flavour sector also contains more LECs than the two-flavour sector. There are 16 LECs in the order $\mathcal{O}(q^2)$ Lagrangian and 78 at order $\mathcal{O}(q^3)$ [40]. In the two-flavour sector there are 7 LECs at $\mathcal{O}(q^2)$ and 23 at order $\mathcal{O}(q^3)$ [41].

For three-flavour calculations, we end up with a series in M_π, M_K and M_η. As the kaon and eta masses are larger than the pion mass it can be expected that a series may converge more slowly in the SU(3) sector.

2.3 The decuplet

As well as removing divergences from integrals, LECs also encode the effects of resonances that are not included in the chiral Lagrangian. When a particle has

a large mass, m, compared to the typical energy scales of an interaction, it can be "integrated out" so that the effects of the particle are modelled as a series of point interactions of successively higher order in q^2/m^2. The larger the mass of the particle, the better this approximation is. Certain LECs strongly encode the effects of heavy particles, and in the mesonic sector the idea of resonance exchange, where we attribute a particular counter term to a particular resonance (or particle) has been quite successful [42, 43]. However, if a resonance is only separated from the chiral scale by a small amount, we would expect to see slow convergence of the perturbative series. The mass difference between the nucleon and the Δ is $m_{N-\Delta} = 0.290$ GeV, approximately twice the mass of the pion. This small separation suggests that integrating out the Δ may not always be a good approximation. One method to counter this is to include the resonance explicitly as a degree of freedom. We can see the impact of the Δ resonance particularly strongly in two-flavour ChPT, where the LECs c_{2-4} are notably reduced in fits to data when the Δ resonance is included as an explicit degree of freedom [44].

We can see in table 2.3 that the decuplet couples strongly to the octet, with the decays of the Δ, Σ^* and Ξ^* being predominantly strong decays to the baryon octet. The Ω cannot decay via the strong force, as its mass is too low to decay to the $s = -3$ combination of Ξ and K. The fact that it must decay via the weak interaction gives it a much longer life than the other members of the decuplet.

The average mass of the baryon decuplet is close to that of the baryon octet. This suggests that integrating out the decuplet degrees of freedom may not always be advised. An alternative method is to include the degrees of freedom explicitly.

As the decuplet has spin 3/2, it is not described by the Dirac equation, but

instead by the Rarita Schwinger equation [45]

$$\begin{aligned}\mathcal{L} = \bar{\Psi}_\mu \Big(&- (i\partial\!\!\!/ - m_\Delta) g^{\mu\nu} - iA(\gamma^\mu \partial^\nu + \gamma^\nu \partial^\mu) \\ &- \frac{i}{2}(3A^2 + 2A + 1)\gamma^\mu \partial\!\!\!/ \gamma^\nu - m_\Delta (3A^2 + 3A + 1)\gamma^\mu \gamma^\nu \Big) \Psi_\nu \end{aligned} \tag{2.27}$$

where $A \neq 1/2$ is an arbitrary real parameter taken by Rarita and Schwinger to be $A = -1/3$ [27]. The Lagrangian is invariant under the transformation

$$\Psi_\mu \to \Psi'_\mu = \Psi_\mu + \partial_\mu \varepsilon \tag{2.28}$$

with ε a spinor. The fields must also satisfy the equations

$$\gamma_\mu \Psi^\mu = 0, \quad \partial_\mu \Psi^\mu = 0. \tag{2.29}$$

It is important to note that the vector field Ψ^μ is constructed by coupling a spin 1 vector and a spin 1/2 Dirac spinor. As a result of this, Ψ^μ contains both spin 1/2 and spin 3/2 degrees of freedom. To remove the unwanted spin 1/2 degrees of freedom, it is common to introduce a set of orthonormal spin projection operators to separate the spin 1/2 and spin 3/2 components [46]

$$(P^{3/2})_{\mu\nu} + (P^{1/2}_{11})_{\mu\nu} + (P^{1/2}_{22})_{\mu\nu} = g_{\mu\nu} \tag{2.30}$$

with the spin 3/2 projection operator defined as [47]

$$(P^{3/2})_{\mu\nu} = g_{\mu\nu} - \frac{\gamma_\mu \gamma_\nu}{d-1} - \frac{1}{(d-1)p^2}(p\!\!\!/ \gamma_\mu p_\nu + p_\mu \gamma_\nu p\!\!\!/) - \frac{(d-4)p_\mu p_\nu}{(d-1)p^2}. \tag{2.31}$$

The Rarita-Schwinger propagator can be written

$$S_{\mu\nu}(p) = \frac{p\!\!\!/ + m_T}{m_T^2 - p^2}(P^{3/2})_{\mu\nu}. \tag{2.32}$$

The interaction of the decuplet with the baryon and meson octet must be consistent, meaning that it must have the correct number of degrees of freedom. The relationship between consistent and inconsistent couplings was formalised by Pascalutsa [48]. Pascalutsa points out that a Lagrangian written as

$$\mathcal{L}_{\rm RS} + \mathcal{L}_{\rm int} = \bar{\Psi} \cdot \Lambda \cdot \Psi + g(\bar{\Psi} \cdot j + \bar{j} \cdot \Psi) \tag{2.33}$$

must obey the constraint $\partial \cdot j = 0$ in order for the Lagrangian to be invariant under the transformation given in eq. (2.28). However, if $\partial \cdot j \neq 0$ the interaction will be inconsistent. By making a field redefinition

$$\Psi_\mu \to \Psi_\mu + g\xi_\mu \tag{2.34}$$

then the Lagrangian can be written in terms of a consistent coupling plus a term that is quadratic in the coupling constant [48].

The three-flavour chiral Lagrangian describing interactions with the baryon and meson octet is

$$\begin{aligned}\mathcal{L} = {} & \bar{T}^{abc}_\mu (i\gamma^{\mu\nu\alpha} D_\alpha - m_T \gamma^{\mu\nu}) T^{abc}_\nu + \frac{H}{m_T} \bar{T}^{abi}_\mu \gamma^{\mu\nu\rho\sigma} \gamma_5 (\partial_\rho T^{abj}_\nu) u^{ij}_\sigma \\ & + \frac{C_A}{m_T} \varepsilon^{abc} (\partial_\alpha \bar{T}^{ade}_\mu) \gamma^{\alpha\mu\nu} B^{ce} u^{bd}_\nu \end{aligned} \tag{2.35}$$

with the totally symmetric fields T_{ijk}

$$\begin{gathered} T_{111} = \Delta^{++} \qquad T_{112} = \tfrac{\Delta^+}{\sqrt{3}} \qquad T_{122} = \tfrac{\Delta^0}{\sqrt{3}} \qquad T_{222} = \Delta^- \\ T_{113} = \tfrac{\Sigma^{*+}}{\sqrt{3}} \qquad T_{123} = \tfrac{\Sigma^{*0}}{\sqrt{6}} \qquad T_{223} = \tfrac{\Sigma^{*-}}{\sqrt{3}} \\ T_{133} = \tfrac{\Xi^{*0}}{\sqrt{3}} \qquad T_{233} = \tfrac{\Xi^{*-}}{\sqrt{3}} \\ T_{333} = \Omega^-. \end{gathered} \tag{2.36}$$

Including the decuplet explicitly also introduces another non-chiral mass scale. One method of maintaining power counting, introduced by Pascalutsa and Phillips [49], is known as the δ expansion. This used the hierarchy of mass scales

$$M_\pi \ll m_\Delta - m_N \ll \Lambda \sim 1 \text{ GeV} \tag{2.37}$$

where the difference $m_\Delta - m_N$ is commonly labelled Δ. Pascalutsa and Phillips introduce the parameter δ

$$\delta = \frac{\Delta}{\Lambda} \sim \frac{M_\pi}{\Delta} \tag{2.38}$$

and perform an expansion to a consistent order in δ. In this scheme, we can clearly see that a term M_π^2 is of order $\mathcal{O}(\delta^2)$.

A previous scheme, developed by Hemmert et al. [50] known as the ε expansion and treats $M_\pi \sim \Delta \sim \varepsilon$. The scheme of Pascalutsa and Phillips [49] accounts for the fact that in the two-flavour sector, the pion mass is smaller than Δ, whereas the scheme of Hemmert et al. [50] does not.

In the three-flavour sector, where we include the heavier K and η mesons, it can be argued that the ε scheme is the most sensible to use.

2.4 Some successes of ChPT

With the development of ChPT came the chance to study hadronic physics with a theory based solely on the symmetries of QCD. Previously, physicists used models based on some of the observed properties of hadrons, and so with the powerful tool of ChPT, many hadronic properties could be re-investigated.

Indeed, when BChPT was first formulated by Gasser et al. [33], it was used to study pion-nucleon scattering, which at the time was a field of study with over 30 years of investigation. In this section we shall briefly mention a few key results

from the field of baryon ChPT.

2.4.1 πN Scattering

Prior to ChPT calculations, the best theoretical description of πN scattering was from Weinberg, who used current algebra to calculate S-wave πN scattering lengths [51]. Using HBChPT, Bernard et al. [52] calculated corrections due to pion loops to Weinberg's current algebra predictions for the two S-wave πN scattering lengths $a^{\pm}$. Bernard et al. found that the corrections to a^{-} were small relative to the tree-level terms, but a^{+} was found to depend rather heavily on the LECs, suggesting convergence may be slow.

More recently Alarcón et al. [53] studied πN scattering using EOMS ChPT and explicitly including the Δ. They found that including the Δ led to an improved fit with good convergence in the perturbative series. After fitting the available LECs to experimental data, Alarcón et al. investigated the Goldberger–Treiman relation and the πN sigma term, $\sigma_{\pi N}$. Work on $\sigma_{\pi N}$ has currently been extended to $\mathcal{O}(p^4)$ by Alvarez-Ruso et al. [54].

Including the strange quark allows for the study of $K - N$ scattering. Mai and Meißner investigated antikaon-nucleon scattering in the framework of ChPT and found that it was possible to match kaon-nucleon scattering lengths well [55]. They also determined values for several LECs. Meson baryon scattering with decuplet contributions have also been studied in the heavy-baryon sector by Liu and Zhu [56], and meson decuplet scattering lengths have also been investigated [57].

Chapter 3

Lattice QCD

QCD is an important part of the standard model that describes how quarks and gluons interact. It is also very difficult, particularly in the low-energy regime. At low energies, quarks are always observed in a bound state, the coupling to gluons (and between gluons) is large and we cannot use perturbation theory to help us. It is possible to use non perturbative methods to study QCD at low energies; this is what lattice QCD allows us to do.

Lattice QCD was pioneered by Wilson [58]. The basic idea is to discretize space-time, replace the conventional action with a discrete lattice action and use the path integral formulation of quantum field theory to calculate Green's functions. One of the benefits of this approach is that the lattice spacing (often denoted a, and not necessarily uniform in both the space and time directions) provides a natural large momentum cut off in calculations. With lattice spacing a, the momentum must lie within the first Brillouin zone $-\pi/a < p_\mu < \pi/a$ and the inverse of the lattice spacing can be thought of as a momentum cut off. It is possible to think of lattice field theory as simply a different regularization scheme.

In lattice QCD the discretized path integrals cannot be solved analytically. Basic numerical methods for solving integrals are not practical either, due to the

incredibly large number of degrees of freedom involved. The first use of statistical methods to solve the path integrals was by Creutz [59] and Creutz, Jacobs and Rebbi [60, 61]. As each integral is weighted by an action, the main contribution comes from a relatively small region of parameter space and Monte Carlo methods can be used to obtain fairly accurate numerical results.

The numerical calculation of path integrals is a highly non trivial process. Further complications arise as computational time greatly increases with lower quark masses [62, 63]. The effects of discretization (the finite extent of the lattice and the non zero lattice spacing) cannot be quantified easily, and require careful consideration.

Although lattice QCD has applications to many areas of physics, we shall concentrate on its connections with low-energy QCD and with ChPT. As a non perturbative method, lattice QCD complements ChPT rather well. In the early days of lattice QCD, ChPT was frequently used to extrapolate results from high quark masses down to physical masses. More recently, as lattice QCD techniques improve and computer power has increased, there is less need for lattice QCD results to use chiral extrapolations, though ChPT can still benefit directly from lattice results.

In this chapter, we will provide a short description of the key points of lattice QCD. We will introduce scalar fields, fermion fields and gauge fields on the lattice and give a short description on the role of two and three point functions. We shall also mention some of the effects of discretization and the impact of performing calculations with physical quark masses.

3.1 Scalar fields on the lattice

Lattice QCD is a gauge theory set up on a four dimensional discrete Euclidean space time lattice. It is worth mentioning that although we live in Minkowskian space time, the use of Euclidean space time for QCD is not overly prohibitive for the theory. The Green's functions of interest are expressed in terms of a path integral, and the path integral is solved, nearly always computationally.

As an illustrative example, let us consider a real scalar field on the lattice. The action for a scalar field in Euclidean space-time is

$$S = \frac{1}{2}\int d^4x\phi(x)(-\partial^2 + M^2)\phi(x). \tag{3.1}$$

To perform calculations on a lattice, we must convert the integral to a sum and replace the derivative with a finite difference. We must also redefine our field $\phi(x)$ which can only exist at discrete lattice points.It is convenient to define the dimensionless quantities

$$\hat{\phi}(na) = a\phi(na) \tag{3.2}$$

$$\hat{M} = aM \tag{3.3}$$

where we have introduced the four vector $n = (n_1, n_2, n_3, n_4)$ and the lattice spacing a. We can now write the discrete lattice action [64]

$$S = \frac{1}{2}\sum_{n,m}\hat{\phi}_n\left(\hat{M}^2\delta_{n,m} - \sum_{\mu=1}^{4}(\delta_{n+\mu,m} + \delta_{n-\mu,m} - 2\delta_{n,m})\right)\hat{\phi}_m \tag{3.4}$$

and define the parameter K_{nm}

$$S \equiv \frac{1}{2}\sum_{n,m}\hat{\phi}_n K_{nm}\hat{\phi}_m \tag{3.5}$$

where n and m sum over every lattice site and μ is a unit vector in directions 1-4.

We can directly relate each part of the lattice action to the continuum action, however it is sometimes advantageous to add terms to the action that do not have any direct physical counterpart and vanish in the continuum limit; these actions are know as improved actions, and give better numerical results.

The generating functional is given by

$$Z[J] = \int \mathcal{D}\phi \exp\left[-S + J\phi\right] \tag{3.6}$$

where the integration measure $\mathcal{D}\phi$ tells us we need to integrate over every possible path. On the lattice we can write the generating functional as

$$Z[J] = \int \prod_l d\hat{\phi}_l \exp\left[-\frac{1}{2}\sum_{n,m} \hat{\phi}_n K_{nm} \hat{\phi}_m + J_n \hat{\phi}_n\right], \tag{3.7}$$

where the path integral has now become the product of a large number of integrals. A key feature of lattice QCD is that it allows for a rigorous definition of the path integral, although a lot of computational and theoretical time and effort must be put into arriving at a solution.

The scalar propagator is the inverse of K_{nm}, given by [64]

$$\langle \phi(x)\phi(y)\rangle = K^{-1}_{nm} = \int \frac{d^4p}{(2\pi)^4} \frac{e^{ip(n-m)}}{\hat{M}^2 + 4\sum_\mu \sin^2 \frac{p_\mu}{2}}. \tag{3.8}$$

In the limit $a \to 0$, the sin term can be replaced by p^2, and we get the same result for a scalar propagator using lattice regularisation that we would expect from QFT

$$K^{-1}_{nm} \to_{a\to 0} \int_{-\infty}^{\infty} \frac{d^4p}{(2\pi)^4} \frac{e^{ip(x-y)}}{M^2 + p^2}. \tag{3.9}$$

For a scalar field theory there are no adverse effects produced by the lattice, and

the continuum limit is arrived it in a fairly straight forward manner. The situation is rather less clear for fermions.

3.2 Fermion fields on the lattice

To arrive at a lattice action for a scalar field, we have seen that it is possible to start with a continuum action and replace integrals with sums, and derivatives with finite differences. For a fermion field taking a similar approach does not work.

Based on the Lagrangian for a fermion field we could create a lattice action in Euclidean space-time [64]

$$S = \int d^4x \bar{\psi}(x)(\gamma_\mu \partial^\mu + m)\psi(x) \tag{3.10}$$

$$\rightarrow \sum_{\mu,n} \left(\hat{\bar{\psi}}_n \gamma_\mu^{\mathrm{E}} (\hat{\psi}_{n+\mu} - \hat{\psi}_{n-\mu}) + \hat{m} \hat{\bar{\psi}}_n \hat{\psi}_n \right). \tag{3.11}$$

We have replaced the gamma matrix γ_μ with a Euclidean gamma matrix γ_μ^{E}, replaced the derivative with a finite difference and the integral with a sum. There is also a non local term due to the derivative becoming a finite difference. We shall see in the next section how including gauge fields restores locality. From this action we can write down a matrix with elements K_{nm} as we did in the previous section, and the quantity K_{nm}^{-1} should represent the fermion propagator. Following through these steps, we would find that

$$\langle \bar{\psi}(x)\psi(y) \rangle = \int \frac{d^4p}{(2\pi)^4} \frac{(-i/a)\gamma_\mu \sin(p^\mu a) + m}{(1/a^2)\sin^2(p_\mu a) + m^2} e^{-p(x-y)}. \tag{3.12}$$

To arrive at a continuum propagator, we need to take the limit of zero lattice spacing. For a scalar field, we could use the small angle approximation in the denominator of eq. (3.8) because, over the domain of the integral, there was only

one zero at $p_\mu = 0$. For the fermion propagator, the argument of the sin term in the denominator is twice that of the scalar propagator. This means that the radius of convergence is now the same size as the Brillouin zone; there are additional poles at the edges of the Brillouin zone (at $p_\mu = \pm\pi/a$). So now we have an integral that will still receive contributions at zero momentum, but will also receive equally important contributions at $p_\mu = \pm\pi/a$. There will be 16 regions (in a 4 dimensional integral) that all give non zero contributions to the propagator, so there are, in effect, 16 fermions on the lattice. In d dimensions, including fermions in this manner will lead to 2^d fermions for every one that was intended, so this problem was termed the fermion doubling problem and was noticed by Wilson [65] and Susskind [66]. There is a theorem by Nielsen and Ninomiya [67] which states that the fermion problem cannot be solved without violating either causality, locality or chiral symmetry.

An early solution to the doubling problem was given by Wilson [65]. A continuum action does not have a unique lattice equivalent; we can take a lattice action and add to it terms with positive powers of the lattice spacing a. In the continuum limit, these terms should have no effect on any observables. Wilson added a term to the action that removed the unwanted zeros from the propagator. If we change the action to include the extra "Wilson" term, it becomes

$$S \to S - \frac{r}{2}\sum_n \hat{\bar{\psi}}_n \hat{\partial}^2 \hat{\psi}_n \tag{3.13}$$

where r is known as the Wilson parameter. The propagator now reads [64]

$$\int \frac{d^4p}{(2\pi)^4} \frac{-i/a\gamma_\mu \sin(p^\mu a) + M}{1/a^2 \sin^2(p_\mu a) + (M + 2r/a \sin^2(p_\mu a/2))^2} e^{-p(x-y)}. \tag{3.14}$$

The extra term in the denominator serves to remove the extra fermions, and also tends to zero as $a \to 0$. Unfortunately, this creates another problem, the lattice

action is now no longer chirally invariant. Nielsen and Ninomiya [67] showed that it is only possible to avoid doubling if you violate chiral symmetry, locality or Hermiticity.

Another solution to the fermion doubling problem is to use staggered fermions, introduced by Kogut and Susskind [68]. This involves spreading out the fermion degrees of freedom over the lattice so that the effective lattice spacing of the fermions is twice the regular lattice spacing [64]. This staggering reduces the number of fermions from 16 down to 4. These four remaining species of fermions could be interpreted as physical flavours of quarks, however giving them different masses leads to problems such as fine tuning and complex determinants [69]. To move from 4 down to 2 species it is possible to square root the determinant. These two species can be taken to be the up and down quark fields.

Another method to treat the problem is to use domain wall fermions. Kaplan [70] showed that it is possible to simulate chiral fermions in $2d$ dimensions using Dirac fermions in $2d+1$ dimensions with a space dependent mass term, calculations using domain wall fermions are done in five dimensions. In the limit where the fifth dimension tends to infinity, chiral symmetry is completely restored. The great advantage of domain wall fermions is that chiral symmetry can be made arbitrarily exact by increasing the size of the fifth dimension, although the disadvantage of this is that it will increase calculation times [71].

A fourth method of including fermions on the lattice that is quite common is to use twisted mass QCD. This involves adding a pseudoscalar term to the fermion Lagrangian [72]. Twisted mass fermions violate parity and time-reversal, although these symmetries are recovered in the continuum limit [72]. One of the advantages of the twisted mass method are that physical quantities are free of $\mathcal{O}(a)$ effects.

3.3 Gauge fields on the lattice

One of the great advantages of lattice QCD over other non perturbative methods is that lattice QCD is manifestly gauge invariant [1]. Fermion fields exist only on lattice points, and between the lattice points there exist link variables which are elements of SU(3) [64]

$$U_\mu(x) = U(x, x + a\mu) \in \mathrm{SU}(3) \tag{3.15}$$

$$U_\mu^\dagger(x) = U(x + a\mu, x) \in \mathrm{SU}(3) \tag{3.16}$$

and which are directed from x to $x + a\mu$ or $x + a\mu$ to x respectively. It is these parallel transporters that avoid having non local $\bar{\psi}_n\psi_{n+\mu}$ terms. The link variable $U(x, y)$ transforms as

$$U(x, y) \to G(x)U(x, y)G^{-1}(y) \tag{3.17}$$

$$G, G^{-1} \in \mathrm{SU}(3) \tag{3.18}$$

and the fermion fields transform as

$$\psi(x) \to G(x)\psi(x) \tag{3.19}$$

$$\bar{\psi}(x) \to \bar{\psi}(x)G^{-1}(x). \tag{3.20}$$

Gauge invariant quantities can be fermion bilinears that are connected via link variables, or closed loops consisting solely of link variables. The simplest closed loop is around a 1×1 square and is known as a plaquette [64].

Defining

$$U_P = U_{\mu\nu}(x) = U_\mu(x)U_\nu(x + \mu)U_\mu^\dagger(x + \nu)U_\nu^\dagger(x) \tag{3.21}$$

Wilson chose to write the action as [58, 73]

$$S_W = -\sum_{\mu} \frac{\beta}{N} \mathrm{Re}[\mathrm{Tr}(U_P)] \tag{3.22}$$

where $\beta = 2N_C/g^2$, N_C is the number of colours and g is the QCD coupling constant. Introducing the gauge variables via

$$U_\mu = e^{igaA_\mu} \tag{3.23}$$

it is possible to show that

$$U_P = e^{iea^2 F_{\mu\nu}} \tag{3.24}$$

where we have used $F_{\mu\nu}$ as the discrete field strength tensor. Expanding the Wilson action in terms of the fields $F_{\mu\nu}$ it can be shown that the leading order action reproduces the standard kinetic term for a gauge field [64, 73]

$$S = \frac{\beta g^2}{8N} \sum_x a^4 F_{\mu\nu} F^{\mu\nu} + \mathcal{O}(a^5). \tag{3.25}$$

3.4 Fermion determinant

The Euclidean partition function can be written as [74]

$$\mathcal{Z} = \int \mathcal{D}A_\mu \mathcal{D}\psi \mathcal{D}\bar{\psi} \exp\left(- \int d^4x \frac{F_{\mu\nu}F^{\mu\nu}}{4} - \bar{\psi}\mathcal{O}_{\mathrm{Dirac}}\psi \right) \tag{3.26}$$

where $\mathcal{O}_{\mathrm{Dirac}}$ is the Dirac operator. It is possible to integrate out the fermion fields, meaning the partition function can now be written as [74]

$$\mathcal{Z} = \int \mathcal{D}A_\mu \det(M_{\mathrm{Dirac}}) \exp\left(- \int d^4x \frac{F_{\mu\nu}F^{\mu\nu}}{4} \right). \tag{3.27}$$

Calculating the determinant of the Dirac operator matrix requires a large amount of computational power. The quenched approximation in lattice QCD allows for a large reduction in calculation times by assuming the determinant of the matrix to be a constant. Physically, this approximation equates to ignoring contributions from the sea quark loops [74].

Chen [75] observed that in the large N_c limit, quenched and unquenched QCD become identical, which suggests that the errors associated with the quenched approximation should be less than 30%.

There is another way to deal with sea quarks. It is possible to set the sea quark masses to be greater than the valence quark masses; this is known as partial quenching, or mixed action. While it is clearly not physically realistic, is does allow effects of the sea quarks to be studied much better than in a quenched calculation and is less intensive than the unquenched case.

Most modern lattice calculations are fully unquenched which allows better determination of errors, and generally better agreement with experimental data.

3.5 Two and three point functions

In lattice calculations it is common to take the ratio of lattice correlators to extract the required observable [74]. For instance, the correlation function used to determine the mass of a particle is [74]

$$\Gamma(\tau) = \sum_n \langle 0|\mathcal{O}_f|n\rangle \langle n|\mathcal{O}_i|0\rangle \frac{e^{-M_n\tau}}{2M_n} \tag{3.28}$$

where $\mathcal{O}_f$ and $\mathcal{O}_i$ are operators that create and destroy the relevant current, and the sum over n represents the insertion of a complete set of states with mass M_n. If the particle spectrum contains a mass gap, then the lowest mass state will be

the only non negligible state for large times. The ratio

$$M(\tau) = \ln\left(\frac{\Gamma(\tau+1)}{\Gamma(\tau)}\right) \tag{3.29}$$

should have a plateau for $\tau \gg 1$ [74]. Due to the statistical nature of lattice calculations however, the plateau is not flat and fluctuates around the desired result [76]. The statistical errors also grow for large τ.

Another complication is contamination from nearby excited states. If there are a range of particles with the same quantum numbers but different masses, the closer the two masses, the more difficult it is to calculate the observables of the individual particles.

For the calculation of form factors, it is necessary to consider three point functions [1]. For example, to calculate the axial form factor for the nucleon, the nucleon is created at time t_i, the axial current couples to a quark at a later time, and the nucleon is annihilated at time t_f [77]. The calculation of a form factor generally requires both three point and two point functions, meaning calculating form factors on the lattice is more involved than calculating, for instance, a particle's mass.

To calculate the axial coupling constant of the nucleon, the following two and three point functions are required [77]

$$G(q, t_f) = \sum e^{-ix\cdot q}\Gamma^0_{\beta\alpha}\left\langle J_\alpha(t_f, x_f)\bar{J}_\beta(t_i, x_i)\right\rangle \tag{3.30}$$

$$G^\mu(\Gamma^\nu, q, t) = \sum e^{-ix\cdot q}\Gamma^\nu_{\beta\alpha}\left\langle J_\alpha(t_f, x_f)A^\mu(t, x)\bar{J}_\beta(t_i, x_i)\right\rangle \tag{3.31}$$

where J_α is a nucleon interpolating field and A_μ is the axial current. Defining the ratio

$$R^\mu(\Gamma, q, t) = \frac{G^\mu(\Gamma, q, t)}{G(0, t_f)}\sqrt{\frac{G(p, t_f - t)G(0, t)G(0, t_f)}{G(0, t_f - t)G(p, t)G(p, t_f)}} \tag{3.32}$$

the axial (G_A) and pseudoscalar (G_P) form factors are given by

$$\lim_{t_f - t \to \infty, t - t_i \to \infty} R^i(\Gamma^j, q, t) = \frac{i}{4m_N}\sqrt{\frac{2m_N^2}{E(E+m_N)}}\Big(\frac{q_i q_j}{2m_N}G_P(Q^2) - (E+m_N)\delta_{ij}G_A(Q^2)\Big). \tag{3.33}$$

Form factors are further complicated by the presence of disconnected diagrams. This is where the current couples to an intermediate sea quark instead of a valence quark. These calculations often contain a large amount of noise and are not as simple to calculate as connected diagrams [78].

3.6 Discretization effects

To compare observables calculated on the lattice to experimental results, or to ChPT, or even to other lattice calculations, the lattice observables must be extrapolated from the discrete lattice to the continuum. This means taking the limit $L \to \infty$ and $a \to 0$. This process is rather involved, and as we will see actually requires the value of a to be inferred after the lattice calculation is over. Typically, calculating lattice results on various volumes and spacings is required. However, simple extrapolation techniques are often not good enough, and more detailed extrapolations are needed.

3.6.1 The continuum limit

In lattice QCD the lattice spacing a sets a momentum scale; the momentum on the lattice is restricted to the range $-\pi/a < p^\mu < \pi/a$. In order to compare lattice results with experimental data or other theoretical predictions, the lattice spacing must be sent to zero whilst keeping observables finite, and to do this the lattice spacing must first be determined.

The value of the lattice spacing (or equivalently the lattice cut off, a^{-1}) is not a direct input in lattice calculations. Instead the strong coupling constant is used as an input, or more commonly the value $\beta = 6/g^2$. In order to determine the lattice spacing for a particular value of β, a particular observable is calculated on the lattice and compared to a known value. For example the masses of the ρ meson or the Ω baryon can be calculated on the lattice and compared to the experimental values. Other variables such as the Sommer parameter [79] have also been used fairly commonly in lattice calculations. This process is known as setting the scale. For instance, if the ρ meson was used to set the scale, then the lattice spacing would be calculated via the ratio of the value calculated on the lattice to the experimental value

$$a = \frac{\hat{m}_\rho^{\text{lattice}}}{m_\rho^{\text{expt}}} \tag{3.34}$$

where the quantity $\hat{m} = am$ is calculated directly on the lattice. It is important to choose quantities that are thought to have very little dependence on either the light quark masses or the lattice size to get a reliable value of a.

The observable of interest can then be calculated at various values of β, the corresponding lattice spacings inferred, and the observable can be extrapolated to the continuum.

Although lattice calculations using different actions should all converge to the same result as $a \to 0$, discretization errors are necessarily introduced in lattice theory which make the extrapolation more complicated. Symonzik [80] introduced the idea of including superficially irrelevant higher dimension terms in the action that would cancel the leading order discretization errors. Actions with these terms included are referred to as improved actions. Using improved actions means that calculations require less computational power and have less dependence on the lattice spacing [74].

There is quite a wide choice of actions available to use on the lattice. Different

collaborations tend to use different actions, and this naturally provides a method of comparing different methods in lattice QCD.

3.6.2 The finite box

Taking the continuum limit alone is not enough to ensure that results will be a true representation of "real world" results; the finite size of the lattice must also be accounted for. It is a common feature of numerical simulations in general that if the extent of the simulation is too small then results may not be correct. In the case of lattice QCD, Lüscher [81] showed that finite volume effects are suppressed by factors of $e^{-M_\pi L}$.

Lattice observables will be independent of the size of the lattice if it is large enough. However, there is no definitive guide to exactly when the extent of the lattice would be large enough to completely ignore finite size effects. The brute force approach of simply making the lattice volume incredibly large is not very practical.

If we consider the effects of having a lattice volume that is too small, the pion should be the first particle to be directly affected as it has the smallest mass and therefore the longest wavelength [72]. The metric often used when discussing lattice volume is the product $M_\pi L$. When the lattice is too small there is a chance of a pion exiting the box on one side and entering on the other due to the boundary conditions employed, and is referred to as the pion travelling round the world [82]. There does not appear to be a firm theoretical limit to how low $M_\pi L$ can be before the results are no longer trustworthy, however Hall et al. [82] showed that when calculating the axial coupling constant, for pion masses lower than $M_\pi \sim 400$ MeV finite size effects are significant unless $M_\pi L > 5$ [82].

To quantify finite size effects, it is possible to use ChPT. Gasser and Leutwyler showed that the conventional infinite volume Lagrangian can be used in a finite

volume [83, 84, 85]. The LECs for finite volume ChPT can be taken to be the same as the infinite volume LECs, as the discrepancy is expected to be much smaller than the typical error in an LEC [72].

As an example we have shown two plots from work by Horsley et al. [86], reproduced in figure 3.1, where the axial coupling constant g_A is calculated. For a given light quark mass, g_A is calculated on several different lattice extents and then the infinite volume limit is predicted using an expression from finite volume ChPT calculated by Ali Khan et al. [87]. Both graphs show a sharp drop in the calculated value of g_A as the lattice size is shortened, and with the lighter pion mass (the right hand graph in figure 3.1) the sharp decrease occurs at a much larger lattice size. Calculations with light pions require larger lattice sizes. After accounting for both discretization effects and finite volume effects, it should be possible to compare calculations of the same observables from different lattice groups, each using slightly different lattice techniques.

3.7 The physical pion limit

Towards the beginning of the 2000s, there was strong evidence for an incredibly steep rise in computational cost as the pion mass was lowered to the physical point. The large cost of performing calculations with low pion mass was discussed at a lattice conference in Berlin [88], and the problem was referred to as the Berlin Wall.

The computational cost of lowering the pion mass was summarised by Ukawa [62] where he derived an empirical formula to estimate the time a calculation should take. Ukawa concluded that calculations with a lattice size $L = 2$ fm, spacing $a^{-1} = 2 - 3$ GeV and pion mass $M_\pi = 450$ MeV were feasible, but increasing the lattice length to $L = 3$ fm would require an order of magnitude

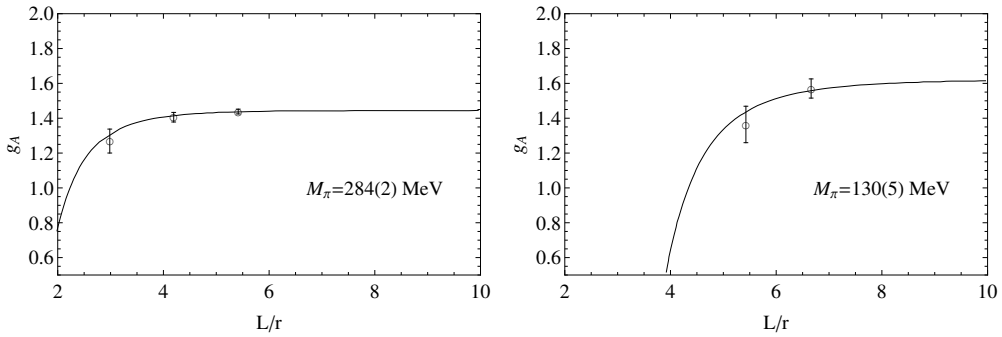

Figure 3.1: Volume dependence for the axial coupling constant g_A reproduced from Horsley et al. [86]. The axial coupling constant is being plotted against the lattice extent, L. The parameter r sets the scale and is taken to be 0.50(1) fm. The left hand graph shows data with a pion mass of 284(2) MeV, and the right hand graph shows data with a pion mass of 130(5) MeV. The solid lines are the predictions of finite volume ChPT calculated by Ali Khan et al. [87].

increase in computer power [62].

More recently, Jung [63] performed a similar analysis. Jung collected data on the cost of simulations from various collaborations, and we have shown some of his results in figure 3.2. The time taken was defined to be the time (in TFlop years) to generate either 1000 molecular dynamics units or 100 statistically independent configurations.

Jung also derived empirical expressions for the length of time a calculation should take, and we have compared the newer expression of Jung [63] with the older one of Ukawa [62] in figure 3.3. We have used $L = 3$ fm and $a^{-1} = 2 - 3$ GeV. We can see that there has been an order of magnitude improvement in computational time over the course of a decade.

One of the most expensive parts of a lattice calculation is the fermion determinant. Using preconditioning, where the determinant is separated into two or more

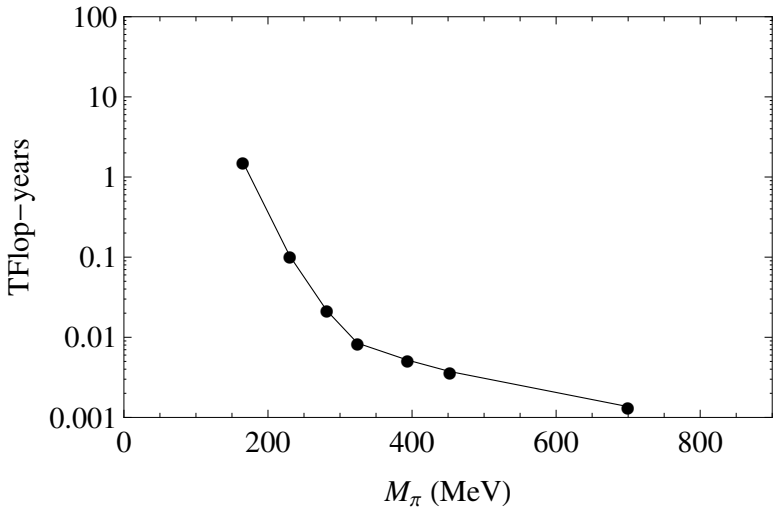

Figure 3.2: Cost of lattice simulation as a function of pion mass. Graph is taken from work by Jung [63].

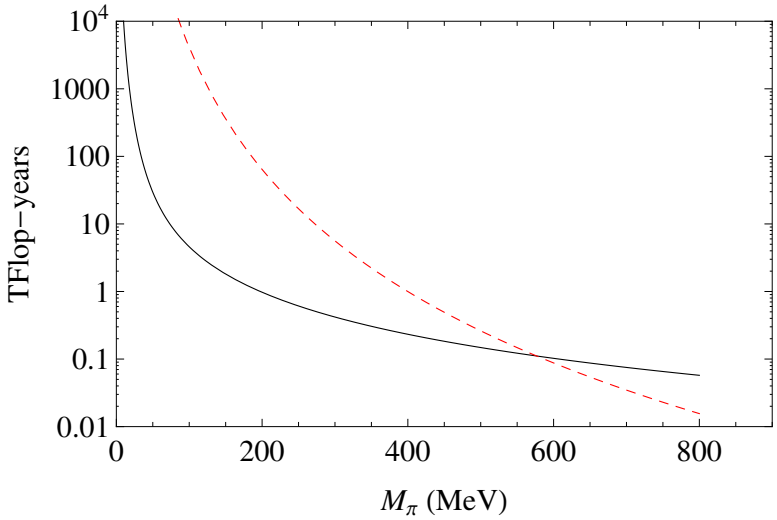

Figure 3.3: Comparison of estimates of computational time for lattice calculations from 2002 (red dashed line) and 2010 (black solid line). We have used the empirical predictions from Ukawa [62] for the 2002 curve (red, dashed) and the predictions from Jung [63] for the 2010 curve (black, solid).

parts, for example techniques by Hasenbusch [89] and Lüscher [90] among others, has helped to reduce calculation times. The wall has been shifted to lower pion masses over the years due to a combination of improvements in computer speed, algorithm efficiency and theoretical improvements in lattice QCD [91]. This has enabled lattice calculations to use much more realistic pion masses.

Although some calculations have been done with physical pion masses, when observables are calculated using larger values of the pion mass, predictions must be made for the observables at a physically realistic pion mass. To extrapolate down to the physical pion mass, ChPT can be of use as it provides a model independent prediction of the dependence on M_π of hadronic properties. There are some caveats to this however. Since ChPT is a low-energy theory of QCD, it is only expected to converge well for $M_\pi/(4\pi F) \ll 1$, so at heavier pion mass we might see poor convergence. Ideally, ChPT should be used to extrapolate lattice data for $M_\pi < 300$ MeV.

A simple reason to see why a linear extrapolation of lattice data to the physical limit may not be reasonable is to consider chiral logarithms. For values of $M_\pi \sim 300$ MeV the curve for a chiral logarithm and a term simply proportional to M_π^2 could have very similar gradients [72]. However, in the chiral limit the chiral logarithm will increase leading to a sizeable under-prediction from the lattice results. Unless the LECs in the ChPT expression are already well known, it is possible that a ChPT fit to lattice data could also lead to the wrong behaviour in the chiral limit.

Several years ago, the best method of extrapolating lattice data to the chiral limit was by fitting an expression derived from ChPT to the lattice data. As there are many LECs in ChPT, if they are not constrained by previous data then they can be treated as free parameters. In some situations this could limit the predictive power of the ChPT expression.

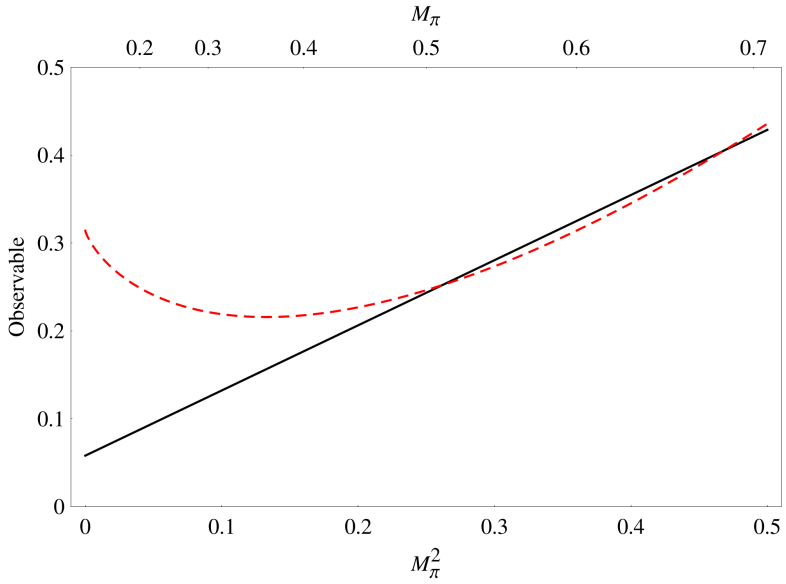

Figure 3.4: A simple example showing how a logarithm and a straight line could be confused for values of $M_\pi > 0.25$. A naive linear extrapolation to the physical pion mass, or to the chiral limit, can give misleading results.

Now we are in the situation where current lattice data is released with pion masses very close to (and in some cases, at or slightly below) the physical pion mass. If the lattice data is already calculated at the pion mass with small a and large L, there is no need to use any extrapolation. This means it is possible to use lattice data to predict the values of the LECs. For example, two of the LECs from ChPT (without baryons) l_3 and l_4 have been calculated by Baron et al. [92] and Brandt et al. [93]. These results, along with others, have been collated by the FLAG collaboration [94] to give

$$l_3 = 3.41(41) \tag{3.35}$$

$$l_4 = 4.62(22). \tag{3.36}$$

3.8 Summary

It can be argued that there are two main theoretical tools for calculating QCD at low energies, lattice QCD and effective field theory (most notably, ChPT). It can also be considered quite lucky that, of the only two methods available, one is perturbative and the other non perturbative. Both techniques are powerful in their own right, and are also very mutually beneficial. In the earlier days of lattice QCD, ChPT was crucial for extrapolating results to the physical quark mass region. However effective field theories can also be constructed in discrete space to investigate the effects of lattice spacing, and they can be constructed in a finite box to help understand finite volume effects. Although lattice QCD is an incredibly powerful tool, we should still remember that it does not truly replicate the real world.Effective field theories can be constructed to help us understand how important these effects are, if they can be ignored and perhaps even how to correct for them.

It is important to not look at the situation purely in terms of using effective field theories to constrain errors in lattice QCD. As lattice calculations become better, there is in fact less need for direct input from effective theories and we can use lattice QCD on its own to investigate properties of single and multiple hadrons.

Chapter 4

Axial coupling constant

The axial coupling constant is a measure of the interaction strength between a nucleon and the weak axial current and is defined as the zero-momentum limit of the axial form factor. The hadronic axial current can be written

$$\langle B_f|A_\mu|B_i\rangle = \bar{u}(p_f)\left(G_A(q^2)\gamma_\mu\gamma_5 + G_P(q^2)\frac{q_\mu}{2M_N}\gamma_5\right)u(p_i) \tag{4.1}$$

with G_A the axial form factor, G_P the pseudoscalar form factor and $q = p_i - p_f$ the momentum transfer.

The axial coupling constant can be measured experimentally to a high degree of accuracy via β decay experiments. It can also be calculated using lattice QCD. Experimental results put the value of g_A^{pn} at 1.2723 ± 0.0023 [1], but lattice calculations performed with an unphysical pion mass historically under-predicted g_A^{pn}. Recent results suggest that this is partly due to pion exchange forces on a small lattice volume [82]. Lattice calculations also tend to show very little dependence on the pion mass.

We can calculate g_A in chiral perturbation theory, where we perform a perturbative expansion in powers of the ratio of the light Goldstone bosons (meson

octet) to a higher energy scale $\Lambda_{\mathrm{QCD}} \sim 1$ GeV. However, the mass difference between the Δ and the nucleon is approximately $M_\Delta - M_N \approx 293$ MeV, less than the average meson octet mass, which gives us an extra non-chiral small scale. When dealing with SU(2) ChPT, the only meson mass we consider is the pion which, at 140 MeV, is significantly lower than the Δ-nucleon mass difference, so at low energies Δ excitations could justifiably be ignored and its effects absorbed into LECs. When we consider the SU(3) sector, the K and η masses are greater than the Δ nucleon mass difference, so it becomes harder to justify not including the spin 3/2 Δ field explicitly.

The axial coupling constant was calculated using two-flavour HBChPT up to $\mathcal{O}(p^4)$ with no explicit Δ contributions by Kambor and Mojzis [95] who found that higher order terms were larger than expected. This slow convergence was also noted by Bernard and Meissner [96], who calculated the two-loop leading logarithmic contribution to g_A^{pn} using two-flavour HBChPT. Calculations using two-flavour relativistic ChPT with the infra-red renormalisation scheme by Schindler et al. [97] give the same result as HBChPT up to $\mathcal{O}(M_\pi^4)$. The EOMS renormalisation scheme has different analytic terms, although this difference is compensated by different values of the renormalised LECs [97]. The decuplet contribution to g_A^{pn} was first calculated in the two-flavour heavy-baryon framework by Bernard et al. [98] where the decuplet was included using the small-scale expansion, and three-flavour calculations without [99] and with decuplet contributions [100] have also been studied. In [100], the axial decays of other members of the baryon octet were also studied in the heavy-baryon framework.

Lattice calculations of g_A^{pn} have used pion masses that are low enough that we should be able to apply ChPT with confidence to the results [101, 87, 102, 93, 103, 77, 104, 105, 86]. It has been noted previously that ChPT calculations up to $\mathcal{O}(p^4)$ without the decuplet cannot simultaneously match both the experimental

data and the lattice data [96, 106]. Bernard and Meissner [96] showed that the two-loop leading logarithmic expression for g_A has very little dependence on pion mass, although there was not a great deal of lattice data available at the time, 2006, to constrain the free parameters. Many lattice collaborations use the SU(2) SSE HBChPT result of Bernard et al. [98] to perform chiral extrapolations (e.g. [101, 77, 87, 103, 107]). Lattice calculations are performed without a strange quark ($N_f = 2$) or with a strange quark ($N_f = 2 + 1$), and currently it appears that results of the two types of calculations give very similar results for g_A^{pn}. It is now possible to perform calculations with the pion mass at, or very near to, the physical pion mass, although it appears uncertain whether questions such as finite size effects have been sufficiently addressed; lattice studies of g_A^{pn} are an ongoing area of research. We shall discuss the lattice results for g_A^{pn} in slightly more detail in section 4.1.

In this chapter, the axial coupling constant for the baryon octet is calculated to order $\mathcal{O}(p^4)$ and regularised using the extended on mass shell (EOMS) scheme [38] with explicit decuplet contributions. A full $\mathcal{O}(p^4)$ calculation would take into account the different masses of the baryon octet. We have not included this effect, so our calculation is a partial $\mathcal{O}(p^4)$ calculation. We believe that our results are still valid however. We have chosen to absorb into LECs terms that are of order $(M_\Delta - M_N)^2$ so that the contribution from the decuplet vanishes in the chiral limit. We are primarily interested in whether we can match the available lattice data for the axial coupling constant of the nucleon, g_A^{pn}. We fit the available free parameters using a combination of lattice data for g_A^{pn} at unphysical pion masses [101, 87, 102, 93, 103, 77, 104, 105, 86], lattice data for $g_A^{\Sigma^+\Sigma^+}$ and $g_A^{\Xi^0\Xi^0}$ [108, 109]

and the experimentally determined values [1]

$$\begin{array}{lll} g_A^{pn} = 1.2723(23) & g_A^{\Lambda p} = -0.879(18) & g_A^{\Sigma^-\Lambda} = 0.570(27) \\ g_A^{\Sigma^- n} = 0.340(17) & g_A^{\Xi^-\Lambda} = 0.306(61) & g_A^{\Xi^0\Sigma^+} = 1.21(05). \end{array} \tag{4.2}$$

We shall discuss the experimental determination of these values in section 4.2. Lattice data incorporates both $N_f = 2$ and $N_f = 2+1$ results, and we have combined both $N_f = 2$ and $2+1$ lattice data into one dataset. Ignoring K and η loops (more formally, setting M_K, $M_\eta \to \infty$) allows us to study the SU(2) limit of g_A^{pn}. In this limit we can set $D_0 + F_0 = g_0$ as there is only one unique SU(2) baryon-meson-baryon operator compared to two for SU(3). For both the SU(2) and SU(3) cases we can expand our result in powers of $1/M_N$, with the leading term giving an $\mathcal{O}(p^3)$ heavy-baryon expression. Retaining terms of order $\mathcal{O}(1/M_N)$ will give an $\mathcal{O}(p^4)$ heavy-baryon expression. In section 4.3 we show the relevant terms of the SU(3) Lagrangian and present our calculation of g_A. In section 4.1 we discuss existing lattice data for g_A^{pn} and in section 4.4 we show which parameters we have kept free in our fits and which we have fixed. In section 4.5 we show our fits to lattice and experimental data, along with the parameters used in the fits and we discuss our conclusions in section 4.7.

4.1 Existing lattice QCD results for g_A^{pn}

The axial form factor has been calculated many times on the lattice. Historically, results have shown very little dependence on the pion mass and have consistently produced results of the order 10% lower than the experimental value of 1.2723±0.0023 [1]. Recent lattice results have a lowest pion mass very close to [105] or lower than [86] the physical pion mass, and only Horsley et al. [86], with $M_\pi = 0.13$ GeV, have obtained a value of g_A close to the true one, however the

results from Horsley et al. relied on finite volume ChPT to extrapolate to infinite volume, and as we shall see, lattice and ChPT do not match particularly well for g_A^{pn}. It has been suggested that finite volume effects could explain the low results for g_A, with Yamazaki et al [102] showing the variation of g_A with the parameter $M_\pi L$ for both $N_f = 2$ and $N_f = 2 + 1$ calculations. They noted that with smaller values of $M_\pi L$ g_A tended to decrease. To keep finite volume effects below 1% for M_π=0.330 GeV, spatial grids of 3.4 - 4.1 fm could be necessary [102]. Although finite volume effects can be calculated, they are based on ChPT. As ChPT is not in the best agreement with all available lattice data, it may be the case that finite volume calculations are inaccurate. It is still recommended that the spatial grid be kept such that the parameter $M_\pi L$ stays above 4 [110], and even as high as 6 [111].

We have collected lattice data from nine different collaborations [101, 87, 102, 93, 103, 77, 104, 105, 86] which have values of M_π between 0.13 GeV and 0.77 GeV. Three of these groups calculated g_A with $N_f = 2 + 1$ [93, 102, 101] with the other six using $N_f = 2$. For the groups using $N_f = 2 + 1$, Edwards et al. [101] used a mixed action and had different quark masses for the sea and valence quarks, though the mass of the sea quarks were kept to 1% of the mass of the valence quarks. Yamazaki et al. [102] performed a fully unquenched calculation where they kept the strange quark mass constant while varying the light quark mass. Bratt et al. [93] used a mixed action, keeping the sea quark mass close to the valence quark mass; they kept the strange quark mass constant while varying the light quark mass. As the efficacy of extrapolating ChPT results to large pion masses is questionable, we have decided to fit our equation to lattice results where $M_\pi^2 < 0.15$ GeV^2 ($M_\pi < 0.387$ GeV), which means we have ignored 44 data points from the original set of 82 points. This data is shown in figure 4.1 where we have also included the experimental data point along with its error which is too small

to be seen on the scale we have used.

Data from Wittig et al [104] have two values of g_A for each value of the pion mass. This is because their work used two different methods to extracting g_A from their simulations: the conventional plateau method and an alternative summation method. The summation method appears to give higher values for g_A but with larger statistical uncertainty [104]. Pleiter et al [103] and Green et al [105] have calculated g_A close to the physical pion mass, but are lower than the experimental result. The results of Pleiter et al [103] for the ratio g_A/F_π are in good agreement with experiment, with Pleiter et al. suggesting that the poor agreement for g_A could be due to the renormalisation constant which drops out in the ratio g_A/F_π. Green et al [105] observe that increasing the source-sink separation with a small value of $M_\pi L_t$ moves their results away from the experimental point and increasing the separation with a larger value of $M_\pi L_t$ moves their data towards the experimental value. They suggest that this is caused by thermal pion states [105]. It should be noted that only the results with the lowest pion mass from Pleiter et al [103] and Green et al [105] appear anomalous, with the rest of their data agreeing with other collaborations.

4.2 Experimental measurements

Current experimental results for the axial coupling constant are based on neutron decay experiments, however a new method has been proposed which measures g_A via the weak charged current reaction $e + p \to \nu + n$

Neutron β decay, at low energy, can be described by only two parameters, the ratio $\lambda \equiv g_A/g_V$ and the CKM matrix element V_{ud} [112]. Writing the hadronic

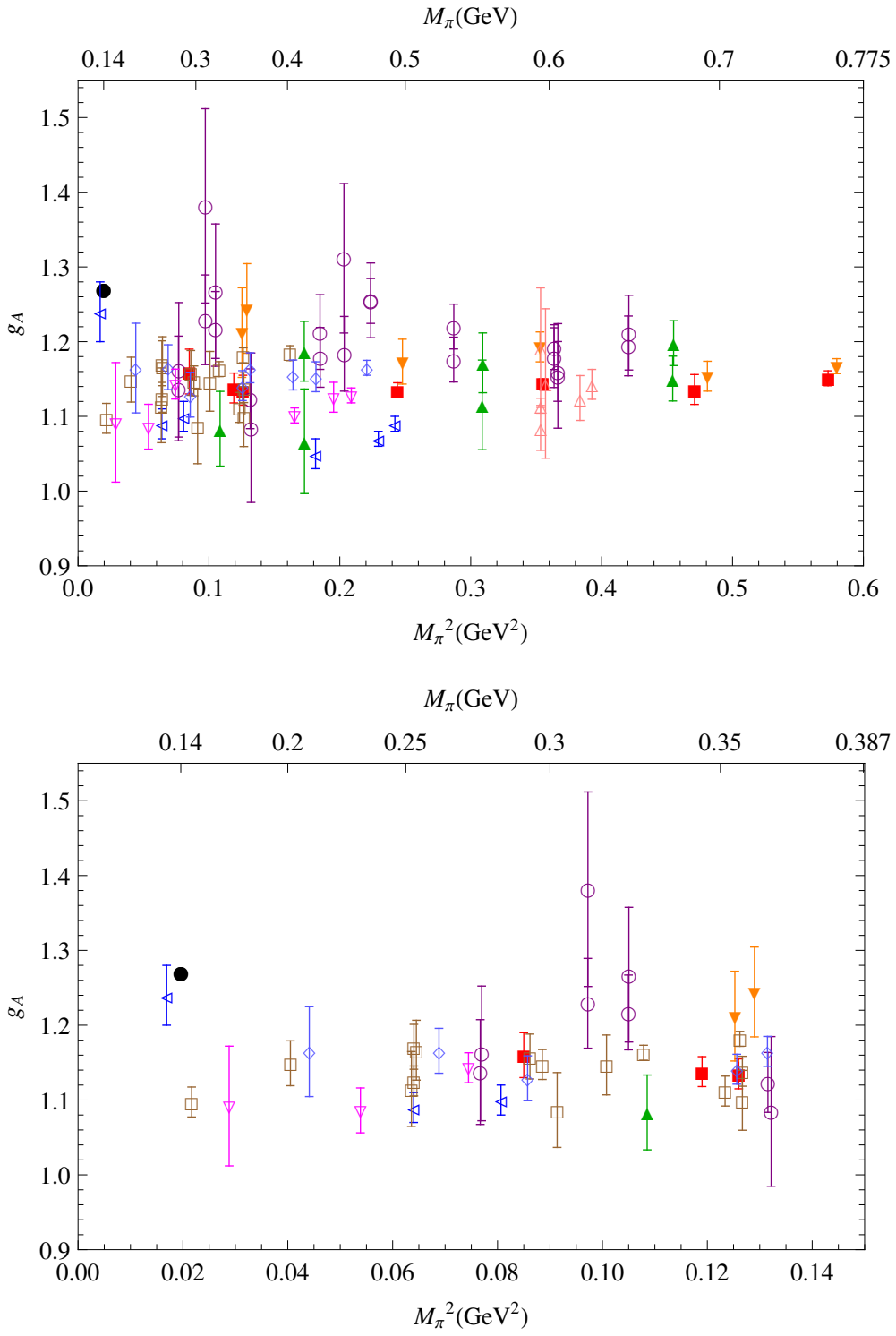

Figure 4.1: Lattice results for g_A^{pn} plotted against M_π^2 from various collaborations. The experimental value is the black dot, and the error on the experimental result is smaller than the size of the dot. The top plot shows all of the data from the collaborations, and the bottom plot shows the data with $M_\pi^2 < 0.15$ GeV^2 that was used in this work. The meanings of the symbols are shown in table 4.1.

	Collaboration	Lead author	N_f	Fermion	Min M_π (MeV)
●	Experimental	n/a	n/a	n/a	n/a
▼	LHPC	Edwards [101]	2+1	DWF/Asqtad	350
△	QCDSF	Ali Khan [87]	2	Wilson	590
▲	RBC+UKQCD	Yamazaki [102]	2+1	DWF	330
■	LHPC	Bratt [93]	2+1	DWF	290
▽	QCDSF/UKQCD	Pleiter [103]	2	Clover	170
◇	Twisted Mass	Alexandrou [77]	2	Twisted mass	210
○	(CLS)	Wittig [104]	2	Imp. Wilson	280
□	(BMW)	Green [105]	2	Clover	150
◁	(QCDSF)	Horsley [86]	2	Wilson	130

Table 4.1: Key to graph for lattice and experimental data on g_A^{pn}. The collaboration shown in brackets signifies that the configurations came from the collaboration, but the work on g_A was not done as part of the collaboration. CLS is the Coordinated Lattice Simulations collaboration and BMW is the Budapest-Marseille-Wuppertal collaboration. We have ordered the table chronologically. Empty symbols denote 2 flavour lattice data and solid symbols (excluding the black circle) denote $2+1$ flavour lattice data.

matrix element for neutron decay as

$$\langle p|J^\mu|n\rangle = \bar{u}_p\Big(g_V\gamma^\mu + g_A\gamma^\mu\gamma_5 + g_P\gamma_5\frac{q^\mu}{m_N} + g_S\frac{q^\mu}{2m_N} - ig_T\sigma^{\mu\nu}\gamma_5\frac{q_\nu}{2m_N} - ig_{\mathrm{WM}}\sigma^{\mu\nu}\frac{q_\nu}{2m_N}\Big)u_n \tag{4.3}$$

where the (q^2 dependent) parameters $g_{V,A,P,S,T,\mathrm{WM}}$ are known as the vector, axial vector, pseudoscalar, scalar, tensor and weak-magnetic form factors, the scalar and tensor form factors are taken to be negligible (under G parity symmetry they are zero, however the standard model slightly violates this symmetry). Under the conserved vector current hypothesis (CVC), $g_V = 1$ (for the nucleon) and $g_{\mathrm{WM}} = \kappa_p - \kappa_n$, where κ_p and κ_n are the anomalous magnetic moments of the proton and neutron, and the pseudoscalar form factor has been calculated to be negligibly small as $q^2 \to 0$. The ratio λ can be measured via the lifetime of the neutron, and its angular correlation coefficients. The neutron lifetime depends

on both λ and V_{ud}, but the angular correlation coefficients, which parametrise the correlation between the spin of the neutron and the momentum of its decay products, is dependent on λ only to lowest order [112].

The most accurate measurement of g_A^{pn} is from the ultra cold neutron asymmetry collaboration (UCNA) [113]. They measured the energy dependent parameter $A(E)$ measured from the angular distribution of emitted electrons from decays of a polarized neutron ensemble via

$$W(E) \propto \frac{v}{c} \langle P \rangle A(E) \cos(\theta) \tag{4.4}$$

where P is the mean neutron polarization. The experiment was performed with electron energies over the range 220 to 670 keV. The leading order contribution to $A(E)$ is given by [113]

$$A_0 = \frac{-2(\lambda^2 - |\lambda|)}{1 + 3\lambda^2} \tag{4.5}$$

where $\lambda \equiv g_A/g_V$. To extract A_0 from the measured $A(E)$, recoil contributions and radiative corrections are calculated.

Where there is an energy dependence on the parameters $g_A(q^2)$ and $g_V(q^2)$ (it is the ratio g_A/g_V that is measured) they are assumed to have a dipole dependence on the energy. The $q^2 \to 0$ limit is then taken from a fit of

$$g(q^2) = g(0) \left(1 + 2\frac{q^2}{M^2}\right) \tag{4.6}$$

(and similarly for f) to the data [114]. The parameter M^2 is known as the axial mass and is determined by fitting to data for the nucleon axial form factor.

The current PDG value for g_A is based entirely on data from neutron experiments, and the individual results that make up the PDG world average are shown in table 4.2.

When considering the SU(3) axial coupling constants, it is important to realise that the values of g_V^{ij} are not all equal to one, so we must multiply the experimental ratios by the leading order SU(3) values of g_V^{ij}.

The non-nucleon axial coupling constants are extracted from measurements of the differential decay rate of the initial baryon [114].

For the decay $\Sigma^- \to \Lambda$ the value of $g_V^{\Sigma^-\Lambda}$ is 0 [1] and so the axial coupling constant is calculated from the experimental branching ratio $\Gamma(\Sigma^- \to \Lambda)/\Gamma(\Sigma^- \to$ everything).

The values of g_V for each axial coupling constant, up to second-order effects in SU(3) symmetry-breaking, are

$$\begin{array}{lll} g_V^{pn} = 1 & g_V^{\Lambda p} = -\sqrt{\frac{3}{2}} & g_V^{\Sigma^-\Lambda} = 0 \\ g_V^{\Sigma^- n} = 1 & g_V^{\Xi^-\Lambda} = \sqrt{\frac{3}{2}} & g_V^{\Xi^0\Sigma^+} = 1. \end{array} \tag{4.7}$$

g_A^{pn}/g_V^{pn}	Mendenhall [113]	1.2755(3)
	Mund [115]	$1.2748(8)^{+0.0010}_{-0.0011}$
	Schumann [116]	1.275(6)(15)
	Mostovoi [117]	1.2686(46)(7)
	Liaud [118]	1.266(4)
	Yerozolimsky [119]	1.2594(38)
	Bopp [120]	1.262(5)
	PDG [1]	1.2723(23)
$g_A^{\Lambda p}/g_V^{\Lambda p}$	Dworkin [121]	0.719(16)(12)
	Bourquin [122]	0.70(3)
	Wise [123]	0.734(31)
	PDG [1]	0.718(15)
$\sqrt{\frac{3}{2}}g_A^{\Sigma^-\Lambda}$	PDG [1]	0.698
$g_A^{\Sigma^- n}/g_V^{\Sigma^- n}$	Hsueh [124]	0.327(7)(19)
	Bourquin [122]	0.34(5)
	Tanenbaum [125]	0.385(37)
	PDG [1]	0.340(17)
$g_A^{\Xi^-\Lambda}/g_V^{\Xi^-\Lambda}$	Bourquin [122]	0.25(5)
$g_A^{\Xi^0\Sigma^+}/g_V^{\Xi^0\Sigma^+}$	Batley [126]	1.21(5)
	Alavi-Harati [127]	$1.32^{+0.21}_{-0.17}(5)$
	Bately [128]	1.20(4)(3)
	PDG [1]	1.22(5)

Table 4.2: Experimental results for axial coupling constants that make up the PDG world averages.

4.3 Effective Lagrangian

We use the lowest order baryon octet and decuplet Lagrangians shown in chapter 2. The baryon octet Lagrangian is given by

$$\mathcal{L}_B^{(1)} = \mathrm{Tr}(\bar{B}(i\not{D} - m_B)B) - \frac{D_0}{2}\mathrm{Tr}(\bar{B}\gamma^\mu\gamma_5\{u_\mu, B\}) - \frac{F_0}{2}\mathrm{Tr}(\bar{B}\gamma^\mu\gamma_5[u_\mu, B]) \quad (4.8)$$

with B the baryon field, m_B the baryon mass and Clebsch-Gordan coefficients D_0 and F_0. The baryon decuplet Lagrangian is

$$\begin{aligned}\mathcal{L}_T^{(1)} &= \bar{T}_\mu^{abc}(i\gamma^{\mu\nu\alpha}D_\alpha - m_T\gamma^{\mu\nu})T_\nu^{abc} + \frac{H}{m_T}\bar{T}_\mu^{abi}\gamma^{\mu\nu\rho\sigma}\gamma_5(\partial_\rho T_\nu^{abj})u_\sigma^{ij} \\ &+ \frac{C_A}{m_T}\varepsilon^{abc}(\partial_\alpha\bar{T}_\mu^{ade})\gamma^{\alpha\mu\nu}B^{ce}u_\nu^{bd}\end{aligned} \quad (4.9)$$

where T_μ^{abc} is the totally symmetric decuplet field shown in eq. (2.36) and m_T is the decuplet mass. The parameters H and C_A are not well known, so we have used the large N_C results $C_A = 2D_0$ and $H = 3D_0 - 9F_0$ [129].

Terms from the higher order Lagrangian (not including the decuplet) that are relevant for this work are [40]

$$\begin{aligned}\mathcal{L}_B^{(2)} &= b_1\mathrm{Tr}(\bar{B}[u^\mu,[u_\mu,B]]) + b_2\mathrm{Tr}(\bar{B}\{u^\mu,\{u_\mu,B\}\}) \\ &+ b_3\mathrm{Tr}(\bar{B}\{u^\mu,[u_\mu,B]\}) + b_4\mathrm{Tr}(\bar{B}B)\mathrm{Tr}(u^\mu u_\mu) \\ &+ ib_5\mathrm{Tr}\left(\bar{B}[u^\mu,[u^\nu,\gamma_\mu D_\nu B]] - \bar{B}\overleftarrow{D}_\nu[u^\nu,[u^\mu,\gamma_\mu B]]\right) \\ &+ ib_6\mathrm{Tr}\left(\bar{B}[u^\mu,\{u^\nu,\gamma_\mu D_\nu B\}] - \bar{B}\overleftarrow{D}_\nu\{u^\nu,[u^\mu,\gamma_\mu B]\}\right) \\ &+ ib_7\mathrm{Tr}\left(\bar{B}\{u^\mu,\{u^\nu,\gamma_\mu D_\nu B\}\} - \bar{B}\overleftarrow{D}_\nu\{u^\nu,\{u^\mu,\gamma_\mu B\}\}\right) \\ &+ id_1\mathrm{Tr}(\bar{B}\{[u^\mu,u^\nu],\sigma_{\mu\nu}B\}) + id_2\mathrm{Tr}(\bar{B}[[u^\mu,u^\nu],\sigma_{\mu\nu}B]) \\ &+ id_3\mathrm{Tr}(\bar{B}u^\mu)\mathrm{Tr}(u^\nu\sigma_{\mu\nu}B) + \cdots\end{aligned} \quad (4.10)$$

$$\begin{aligned}\mathcal{L}_B^{(3)} &= h_{38}\mathrm{Tr}(\bar{B}u^\mu\gamma_5\gamma_\mu B\chi_+) + h_{39}\mathrm{Tr}(\bar{B}\chi_+\gamma_5\gamma_\mu Bu^\mu) \\ &\quad + h_{40}\mathrm{Tr}(\bar{B}u^\mu\gamma_5\gamma_\mu B)\mathrm{Tr}(\chi_+) + h_{41}\mathrm{Tr}(\bar{B}\gamma_5\gamma_\mu Bu^\mu)\mathrm{Tr}(\chi_+) \\ &\quad + h_{43}\mathrm{Tr}(\bar{B}\gamma_5\gamma_\mu B\{u^\mu,\chi_+\}) + h_{44}\mathrm{Tr}(\bar{B}\{u^\mu,\chi_+\}\gamma_5\gamma_\mu B) + \cdots\end{aligned} \tag{4.11}$$

with $\chi_+ = u^\dagger\chi u^\dagger + u\chi^\dagger u$, $\chi = 2B_0\,\mathrm{diag}(m_u, m_d, m_s)$ and m_u, m_d, m_s being the up, down and strange quark mass respectively (we work in the isospin limit $m_u = m_d$). Values for the LECs b_{1-7} have been determined with and without decuplet contributions by Ren et al. [130] where they matched an EOMS ChPT expression for the baryon-octet masses to lattice and experimental data. The LECs h_{38-41}, $h_{43,44}$ and d_{1-3} are treated as free parameters we have varied to match the data.

For $\mathcal{O}(p^4)$ diagrams that have internal decuplet lines we use the Lagrangian of Lutz and Semke [131]

$$\begin{aligned}\mathcal{L}_T^{(2)} &= -\frac{1}{4}f_1\Big(\mathrm{Tr}\big((\bar{T}^\mu\cdot\gamma^\nu\gamma_5 B)\{u_\mu,u_\nu\}\big) + \mathrm{h.c.}\Big) \\ &\quad - \frac{1}{4}f_2\Big(\mathrm{Tr}\big((\bar{T}^\mu\cdot\gamma^\nu\gamma_5 B)[u_\mu,u_\nu]\big) + \mathrm{h.c.}\Big) \\ &\quad - \frac{1}{4}f_3\Big(\mathrm{Tr}\big((\bar{T}^\mu\cdot u_\nu)\gamma^\nu\gamma_5(u_\mu\cdot B) + (\bar{T}^\mu\cdot u_\mu)\gamma^\nu\gamma_5(u_\nu\cdot B)\big) + \mathrm{h.c.}\Big) \\ &\quad - \frac{1}{4}f_3\Big(\mathrm{Tr}\big((\bar{T}^\mu\cdot u_\nu)\gamma^\nu\gamma_5(u_\mu\cdot B) - (\bar{T}^\mu\cdot u_\mu)\gamma^\nu\gamma_5(u_\nu\cdot B)\big) + \mathrm{h.c.}\Big)\end{aligned} \tag{4.12}$$

where we have employed the compact dot notation used by Lutz and Semke [131] and suggested by Lutz and Kolomeitsev [132]

$$\begin{aligned}(\bar{T}^\mu\cdot A)^m_k &= \bar{T}^\mu_{ijk}A^i_l\varepsilon^{jlm} \\ (A\cdot T_\mu)^m_k &= T^{ijm}_\mu A^l_i\varepsilon_{jik}\end{aligned} \tag{4.13}$$

with A being either the meson or baryon octet matrix. The values of the LECs for the decuplet Lagrangian f_{1-4} have not been determined, although a large N_c analysis by Lutz and Semke [131] gives the constraint $f_1 = 0$.

For our SU(3) results, the full Lagrangian we have used is given by the sum

$\mathcal{L}_B^{(1)} + \mathcal{L}_B^{(2)} + \mathcal{L}_B^{(3)} + \mathcal{L}_T^{(1)} + \mathcal{L}_T^{(2)}$. For our SU(2) results, the relevant terms from the higher order Lagrangians are

$$\mathcal{L}_N^{(2)} = \frac{c_3}{2}\mathrm{Tr}(u_\mu u^\mu)\bar{\psi}\psi - \frac{c_4}{4}\bar{\psi}\gamma^\mu\gamma^\nu[u_\mu, u_\nu]\psi + \cdots \tag{4.14}$$

$$\mathcal{L}_N^{(3)} = \frac{d_{16}}{2}\bar{\psi}\gamma^\mu\gamma_5\mathrm{Tr}(\chi_+)u_\mu\psi + \cdots \tag{4.15}$$

We can express the unrenormalised axial coupling constant as

$$\begin{aligned} g_A^{ij} = T_{ij} + A_{ij} + \sum_\phi^{\pi K \eta} \left(B_T^\phi \alpha_{ij}^\phi + B_{L1}^\phi \beta_{ij}^\phi + B_{L2}^\phi \gamma_{ij}^\phi + D_{L1}^\phi \delta_{ij}^\phi + D_{L2}^\phi \varepsilon_{ij}^\phi \right) \\ + \sum_\phi^{\pi K \eta} \left(B_{L3}^\phi \rho_{ij}^\phi + B_{L4}^\phi \sigma_{ij}^\phi + B_{L5}^\phi \tau_{ij}^\phi \right). \end{aligned} \tag{4.16}$$

where B_i^ϕ and D_i^ϕ are loop integrals given in the appendix and the coefficients are also given in the appendix. We have multiplied the tree level term T_{ij} by

$$1 + \frac{1}{2}Z_i + \frac{1}{2}Z_j \tag{4.17}$$

where Z_i is calculated from the self energy of the initial state baryon and Z_j from the final baryon.

We have checked that all of the SU(3) EOMS results up to $\mathcal{O}(p^3)$ obtained in this chapter reproduce the analytic parts of heavy-baryon results that can be found in the literature (for example Borasoy [100]). Our SU(2) results up to $\mathcal{O}(p^4)$ also reproduce the analytic parts of expressions found in the literature. We have also checked that our $\mathcal{O}(p^3)$ results match a similar study performed by Ledwig et al. [133]. The SU(3) $\mathcal{O}(p^4)$ results with and without the decuplet are new, and so we cannot check them against existing results. However, the same software that was written to produce our $\mathcal{O}(p^3)$ results, a combination of FORM and Mathematica,

was also used to produce our new $\mathcal{O}(p^4)$ SU(3) results, giving us confidence that our new results are correct.

The LECs h_{40} and h_{41} in eq. (4.11) have a similar structure to the tree level LECs D_0 and F_0 in eq. (4.8). The LECs h_{40} and h_{41} that enter eq. (4.16) mirror the tree level terms. More explicitly, the LECs h_{40} and h_{41} can be absorbed into the coefficients D_0 and F_0 via

$$D_0 \to D_0' = D_0 + 2B_0(2m + m_s)(h_{40} + h_{41}) \tag{4.18}$$

$$F_0 \to F_0' = F_0 + 2B_0(2m + m_s)(h_{40} - h_{41}). \tag{4.19}$$

This transformation would introduce higher order terms into our expression (due to terms proportional to, e.g. D_0^3) which would be dropped in the heavy-baryon formulation (which, at order $\mathcal{O}(p^n)$ only includes terms up to M_ϕ^n), but which would remain in the EOMS formulation, (which, at order $\mathcal{O}(p^n)$ can include terms with a power greater than M_ϕ^n).

It is not possible to separate contributions from tree level terms and from h_{40} and h_{41} by only using data at the physical pion mass.

At leading order, a simple fit of D_0 and F_0 to the six experimental values of equation 4.2 gives a χ^2 of 4.5 with $D_0 = 0.80$ and $F_0 = 0.47$ (the leading order ChPT results are given in the appendix in equation B.18). This suggests that symmetry-breaking terms, which are not present at tree level, are not required to get a good fit to the experimental data. We might also expect to see this at higher orders.

In ChPT, the loop diagrams introduce SU(3) breaking terms as well as chiral symmetry-breaking terms. For HBChPT, a calculation to chiral order $\mathcal{O}(p^n)$ introduces symmetry-breaking terms (both SU(3) symmetry and chiral symmetry) up to order $\mathcal{O}(p^n)$. The introduction of symmetry-breaking terms proceeds order

by order.

For EOMS ChPT, the situation is different. EOMS ChPT loops still introduce symmetry-breaking terms, but in a less systematic way. A calculation to order $\mathcal{O}(p^n)$ introduces symmetry-breaking terms of order $\mathcal{O}(p^n)$ and higher, it includes a partial summation of higher order terms.

For a $\mathcal{O}(p^3)$ HB expression, ignoring the effects of logs, we can absorb the symmetry-breaking terms from the loops into the LECs h_{38-39} and h_{43-44} and the expressions for the axial coupling constants can be written in terms of the two SU(3) symmetry conserving terms D_0' and F_0' (which have absorbed h_{40-41}, see equation 4.19) and the four symmetry-breaking LECs h_{38-39} and h_{43-44}. Under these circumstances, the six experimental axial coupling constants shown in 4.2 and the two unmeasured coupling constants, $g_A^{\Sigma^+\Sigma^+}$ and $g_A^{\Xi^0\Xi^0}$, are not all independent, as they can be expressed in terms of six free parameters. We can write two unmeasured axial coupling constants in terms of the other six. It can be shown that

$$g_A^{\Sigma^+\Sigma^+} = 2g_A^{pn} + \sqrt{6}g_A^{\Lambda p} - \sqrt{6}g_A^{\Sigma^-\Lambda} - g_A^{\Sigma^- n} + 2g_A^{\Xi^0\Sigma^+} \tag{4.20}$$

$$g_A^{\Xi^0\Xi^0} = g_A^{pn} + \sqrt{\frac{3}{2}}g_A^{\Lambda p} - \sqrt{6}g_A^{\Sigma^-\Lambda} + \frac{1}{2}g_A^{\Sigma^- n} + \sqrt{\frac{3}{2}}g_A^{\Xi^-\Lambda} + \frac{1}{2}g_A^{\Xi^0\Sigma^+}. \tag{4.21}$$

A fit of the experimental data to the six free parameters shows that the symmetry-breaking terms are very small. We use this fact to justify our assumption that the symmetry-breaking terms for $g_A^{\Sigma^+\Sigma^+}$ and $g_A^{\Xi^0\Xi^0}$ are also small. Equations 4.20 and 4.21 are valid for HBChPT up to order $\mathcal{O}(p^3)$.

Using these equations, along with the experimental data shown in equation 4.2 we can predict "experimental" results at the physical pion mass for the ratios

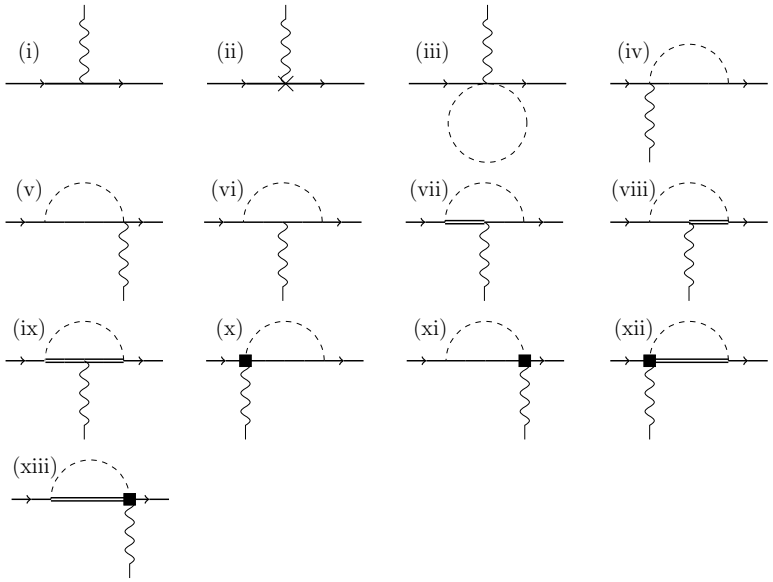

Figure 4.2: Diagrams contributing to the axial form factor up to order $\mathcal{O}(p^4)$. The the cross is a third-order vertex, the solid squares are second order vertices and all other vertices are from the lowest order Lagrangian. The dashed lines are pions, the solid lines are octet baryons, the double solid lines are decuplet baryons and the wavy lines are external axial sources.

$g_A^{\Sigma^+\Sigma^+}/g_A^{pn}$ and $g_A^{\Xi^0\Xi^0}/g_A^{pn}$. This gives us

$$g_A^{\Sigma^+\Sigma^+}/g_A^{pn} = 0.84(10) \tag{4.22}$$

$$g_A^{\Xi^0\Xi^0}/g_A^{pn} = -0.04(8) \tag{4.23}$$

where the errors were calculated using standard error propagation. We have included these two "data points" in our fits, to try to ensure that the behaviour of our expressions for $g_A^{\Sigma^+\Sigma^+}/g_A^{pn}$ and $g_A^{\Xi^0\Xi^0}/g_A^{pn}$ near the chiral limit respects the low level of SU(3) symmetry-breaking we might expect, based on the smallness of the symmetry-breaking terms mentioned above.

4.4 Fitting parameters

The combination of third-order LECs that contribute to g_A is shown in equations B.19 to B.26. Although the LECs from the third-order Lagrangian are not known with any certainty, it is possible to uniquely constrain them using a combination of experimental and lattice data. We have explicitly separated the terms into SU(3) symmetry-conserving terms proportional to $2m + m_s$ and symmetry-breaking terms proportional to $m - m_s$.

We have fixed the second order LECs b_{1-7}, which enter through loop diagrams, to the values given by Ren et al. [130]. Ren et al. determined the values of the LECs by fitting an EOMS ChPT expression for the baryon octet masses to lattice and experimental data. The values of the LECs with and without decuplet contributions are shown in table 4.3. There are values for the LECs b_{1-7} and d_{1-3} without decuplet contributions, from Mai and Meissner [55], however when using these parameters we found that the contributions from the $\mathcal{O}(p^4)$ terms was very large and would dominate our expression. We have allowed d_{1-3} to vary.

It is not surprising that the $\mathcal{O}(p^4)$ terms are large, in the SU(2) sector the M_π^3 term is given by

$$-\frac{g_A}{6\pi F^2}(c_3 - 2c_4)M_\pi^3 \approx 90 M_\pi^3 \tag{4.24}$$

where we have taken $c_3 - 2c_4 = -11.7\ \text{GeV}^{-1}$ (from Bernard [37]), $F = 0.094$ GeV and $g_A = 1.27$. If the SU(3) coefficients for M_K and M_η were close to this value it would appear that the expansion of g_A may not converge well until much higher order.

For the SU(2) LECs generated by our $\mathcal{O}(p^4)$ diagrams, c_3 and c_4, we used the values established by Bernard [37]. When including the decuplet we lowered the values of c_3 and c_4 in the same manner as McGovern et al. [134]. These values are also shown in table 4.3.

For the remaining parameters, we have allowed the SU(3) Clebsch Gordon coefficients, D_0 and F_0 to vary. We have set the decuplet-octet-meson coupling to be $C_A = 2D_0$ and the decuplet-decuplet-meson coupling to be $H = 3D_0 - 9F_0$ based on large N_c QCD [129]. We have set F_π at its value at the physical pion mass of 0.0924 GeV, and we have also used a single mass for the baryon decuplet of 1.2 GeV and a single mass for the baryon octet of 0.94 GeV. For our SU(2) fits we have set $C_A = 1.125(1.4)$ for the EOMS (HB) fit [107] and set $H = 9g_0/5$. These values are shown in table 4.4.

To briefly summarise: for our SU(2) expression we allow g_0 and d_{16} to vary and fit to lattice data for g_A^{pn} together with the experimental data point. For our SU(3) expression we allow D_0, F_0, h_{38-41}, h_{43}, h_{44} (and d_{1-3} in our $\mathcal{O}(p^4)$ fits) to vary and fit to lattice data for g_A^{pn}, $g_A^{\Sigma^+\Sigma^+}$, $g_A^{\Xi^0\Xi^0}$ and the six experimental data points shown in equation 4.2. We have not constrained our fits to pass through the experimental data point for g_A^{pn}, however the fact that the experimental error bar is so small ensures that our fits will automatically favour the experimental value.

To include K and η loops with varying M_π, we have used the lowest order mass relationship between the meson octet to write the K and η mass in terms of the pion mass,

$$M_K^2 = \frac{M_\pi^2}{2} + B_0 m_s, \quad M_\eta^2 = \frac{M_\pi^2}{3} + \frac{4}{3} B_0 m_s \tag{4.25}$$

where we have set $B_0 m_s = 0.23$ GeV^2, so that at $M_\pi = 0.14$ GeV we have $M_K = 0.49$ GeV and $M_\eta = 0.56$ GeV. The final SU(3) expression for g_A will have terms that are independent of the pion mass. This means that in the $M_\pi \to 0$ limit, there will be a contribution to g_A from K and η loops, as well as from the third-order LECs h_i multiplied by $B_0 m$ and $B_0 m_s$.

When fitting the parameters to the available data, it is important to ensure they are of natural order. A standard least-squares fit, based on minimizing the

function

$$\chi^2 = \sum_i \left(\frac{\text{expt}_i - \text{theory}_i}{\text{error}_i} \right)^2 , \tag{4.26}$$

does not take into account any prior information that is known about the parameters. Schindler & Phillips [135] have investigated using Bayesian analysis to estimate parameters. They point out some flaws with the standard least-squares approach. Firstly, it asks the question "given this theory and parameter set, is the data matched well" rather than "given the data, is this theory and parameter set a good match". Secondly, it does not allow you to easily include any information you may know about the parameters. And thirdly, the least-squares approach assumes a single functional form for the theoretical expression. To fix these flaws, Schindler & Phillips suggest using a fitting method based on Bayesian statistics.

We are most concerned with the second point, as using a standard least-squares fit many of our parameters took on unphysical values.

For our SU(2) fits we used an augmented χ^2 [135] to ensure the parameters were not unrealistically large

$$\chi^2_{\text{aug}} = \chi^2 + \chi^2_{\text{prior}} \tag{4.27}$$

with

$$\chi^2_{\text{prior}} = \sum_{i=0}^{n} \frac{a_i^2}{R_i^2} \tag{4.28}$$

for n free parameters where a_i is the parameter we are fitting and R_i represents the constraint of naturalness. With this method we can limit the values of the free parameters without imposing any boundaries on the area of phase space the χ^2 function can explore. For g_0 we have used a value of R of 1, and for the remaining SU(2) LEC we have used $R = 10$.

When performing our SU(3) fits, we found that the augmented χ^2 alone did

	SU(3)							SU(2)	
	b_1	b_2	b_3	b_4	b_5	b_6	b_7	c_3	c_4
$\not\Delta$	0.55	−0.71	−0.67	−0.84	−0.56	0.16	1.98	−4.7	3.5
Δ	1.01	0.43	−1.83	−1.57	−0.36	−0.42	2.79	−1.6	0.4

Table 4.3: Values of the SU(3) and SU(2) LECs from $\mathcal{L}^{(2)}$. Units are all GeV^{-1}. The SU(3) LECs b_{1-7} are taken from Ren et al. [130] and the SU(2) LECs are taken from Bernard [37]. When including the decuplet we have lowered the SU(2) LECs in the same manner outlined by McGovern et al. [134].

Parameter	Value
C_A	$1.4/1.125/2D_0$
F	0.0924 GeV
M_N	0.94 GeV
M_Δ	1.2 GeV
$B_0 m_S$	0.23 GeV^2
b_{1-7}, $c_{3,4}$	fixed, see table 4.3
D_0, F_0	allowed to vary
g_0	allowed to vary
h_i, d_i	allowed to vary

Table 4.4: Table showing values given to parameters that were held constant and the parameters that were allowed to vary throughout this work.

not prevent the parameters taking unrealistic values. In particular we found that higher order terms would often dominate over the leading order terms. To mitigate this we included a term in our χ^2 function proportional to the ratio of the leading order and higher order terms. More explicitly, we alter our χ^2 function by

$$\chi^2 \to \chi^2 + \left(\frac{g^{ij}_{\text{loop}}}{g^{ij}_{\text{tree}}} \right)^2 \tag{4.29}$$

for each of the eight axial coupling constants we studied (the six experimental values and the lattice data for $g_A^{\Sigma^+\Sigma^+}$ and $g_A^{\Xi^0\Xi^0}$).

4.5 Fits to lattice and experimental data

We show results for our calculation with and without decuplet contributions, and for each case both with and without contributions from K and η loops (SU(2) and SU(3) fits). We also explicitly show the effect of excluding $\mathcal{O}(p^4)$ terms. There are a large number of free parameters at order $\mathcal{O}(p^4)$. We found that the $\mathcal{O}(p^4)$ baryon octet loop contributions are potentially large, whilst the $\mathcal{O}(p^4)$ baryon decuplet loop contributions are rather small, and are very small compared to the octet loop contributions. Assuming that the LECs f_{1-4} are of natural order, we found that the $\mathcal{O}(p^4)$ decuplet contribution to the axial form factor is of the order 1%. Due to the small size of the decuplet contributions at $\mathcal{O}(p^4)$ we have set the LECs $f_{1-4} = 0$ to reduce the number of free parameters.

4.5.1 SU(2) fits

The SU(2) fits at $\mathcal{O}(p^3)$ with and without the decuplet are all quite similar, and do not match the lattice data well (figure 4.3, red dashed line). They do not pass through the well known experimental value at the physical pion mass (none of our fits were constrained to pass through the experimental value).

At $\mathcal{O}(p^4)$ the fit to the data is generally improved and we can see a notable difference in the fits without and with the decuplet (black solid line in the top row and bottom row of figure 4.3 respectively). Without the decuplet, we see that g_A varies considerably with the pion mass, and although the EOMS fit has a low χ^2, the parameters g_0 and d_{16} are rather large. The $\mathcal{O}(p^4)$ HB without decuplet fit to the lattice data however is very poor. The new LECs entering at $\mathcal{O}(p^4)$ are matched to pion nucleon scattering data [136] and so we cannot vary them to optimise our fit. The inability of SU(2) HBChPT (without decuplet contributions) to fit lattice data has been noted previously [107], and we have confirmed that including $\mathcal{O}(p^4)$

terms does not help.

Including the decuplet explicitly (figure 4.3, bottom row) we see that g_A varies much less with the pion mass. At $\mathcal{O}(p^4)$ with the decuplet included, we get much lower values of the LEC d_{16} compared to our expression without an explicit decuplet. Bernard [37] predicted that d_{16} should lie in the range $-3.4 \leqslant d_{16} \leqslant -0.92$ based on a fit to $\pi N \to \pi\pi N$ data (without decuplet contributions). Our best SU(2) fit (HB at $\mathcal{O}(p^4)$ with decuplet) has a value of d_{16} that is outside this range.

The two data points with the lowest pion mass from Green et al. [105] and Pleiter et al. [103] are not compatible with the experimental point, however removing them does not significantly alter any of our fits, so we have not excluded them from our fits.

The parameters used to achieve the fit shown in figure 4.3 are shown in table 4.5. To calculate the errors on our fitting parameters we increased the value of each parameter from its best fit value until the χ^2 value became greater than $\chi^2_{\text{min}} + 1$. The best fit was for the $\mathcal{O}(p^4)$ results with decuplet contributions, and we can see that going from $\mathcal{O}(p^3)$ to $\mathcal{O}(p^4)$ increases the values of the LECs in every case, although for the $\mathcal{O}(p^4)$ EOMS results the value of d_{16} is not abnormally large. We cannot match the lattice data below $M_\pi \sim 0.25$ GeV with the exception of the lowest data point from Horsley et al. [86], although we do not match the data from Horsley et al. [86] at larger pion masses.

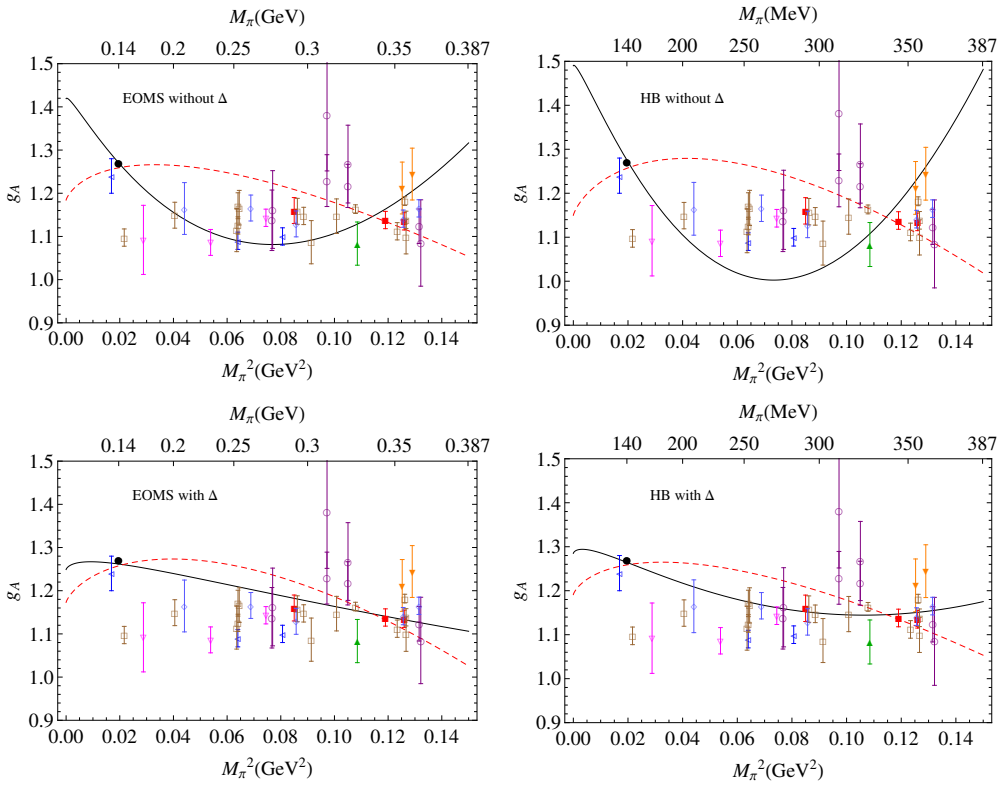

Figure 4.3: SU(2) result for g_A^{pn} without (top) and with (bottom) Δ contributions matched to lattice QCD data. Results are plotted against the squared pion mass. The left plot shows the relativistic fit and the right plot shows the heavy-baryon fit. The black solid line is the fit at $\mathcal{O}(p^4)$ and the red dashed line is the fit at $\mathcal{O}(p^3)$. The meaning of the symbols can be found in table 4.1.

		g_0	d_{16} GeV^{-2}	χ^2
$\not\Delta$	EOMS $\mathcal{O}(p^3)$	1.18(2)	−1.28(11)	400/38
	EOMS $\mathcal{O}(p^4)$	1.42(2)	−8.11(60)	217/38
	HB $\mathcal{O}(p^3)$	1.15(2)	−0.33(9)	520/38
	HB $\mathcal{O}(p^4)$	1.49(2)	−9.34(24)	606/38
Δ	EOMS $\mathcal{O}(p^3)$	1.17(2)	0.57(9)	480/38
	EOMS $\mathcal{O}(p^4)$	1.25(2)	−1.46(45)	253/38
	HB $\mathcal{O}(p^3)$	1.19(2)	−1.87(10)	396/38
	HB $\mathcal{O}(p^4)$	1.28(3)	−4.30(67)	162/38

Table 4.5: Results of SU(2) fit. The parameters that were not varied are shown in tables 4.3 and 4.4, and the match to lattice data is shown in figure 4.3. Errors were calculating by finding the minimum value of the parameter that would yield $\chi^2 > \chi^2_{\text{min}} + 1$.

4.5.2 SU(3) fits

For our SU(3) fits we have only used lattice data with $N_f = 2 + 1$ from Edwards et al. [101], Yamazaki et al. [102] and Bratt et al. [93]. The plots in this section are shown with lattice data from these groups only.

To calculate the errors on our fitting parameters we increased the value of each parameter from its best fit value until the χ^2 value became greater than $\chi^2_{\text{min}} + 1$, as we did in the previous section.

We match to more data with our SU(3) fits. We fit to the six experimental data points shown in equation 4.2, the lattice data for g_A^{pn} with pion mass $M_\pi^2 < 0.15$ shown in the right hand side of figure 4.1 and lattice data for $g_A^{\Sigma^+\Sigma^+}$ and $g_A^{\Xi^0\Xi^0}$.

Our $\mathcal{O}(p^3)$ fits to g_A^{pn} all have a positive gradient at the physical point and do not pass through the majority of the lattice data points (figure 4.4 red dashed lines, top row without decuplet, bottom row with decuplet). This is similar to our SU(2) fits without the decuplet (figure 4.3). The $\mathcal{O}(p^3)$ fits to the ratios g^Σ/g^N and g^Ξ/g^N show very little dependence on the pion mass, see figure 4.5.

Our $\mathcal{O}(p^4)$ fits all show an improved fit to the lattice data for g_A^{pn} (figure 4.4, solid lines). Our fits to the lattice data for the ratios g^Σ/g^N and g^Ξ/g^N, shown in figure 4.5, show more dependence on the pion mass than the $\mathcal{O}(p^3)$ fits. The heavy-baryon $\mathcal{O}(p^4)$ fits have unphysically large values for the LECs d_{1-3}, and the total contribution from $\mathcal{O}(p^4)$ terms is large. The $\mathcal{O}(p^4)$ fits are substantially different to the $\mathcal{O}(p^3)$ fits at the physical pion mass for all of our results.

Comparing our $\mathcal{O}(p^4)$ EOMS results with and without decuplet contributions we can see that the χ^2 value is lower without the decuplet (table 4.6). The fits to the lattice data are quite similar for these two results (solid black line, upper left and lower left plots in figures 4.4 and 4.5); the difference in the χ^2 values is due an improved match to the experimental data when the decuplet is not included, see table 4.8. It is interesting to note in particular the results for g_A^{pn} and $g_A^{\Xi^0\Sigma^+}$.

The experimental values are very close, suggesting that symmetry-breaking terms are small, but we see that our EOMS $\mathcal{O}(p^4)$ results have $g_A^{\Xi^0\Sigma^+}$ more than 10% lower than g_A^{pn}, suggesting that to match the lattice data for g_A^{pn} we have had to introduce large symmetry-breaking terms.

With all of our fits there are large cancellations between third-order tree contributions and loop contributions at the matching scale of m_N.

We match the six experimental axial couplings well without the decuplet, and slightly worse when it is included (see table 4.8). However, this better fit relies on large cancellations that are possible because we have allowed the LECs d_{1-3} to vary. The χ^2 for the $\mathcal{O}(p^4)$ EOMS fit without decuplet is substantially lower than the other fits.

Recently, a similar study of g_A was performed by Ledwig et al. [133]. They looked at axial charges up to order $\mathcal{O}(p^3)$ both with and without decuplet contributions. They used a small amount of lattice data, which consisted of a single data point for g_A^{pn} [109] and the ratio data for g_A^{Ξ}/g_A^N and g_A^{Σ}/g_A^N [108] that we have also used, along with experimental data to uniquely constrain the LECs h_{38-41} and $h_{42,43}$, and they found that a good match could be achieved both with and without decuplet corrections. They also saw that there were large cancellations between loop terms and counter terms which are decreased by the inclusion of the decuplet. However, the running of g_A^{pn} with M_π that they predict does not agree with the vast majority of lattice data.

We agree with these conclusions, however we have included more lattice data for g_A and have found that a good match at $\mathcal{O}(p^3)$ is not possible; the lattice data for g_A does not show the same dependence on M_π as predicted by ChPT at this order. Including $\mathcal{O}(p^4)$ terms does allow for a good fit, but the good fit is only possible due to cancellations between large terms from the $\mathcal{O}(p^3)$ and $\mathcal{O}(p^4)$ loop diagrams. The large terms at order $\mathcal{O}(p^3)$ and $\mathcal{O}(p^4)$ were present even with

the augmented χ^2 explicitly suppressing them, as mentioned in section 4.4 (see equation 4.29).

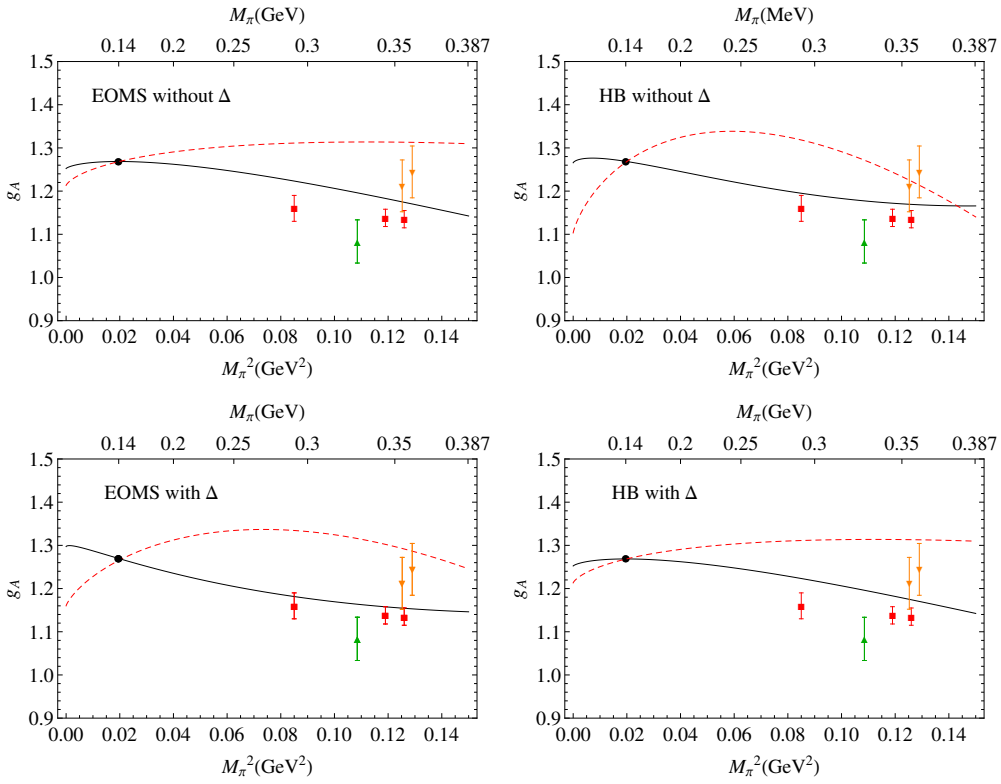

Figure 4.4: SU(3) result for g_A^{pn} without (top) and with (bottom) decuplet contributions matched to lattice QCD data. Results are plotted against the squared pion mass. The left plot shows the relativistic fit and the right plot shows the heavy-baryon fit. The black solid line is the fit at $\mathcal{O}(p^4)$ and the red dashed line is the fit at $\mathcal{O}(p^3)$. The meaning of the symbols can be found in table 4.1.

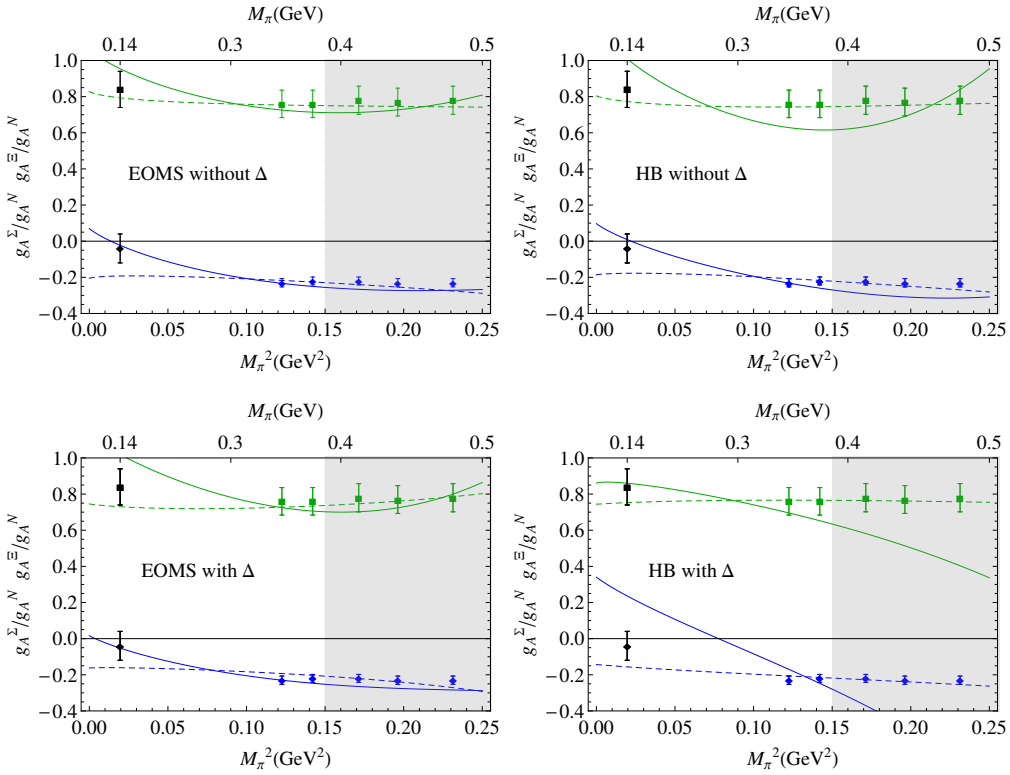

Figure 4.5: SU(3) result for g_A^Ξ/g_A^N and g_A^Σ/g_A^N without (top) and with (bottom) decuplet contributions to lattice QCD data. The solid line shows the $\mathcal{O}(p^4)$ fit (green for g_A^Ξ/g_A^N and blue for g_A^Σ/g_A^N), and the dashed line shows the $\mathcal{O}(p^3)$ fit. We have not included data within the shaded region in our fits. The solid black data points at the physical pion mass are the predicted values based on the available experimental data (see section 4.3 equations 4.20 to 4.23).

	$\not\Delta$		Δ	
	$\mathcal{O}(p^3)$	$\mathcal{O}(p^4)$	$\mathcal{O}(p^3)$	$\mathcal{O}(p^4)$
D_0	0.75 (22)	0.66 (7)	0.64 (7)	0.65 (9)
F_0	0.53 (14)	0.44 (7)	0.46 (7)	0.43 (6)
h_{38} [GeV^{-2}]	0.13 (05)	−0.22 (36)	−0.79 (31)	−0.94 (50)
h_{39} [GeV^{-2}]	0.03 (09)	−1.09 (29)	0.30 (13)	−0.69 (28)
h_{40} [GeV^{-2}]	−0.50 (24)	0.10 (26)	0.90 (27)	0.52 (40)
h_{41} [GeV^{-2}]	−0.04 (08)	0.05 (20)	−0.28 (13)	−0.45 (21)
h_{43} [GeV^{-2}]	0.06 (09)	0.81 (34)	0.37 (14)	1.28 (39)
h_{44} [GeV^{-2}]	−0.18 (05)	−1.30 (61)	0.03 (05)	−1.42 (57)
d_1 [GeV^{-1}]	n/a	−3.70 (94)	n/a	−3.10 (1.00)
d_2 [GeV^{-1}]	n/a	3.48 (1.13)	n/a	3.72 (1.12)
d_3 [GeV^{-1}]	n/a	2.25 (1.71)	n/a	5.11 (1.91)
χ^2/dof	39/10	55/7	202/10	106/40

Table 4.6: Parameters used to fit EOMS SU(3) results to lattice and experimental data. We established the errors by increasing each parameter from its best fit value until the χ^2 value became greater than $\chi^2_{\rm min} + 1$.

	$\not\Delta$		Δ	
	$\mathcal{O}(p^3)$	$\mathcal{O}(p^4)$	$\mathcal{O}(p^3)$	$\mathcal{O}(p^4)$
D_0	0.72(7)	0.56(7)	0.62(7)	0.19(10)
F_0	0.54(8)	0.41(7)	0.40(5)	0.50(33)
h_{38}[GeV^{-2}]	−0.04(7)	−0.75(10)	0.70(15)	−0.75(1.70)
h_{39}[GeV^{-2}]	0.07(7)	−0.53(31)	−0.16(09)	−2.30(75)
h_{40}[GeV^{-2}]	0.00(6)	0.23(28)	−0.77(25)	1.17(4.80)
h_{41}[GeV^{-2}]	0.02(7)	0.14(18)	0.00(8)	1.97(1.00)
h_{43}[GeV^{-2}]	0.09(7)	1.33(38)	0.09(11)	−0.47(1.21)
h_{44}[GeV^{-2}]	0.12(5)	−1.51(70)	−0.02(13)	−1.17(27)
d_1 [GeV^{-1}]	n/a	−7.33(99)	n/a	1.33(31)
d_2 [GeV^{-1}]	n/a	6.55(1.54)	n/a	−3.04(2.23)
d_3 [GeV^{-1}]	n/a	2.19(1.67)	n/a	10.13(5.70)
χ^2/dof	120/10	140/7	65/10	252/7

Table 4.7: Parameters used to fit HB SU(3) results to lattice and experimental data. Errors calculated using the same method for the data in table 4.6.

		$p \to n$	$\Lambda \to p$	$\Sigma^- \to \Lambda$	$\Sigma^- \to n$	$\Lambda \to \Xi^-$	$\Xi^0 \to \Sigma^+$
	expt	1.2725(23)	−0.879(18)	0.570(27)	0.340(17)	0.306(61)	1.21(5)
$\not\Delta$	$\mathcal{O}(p^3)$	1.224	−0.822	0.567	0.322	0.149	1.126
	$\mathcal{O}(p^4)$	1.270	−0.893	0.552	0.341	0.460	1.047
Δ	$\mathcal{O}(p^3)$	1.268	−0.884	0.589	0.341	0.254	1.185
	$\mathcal{O}(p^4)$	1.269	−0.867	0.375	0.357	0.780	0.929

Table 4.8: Match to experimental results using EOMS.

		$p \to n$	$\Lambda \to p$	$\Sigma^- \to \Lambda$	$\Sigma^- \to n$	$\Lambda \to \Xi^-$	$\Xi^0 \to \Sigma^+$
	expt	1.2725(23)	−0.879(18)	0.570(27)	0.340(17)	0.306(61)	1.21(5)
$\not\Delta$	$\mathcal{O}(p^3)$	1.267	−0.850	0.553	0.309	0.122	1.115
	$\mathcal{O}(p^4)$	1.268	−0.898	0.540	0.345	0.545	0.884
Δ	$\mathcal{O}(p^3)$	1.267	−0.881	0.588	0.337	0.253	1.177
	$\mathcal{O}(p^4)$	1.267	−0.864	0.363	0.359	0.775	0.964

Table 4.9: Match to experimental results using HB.

4.6 Fits excluding the lattice data

We mentioned in section 4.3 that the LECs h_{40} and h_{41} and the tree level coefficients D_0 and F_0 enter our expressions in a similar fashion. We also showed an appropriate transformation that would eliminate h_{40} and h_{41} at the cost of introducing terms of chiral order greater than $\mathcal{O}(p^3)$ (in the heavy-baryon limit these terms can be ignored entirely). The fact that these LECs can be absorbed into tree level terms is why we require lattice data at varying pion mass to uniquely determine them. In the EOMS scheme, where a calculation to order $\mathcal{O}(p^n)$ contains terms with a power greater than M_ϕ^n, a transformation absorbing the LECs h_{40} and h_{41} will result in a different expression due to the higher order terms. We can therefore study how varying these two LECs impacts our fit to the experimental data without using the lattice data to constrain any parameters. We can then see how well this fit matches the available lattice data.

As there are eight free parameters up to $\mathcal{O}(p^3)$ we can fix h_{40} and h_{41} at various values and calculate the best fit to the experimental data based on the remaining parameters. Up to $\mathcal{O}(p^4)$ there are additional LECs that are not determined, d_{1-3}. We fixed these parameters to the values from the full fit, given in table 4.6, where we included the extra lattice data. To fit the parameters to the experimental data we included in our χ^2 a term proportional to the ratio of the loop contributions to the tree contributions, as we did with our previous SU(3) fits (see the end of section 4.4 for discussion of our fitting method).

We calculated the χ^2 value at different values of h_{40} and h_{41} and plotted contours of constant χ^2 at values of $\chi^2_{\text{min}} + n$ with $n = 1, \cdots, 8$. The graphs can be seen in figure 4.6. We also show on the graph the values of h_{40} and h_{41} given in table 4.6 using a red dot. The parameters that gave us the best fit are shown in table 4.10.

With no decuplet, as h_{40} decreases the χ^2 increases fairly slowly. We can see

that changing h_{41} has a larger impact on the fit. It appears that the two parameters are largely uncorrelated. When we perform a fit (without the decuplet) including the lattice data, the values of h_{40} and h_{41} do not stray too far from the best fit position.

With the decuplet there is more correlation between the two parameters, where a larger value of h_{40} can be compensated for by lowering h_{41}. We also see that including the lattice data moves the values of h_{40} and h_{41} away from the optimal region in the plot.

We have shown in figure 4.7 how well the fits without the lattice data can match the lattice data, where we have plotted the variation with M_π using the best fit values for h_{40} and h_{41}. We have shown both $N_f = 2$ and $N_f = 2 + 1$ lattice data in the plots, although we have not used the data in our fits. The parameters used are shown in table 4.10. The $\mathcal{O}(p^3)$ fits match the lattice data poorly, however the $\mathcal{O}(p^4)$ fit without decuplet contributions matches the lattice data surprisingly well. In all cases the lattice data for the ratios g_A^Σ/g_A^N and g_A^Ξ/g_A^N is not well described.

	$\not{\Delta}$		Δ	
	$\mathcal{O}(p^3)$	$\mathcal{O}(p^4)$	$\mathcal{O}(p^3)$	$\mathcal{O}(p^4)$
D_0	0.78(14)	0.78 (18)	0.80 (12)	0.80 (12)
F_0	0.48(8)	0.46 (12)	0.49 (9)	0.49 (09)
h_{38} [GeV^{-2}]	0.13(8)	−0.16 (20)	−1.40 (75)	−1.64 (86)
h_{39} [GeV^{-2}]	−0.10(7)	−1.15 (29)	0.28 (20)	−0.47 (9)
h_{40} [GeV^{-2}]	−0.45(35)	−0.20 (30)	1.50 (90)	1.00 (70)
h_{41} [GeV^{-2}]	−0.10(8)	0.05 (8)	−0.35 (19)	−0.70 (20)
h_{43} [GeV^{-2}]	0.05(6)	1.13 (35)	0.42 (25)	1.82 (48)
h_{44} [GeV^{-2}]	−0.18(5)	−1.82 (44)	0.15 (15)	−1.90 (21)
d_1 [GeV^{-1}]	n/a	−3.40	n/a	−2.88
d_2 [GeV^{-1}]	n/a	3.96	n/a	4.03
d_3 [GeV^{-1}]	n/a	2.40	n/a	5.30

Table 4.10: Parameters used to fit EOMS SU(3) results to experimental data only. As there were six free parameters and six data points, the χ^2 value was very small.

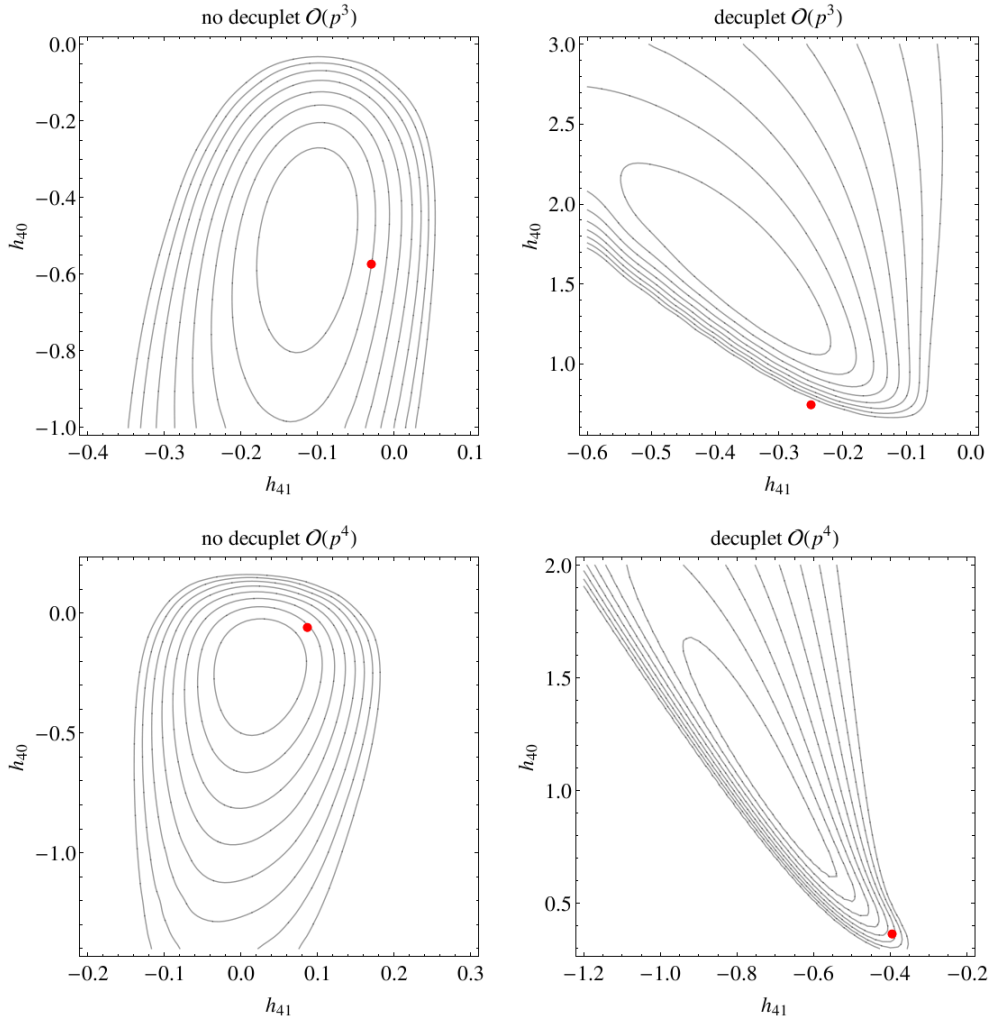

Figure 4.6: Contours of constant χ^2 for fits to the experimental data only. The results are with EOMS ChPT only. The parameters h_{40} and h_{41} were fixed at several different values and a χ^2 fit was performed on the remaining parameters. The red dot shows the value of h_{40} and h_{41} achieved when fitting to the entire set of data (from table 4.6). The contours show $\chi^2_{\rm min} + n$ with $n = 1, \cdots, 8$.

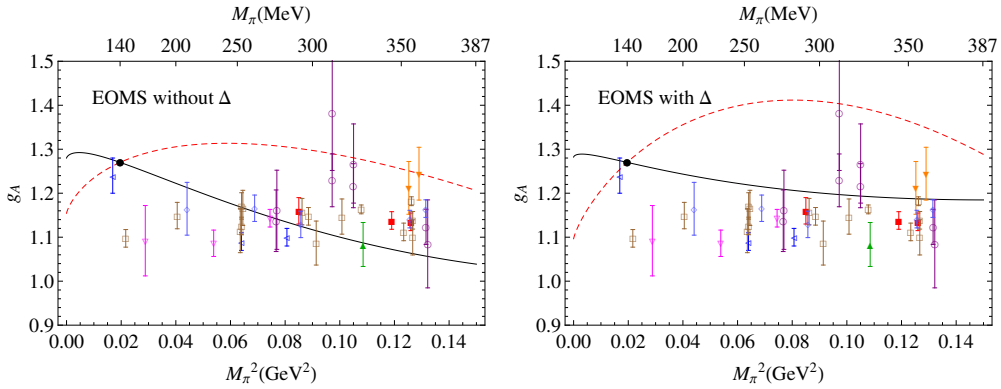

Figure 4.7: Variation of g_A^{pn} with M_π^2 when no lattice data is used in the fit. The black solid line is the fit at $\mathcal{O}(p^4)$ and the red dashed line is the fit at $\mathcal{O}(p^3)$. The meaning of the symbols can be found in table 4.1

4.7 Conclusions

We have collected lattice data on the axial coupling constant g_A from various collaborations, and have calculated an SU(3) expression up to order $\mathcal{O}(p^4)$ in the framework of EOMS ChPT with decuplet contributions, and have fit any free parameters to a combination of lattice data and experimental data. We have also used our expression to derive the corresponding heavy-baryon result by expanding in powers of $1/m_N$, and have looked at the SU(2) flavour limit (for both the HB and EOMS frameworks) by taking the strange quark mass to infinity.

We found that the relativistic and heavy-baryon SU(2) expressions with no decuplet contributions could not fit both the experimental value of the axial coupling constant and the lattice data below $M_\pi^2 = 0.15$ GeV^2. Including the decuplet has, in previous work [107], given a much improved fit to both the lattice and experimental data. When we include the decuplet explicitly we see much less variation in g_A^{pn} with pion mass. If we perform a chiral extrapolation, all of our SU(2) expressions predict a value of $g_A \sim 1.05 - 1.1$ at the physical pion mass.

For our SU(3) results, our $\mathcal{O}(p^4)$ calculation was only a partial calculation as we did not account for the difference in the masses of the baryon octet. Our SU(3) $\mathcal{O}(p^4)$ EOMS fit with no decuplet gave our best fit, although this was mainly due to large cancellations between higher order terms. This was made possible by having the LECs d_{1-3} as free parameters. The presence of large cancellations was a feature in all of our fits, and shows that the perturbative series for the axial coupling constant contains large contributions at $\mathcal{O}(p^4)$. The convergence of SU(3) ChPT is a concern due to the large masses of the K and η particles, and it appears that for the axial coupling constant the perturbative series is not converging well at $\mathcal{O}(p^4)$. Including the decuplet resulted in a comparable, but slightly worse fit at $\mathcal{O}(p^4)$ than when it is omitted. Our decuplet fit was sensitive to the parameter C_A, with lower values ($C_A < 0.2$) yielding a better χ^2 than more realistic values.

We also performed a fit using only the experimental data. Calculating the best fit for various values of h_{40} and h_{41} we found that the parameters could match the lattice data quite well at $\mathcal{O}(p^4)$ without the decuplet. The resulting fit to the lattice data for the ratios g^{Σ}/g^{N} and g^{Ξ}/g^{N} were very poor.

Ledwig et al [133] have performed a similar study of the axial form factor, but up to $\mathcal{O}(p^3)$ and with much less lattice data used to constrain the free parameters. They found that a good fit could be achieved both with and without the decuplet, and while they also saw moderate cancellations between terms at higher order, the magnitude of the cancellations was not as large as we have found when including more lattice data. The running of g_A^{pn} with M_π that is predicted by Ledwig et al. [133] does not match the vast majority of available lattice data.

It appears that the available lattice data for the axial coupling of the nucleon does not agree well with three-flavour ChPT up to $\mathcal{O}(p^4)$. The lattice data for g_A^{pn} does not lend itself to being easily modelled using ChPT.

Chapter 5

Proton decay

The proton is observed to be an extremely stable particle. It is the lightest baryon, and its decay would violate baryon-number conservation. In the standard model, baryon-number violation is allowed only through non-perturbative effects, although the lifetime of the proton due to non-perturbative effects alone is incredibly long.

Experimentally, baryon number violation and $B - L$ violation, which are both conserved to all orders perturbatively in the standard-model, have never been detected. Results from the Super-Kamiokande experiment tell us that, if the proton is unstable, it must have a lifetime greater than 3.6×10^{31} years at a confidence level of 90% [137]. There are proposals for more sensitive experiments that seek to provide better constraints on the proton lifetime [138]. We shall briefly mention some of these proposals in section 5.1.

The standard model currently explains particle interactions in terms of three coupling constants. It was suggested by Georgi and Glashow [139] that at high enough energies, the forces we observe could be unified into a single gauge group. Theories based on the idea of the unification of forces are known as Grand Unified Theories (GUTs). There are many candidate GUTs, and a common feature is

that they predict the proton should not be stable; evidence of proton decay would strongly validate unification. Experimental data on proton decay can be used to rule out GUTs that predict shorter proton lifetimes. For example, the simplest GUT, minimal non-supersymmetric SU(5), has been ruled out because it predicts a proton lifetime that is too short [138]. We shall discuss GUTs in slightly more detail in section 5.2.

It is possible to add to the standard-model Lagrangian higher dimension operators that are suppressed by inverse powers of some large energy scale that do allow for perturbative proton decay. The lowest dimension operators that obey all the standard model local gauge symmetries and allow for proton decay are dimension six, and have been known for some time [140, 141] (we shall show the operators in a later section) . These operators conserve the difference between baryon and lepton number $(B - L)$.

The first calculations of proton decay using chiral perturbation theory were performed by Claudson, Wise and Hall [142]. They deduced a chiral Lagrangian that allowed proton decay based on previously known quark-level operators and then proceeded to calculate certain branching ratios for proton decay. The work of Claudson et al. [142] was done several years before a systematic method of power counting involving baryons was devised, and so their results were tree level. Current calculations using EOMS ChPT are routinely performed to at least the one-loop level.

It is accepted that two-flavour ChPT should converge well due to the ratio of the light pion mass to the chiral-symmetry-breaking scale providing an expansion parameter of the order $M_\pi/\Lambda \sim 0.1$. When we move to three flavours and include the kaon and η, we introduce the additional expansion parameters $M_K/\Lambda \sim M_\eta/\Lambda \sim 0.4$. With the larger expansion parameters, it becomes more important to check that higher order corrections are not large.

In this chapter we show results for one loop corrections to the matrix elements for the proton and neutron decaying into the meson octet (π, K, η) using EOMS ChPT, and fit our results to lattice data. In section 5.1 we shall mention some of the experimental searches for proton decay. We shall then briefly mention some key concepts of GUTs in section 5.2. Section 5.3 shows the quark-level operators that allow for baryon number violation, and the chiral Lagrangian that can be constructed to allow for proton decay is shown in section 5.4. In section 5.5 we shall briefly review some of the available lattice data, and in section 5.6 we discuss the parameters that we shall be varying in our fit and those that are kept constant. In section 5.7 we shall present our results followed by a discussion in section 5.8 and we show our conclusions in section 5.9.

5.1 Experimental results for proton decay

Due to the long lifetime of protons, to have a good chance of detecting proton decay it is prudent to gather a large number of protons together. Experiments that try to detect proton decay are large, for example the Super-Kamiokande experiment is over 20 kton and contains approximately 7.5×10^{33} protons [138]. This is currently the only active experiment searching for proton decay; it is situated in Japan and uses a water Cherenkov detector.

It is designed to detect the decays of either the free protons contained in hydrogen atoms in the water, or the bound protons contained in oxygen atoms [143]. For protons decaying into a neutral pion and positron, the pion energy is $E_\pi \sim 460$ MeV. Simulations show that 37% of these pions will be absorbed or charge-exchanged inside the nucleon [137], while 44 % will escape without scattering, with the remaining 19% being scattered [137]. This makes this particular

channel harder to detect. For protons decaying to kaons and leptons, the maximum kaon energy is $E_K \sim 600$ MeV [143]. Decays to final states that include kaons can be detected via the decays of the kaon into pions or leptons [143]. We show some of the experimental results for the lifetime of the proton in table 5.1.

The most significant background at Super-Kamiokande comes from atmospheric neutrinos. The neutrinos can interact with the nuclei in the detector and produce events that look similar to proton decay events [143]. These effects must be carefully accounted for, and minimizing the background is one of the reasons that the detector is built underground.

The technology to detect proton decay can be divided into three categories, water Cherenkov, liquid argon time projection chambers (LArTPC) and scintillators [138]. Currently there are no other experiments searching for proton decay [138], however there are proposals for LArTPC [144] and scintillator [145] experiments. The advantage of a LArTPC experiment is that it can distinguish between different charged particles and detect protons below the Cherenkov threshold [138]. Scintillators are also able to detect particles that are below the Cherenkov threshold [138].

Decay mode	Time (90% CL) yrs
$p \to \pi^0 e^+$	8.2×10^{33}
$p \to \pi^0 \mu^+$	6.6×10^{33}
$p \to \eta e^+$	4.2×10^{33}
$p \to \eta \mu^+$	1.3×10^{33}

Table 5.1: Some results for the lifetime of the proton from the Super-Kamiokande experiment to show the typical time scales involved in proton decay. Results are taken from Nishino et al. [137].

5.2 Grand Unified Theories

The aim of a GUT is to combine the strong, weak and EM interactions into a single gauge group. The idea of a GUT was first proposed by Georgi and Glashow [139] who proposed that, at high energies, the three forces could be combined into the single gauge group SU(5). Some consequences of this are that the three coupling constants would be unified, lepton and quark matter fields could exist in the same representation, and the proton would no longer be stable.

The reason the proton is stable in the standard model is due to the global $U(1)_V$ symmetry in the QCD Lagrangian. The conserved charge associated with the symmetry is

$$Q_B = \int d^4x \frac{1}{3}(u_i^\dagger u_i + d_i^\dagger d_i) \tag{5.1}$$

where $u_i = (u, c, t)$ and $d_i = (d, s, b)$. This operator counts the number of quarks present, and so the proton is unable to "lose" a quark and decay into lighter particles. This symmetry of the standard model can be seen to be accidental, in that it is not possible to construct renormalisable operators that violate the symmetry. If the lepton and quark fields were combined into the same multiplet, the conserved charge would also count lepton number, and so the baryon number on its own would not be conserved.

The gauge group SU(5) contain $5^2 - 1 = 24$ generators, compared to the 12 recognised in the standard model. The extra 12 generators, known as X_i and Y_i, with $1 \leqslant i \leqslant 6$, allow interactions where quarks are transformed into leptons, and vice versa [146].

Two of the predictions of the SU(5) GUT mentioned earlier, the unification of the coupling constants and the instability of the proton, are both testable. Based on the standard model, the coupling constants are predicted to become close at higher energies, but they do not all converge [147]. The lifetime of the proton

has also been measured to be longer than the SU(5) prediction. Incorporating supersymmetry [148, 149], where every elementary particle has a supersymmetric partner extends the proton lifetime predictions so they are in agreement with current experiments, and also ensures that the coupling constants unify at high energy. However, so far no supersymmetric partner particles have been discovered and the theory remains unproven.

5.3 Baryon decay at the quark level

Weinberg [140] and Wilczek and Zee [141] identified six operators of dimension six that could mediate proton decay. It was realised later that these six operators were not linearly independent, and that two of them could be expressed in terms of the remaining four [150]. The four independent operators can be taken to be

$$\mathcal{O}^1_{abcd} = (\bar{D}^C_{iaR} U_{jbR})(\bar{Q}^C_{\alpha kcL} L_{\beta dL}) \varepsilon_{ijk} \varepsilon_{\alpha\beta} \tag{5.2}$$

$$\mathcal{O}^2_{abcd} = (\bar{Q}^C_{\alpha iaL} Q_{\beta jbL})(\bar{U}^C_{kcR} E_{dR}) \varepsilon_{ijk} \varepsilon_{\alpha\beta} \tag{5.3}$$

$$\mathcal{O}^3_{abcd} = (\bar{Q}^C_{\alpha iaL} Q_{\beta jbL})(\bar{Q}^C_{\gamma kcL} L_{\delta dL}) \varepsilon_{ijk} \varepsilon_{\alpha\delta} \varepsilon_{\beta\gamma} \tag{5.4}$$

$$\mathcal{O}^4_{abcd} = (\bar{D}^C_{iaR} U_{jbR})(\bar{U}^C_{kcR} E_{dR}) \varepsilon_{ijk} \tag{5.5}$$

where α, β, γ and δ are electroweak SU(2) indices, i, j and k are colour SU(3) indices and a, b, c and d are generation indices (distinguishing electron, muon and tau for leptons and the three "up type" and "down type" quarks), and the superscript C stands for charge conjugation. The fields Q and L are left handed SU(2) doublets and D, U, and E are right handed SU(2) singlets. More explicitly

we have

$$Q_{aL} = \begin{pmatrix} u_{aL} \\ d_{aL} \end{pmatrix}, \quad U_{aR} = u_{aR}, \quad D_{aR} = d_{aR}$$
$$L_{aL} = \begin{pmatrix} \nu_{aL} \\ e_{aL} \end{pmatrix}, \quad E_{aR} = e_{aR} \tag{5.6}$$

where the subscript a represents the generation, for example $u_a = (u, c, t)$ and $d_a = (d, c, b)$. Similarly for the leptons, the index describes the generation (electron, muon or tau). These four-fermion interactions allow a proton to decay into a meson and a lepton, or directly into a lepton (although this process is forbidden kinematically). A representation of proton decay at the quark level is shown in figure 5.1, with the left-hand image depicting a proton decaying into a pion and a positron, and the right-hand image showing a proton decaying into a positron.

For nucleon decay into non-strange final states we must take all quark generation indices (a, b, c) to be one. This gives the operators [142]

$$\mathcal{O}^1_{111d} \equiv \mathcal{O}^1_d = (\bar{d}^c_{iR} u_{jR})(\bar{u}^c_{kL} e_{dL} - \bar{d}^c_{kL} \nu_{dL}) \varepsilon_{ijk} \tag{5.7}$$
$$-\frac{1}{2}\mathcal{O}^2_{111d} \equiv \mathcal{O}^2_d = (\bar{d}^c_{iL} u_{jL})(\bar{u}^c_{kR} e_{dR}) \varepsilon_{ijk} \tag{5.8}$$
$$\mathcal{O}^3_{111d} \equiv \mathcal{O}^3_d = (\bar{d}^c_{iL} u_{jL})(\bar{u}^c_{kL} e_{dL} - \bar{d}^c_{kL} \nu_{dL}) \varepsilon_{ijk} \tag{5.9}$$
$$\mathcal{O}^4_{111d} \equiv \mathcal{O}^4_d = (\bar{d}^c_{iR} u_{jR})(\bar{u}^c_{kR} e_{dR}) \varepsilon_{ijk}. \tag{5.10}$$

For strange final states we have the operators [142]

$$\mathcal{O}^1_{211d} \equiv \tilde{\mathcal{O}}^1_d = (\bar{s}^c_{iR} u_{jR})(\bar{u}^c_{kL} e_{dL} - \bar{d}^c_{kL} \nu_{dL}) \varepsilon_{ijk} \tag{5.11}$$
$$-\mathcal{O}^2_{211d} \equiv \tilde{\mathcal{O}}^2_d = (\bar{s}^c_{iL} u_{jL})(\bar{u}^c_{kR} e_{dR}) \varepsilon_{ijk} \tag{5.12}$$

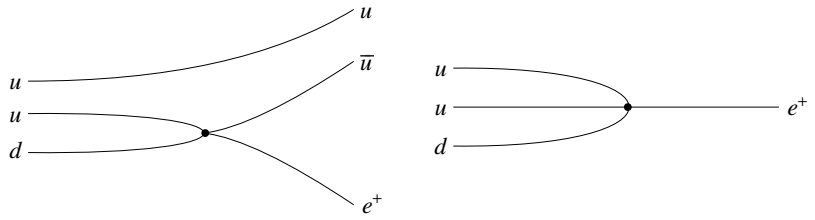

Figure 5.1: Quark-level diagrams showing the type of interaction possible using the baryon-number-violating operators in eqs (5.2) to (5.5).

$$-\frac{1}{2}\mathcal{O}^3_{221d} \equiv \tilde{\mathcal{O}}^3_d = (\bar{s}^c_{iL}u_{jL})(\bar{u}^c_{kL}e_{dL} - \bar{d}^c_{kL}\nu_{dL})\varepsilon_{ijk} \tag{5.13}$$

$$\mathcal{O}^4_{211d} \equiv \tilde{\mathcal{O}}^4_d = (\bar{s}^c_{iR}u_{jR})(\bar{u}^c_{kR}e_{dR})\varepsilon_{ijk} \tag{5.14}$$

$$-\mathcal{O}^1_{112d} \equiv \tilde{\mathcal{O}}^5_d = (\bar{d}^c_{iR}u_{jR})(\bar{s}^c_{kL}e_{dL})\varepsilon_{ijk} \tag{5.15}$$

$$\mathcal{O}^3_{211d} \equiv \tilde{\mathcal{O}}^6_d = (\bar{d}^c_{iL}u_{jL})(\bar{s}^c_{kL}e_{dL})\varepsilon_{ijk} \tag{5.16}$$

after performing some simplifications using Fierz identities [151].

The quark level Lagrangian containing baryon-number-violating terms is given by

$$\mathcal{L} = \sum_{i=1}^{4} C^{(i)}_d \mathcal{O}^i_d + \sum_{i=1}^{6} \tilde{C}^{(i)}_d \tilde{\mathcal{O}}^i_d \tag{5.17}$$

where the coefficients $C^{(i)}_d$ and $\tilde{C}^{(i)}_d$ are known as Wilson coefficients, and can be determined in a given GUT model. The Wilson coefficients are calculated at a scale $\mu = 2$ GeV and regularised using the $\overline{\text{MS}}$ scheme [152].

5.4 Chiral Lagrangian for proton decay

The quark-level operators can be grouped according to the parity of the fermion fields as $\mathcal{O}^{\mathrm{RL}}$ ($\mathcal{O}^1_d$, $\tilde{\mathcal{O}}^1_d$ and $\tilde{\mathcal{O}}^5_d$), $\mathcal{O}^{\mathrm{LR}}$ ($\mathcal{O}^2_d$ and $\tilde{\mathcal{O}}^2_d$), $\mathcal{O}^{\mathrm{LL}}$ ($\mathcal{O}^3_d$, $\tilde{\mathcal{O}}^3_d$ and $\tilde{\mathcal{O}}^6_d$) and $\mathcal{O}^{\mathrm{RR}}$ ($\mathcal{O}^4_d$ and $\tilde{\mathcal{O}}^4_d$), see eqs (5.7-5.16). Due to parity invariance we have [153]

$$\langle \phi \left| \mathcal{O}^{\mathrm{RL}} \right| B \rangle = \langle \phi \left| \mathcal{O}^{\mathrm{LR}} \right| B \rangle \tag{5.18}$$

and

$$\langle \phi \left| \mathcal{O}^{\mathrm{RR}} \right| B \rangle = \langle \phi \left| \mathcal{O}^{\mathrm{LL}} \right| B \rangle \tag{5.19}$$

where ϕ is a meson field and B a baryon field and we are only looking at the strong matrix element. A generic matrix element for proton decay will depend on two types of quark-level operators which can be taken to be

$$\langle \phi \left| \mathcal{O} \right| B \rangle = \langle \phi \left| \mathcal{O}^{\mathrm{RL}} + \mathcal{O}^{\mathrm{LL}} \right| B \rangle. \tag{5.20}$$

On the lattice these two matrix elements can be calculated individually. For a proton or neutron decaying into a meson and a lepton, assuming isospin symmetry, the following list is a set of independent matrix elements [153]

$$W^{(1)} = \langle \pi^0 \left| (ud)_{\mathrm{R/L}}(u_{\mathrm{L}}) \right| p \rangle \tag{5.21}$$

$$W^{(2)} = \langle K^0 \left| (us)_{\mathrm{R/L}}(u_{\mathrm{L}}) \right| p \rangle \tag{5.22}$$

$$W^{(3)} = \langle K^+ \left| (us)_{\mathrm{R/L}}(d_{\mathrm{L}}) \right| p \rangle \tag{5.23}$$

$$W^{(4)} = \langle K^+ \left| (ud)_{\mathrm{R/L}}(s_{\mathrm{L}}) \right| p \rangle \tag{5.24}$$

$$W^{(5)} = \langle K^0 \left| (us)_{\mathrm{R/L}}(d_{\mathrm{L}}) \right| n \rangle \tag{5.25}$$

$$W^{(6)} = \langle \eta^0 \left| (ud)_{\mathrm{R/L}}(u_{\mathrm{L}}) \right| p \rangle. \tag{5.26}$$

We have labelled these matrix elements $W^{(i)}$ for ease of reference.

To calculate matrix elements using ChPT, the quark-level operators, eqs (5.7–5.16), were converted into a chiral Lagrangian by Claudson et al. [142]. The conversion was achieved by noting that the $\mathcal{O}^{\rm RL}$ and $\mathcal{O}^{\rm LR}$ operators transform under $SU(3)_L \otimes SU(3)_R$ like $(3,\bar{3})$ and $(\bar{3},3)$ respectively, and the $\mathcal{O}^{\rm LL}$ and $\mathcal{O}^{\rm RR}$ operators transform like $(1,8)$ and $(8,1)$ respectively. The chiral constructs uBu and $u^\dagger B u^\dagger$ transform like $(3,\bar{3})$ and $(\bar{3},3)$ respectively and $u^\dagger B u$ and $uBu^\dagger$ transform like $(1,8)$ and $(8,1)$ respectively. The chiral Lagrangian for baryon number violation can be written in terms of baryon and meson octet fields as [142]

$$\begin{aligned}
\mathcal{L}_0^{\not B} = \alpha \sum_{d=1}^{2} \Big[& C_d^{(1)} \left(e_{dL} {\rm Tr}\mathcal{F}_1 u B_L u - \nu_{dL} {\rm Tr}\mathcal{F}_2 u B_L u \right) + C_d^{(2)} e_{dR} {\rm Tr}\mathcal{F}_1 u^\dagger B_R u^\dagger \\
& + \tilde{C}_d^{(1)} \left(e_{dL} {\rm Tr}\mathcal{F}_3 u B_L u - \nu_{dL} {\rm Tr}\mathcal{F}_4 u B_L u \right) + \tilde{C}_d^{(2)} e_{dR} {\rm Tr}\mathcal{F}_3 u^\dagger B_R u^\dagger \\
& + \tilde{C}_d^{(5)} \nu_{dL} {\rm Tr}\mathcal{F}_5 u B_L u \Big] \\
+ \beta \sum_{d=1}^{2} \Big[& C_d^{(3)} \left(e_{dL} {\rm Tr}\mathcal{F}_1 u B_L u^\dagger - \nu_{dL} {\rm Tr}\mathcal{F}_2 u B_L u^\dagger \right) + C_d^{(4)} e_{dR} {\rm Tr}\mathcal{F}_1 u^\dagger B_R u \\
& + \tilde{C}_d^{(3)} \left(e_{dL} {\rm Tr}\mathcal{F}_3 u B_L u^\dagger - \nu_{dL} {\rm Tr}\mathcal{F}_4 u B_L u^\dagger \right) + \tilde{C}_d^{(4)} e_{dR} {\rm Tr}\mathcal{F}_3 u^\dagger B_R u \\
& + \tilde{C}_d^{(6)} \nu_{dL} {\rm Tr}\mathcal{F}_5 u B_L u^\dagger \Big] + {\rm h.c.}.
\end{aligned} \tag{5.27}$$

The matrices $\mathcal{F}_i$ are give by

$$\begin{aligned}
\mathcal{F}_1 &= \begin{pmatrix} 0 & 0 & 0 \\ 0 & 0 & 0 \\ 1 & 0 & 0 \end{pmatrix}, \qquad \mathcal{F}_2 = \begin{pmatrix} 0 & 0 & 0 \\ 0 & 0 & 0 \\ 0 & 1 & 0 \end{pmatrix}, \qquad \mathcal{F}_3 = -\begin{pmatrix} 0 & 0 & 0 \\ 1 & 0 & 0 \\ 0 & 0 & 0 \end{pmatrix}, \\
\mathcal{F}_4 &= -\begin{pmatrix} 0 & 0 & 0 \\ 0 & 1 & 0 \\ 0 & 0 & 0 \end{pmatrix}, \qquad \mathcal{F}_5 = \begin{pmatrix} 0 & 0 & 0 \\ 0 & 0 & 0 \\ 0 & 0 & 1 \end{pmatrix}.
\end{aligned} \tag{5.28}$$

As we can set $u = u^\dagger = 1$ the same terms in the chiral Lagrangian give both $N \to \phi l$ and $N \to l$ vertices. There are two new low-energy constants, α and β, distinguishing between $\mathcal{O}^{\mathrm{RL}}$ and $\mathcal{O}^{\mathrm{LL}}$ type operators respectively. They encode the SU(3) symmetry of baryon decay. The Wilson coefficients, that originate from the construction of the quark level Lagrangian eq. (5.17), also appear in the chiral Lagrangian. None of the coefficients (α, β, $C_d^{(i)}$ and $\tilde{C}_d^{(i)}$) can be determined using ChPT. We can match a ChPT expression to lattice data to determine α and β however, as both lattice and ChPT address only the hadronic matrix element. The determination of the Wilson coefficients is not accessible using ChPT, but depends entirely on the specific GUT. We shall only investigate the parameters α and β in this chapter.

For each hadronic matrix element we calculate, we shall consider the parts proportional to α and β independently in order to fit the LECs to lattice data.

Aoki et al. [153] pointed out that the matrix element can be written in terms of two form factors,

$$\left\langle \phi \left| \bar{v}_l \mathcal{O}^{\mathrm{R/L,L}} u_B \right| B \right\rangle = \bar{v}_l (W_0(q^2) + \not{q} W_q(q^2)) P_{\mathrm{L}} u_B, \tag{5.29}$$

where q^2 is the momentum of the lepton, $\bar{v}_l$ and u_B are spinors for the lepton and baryon and $P_{\mathrm{L,R}} = 1/2(1 \pm \gamma_5)$. The W_q term is suppressed by a power of the lepton mass and can be ignored. The terms W_0 and W_q are known as the relevant and irrelevant form factors respectively. We shall study the six relevant form factors, $W_0^{(i)}$, of eqs (5.21–5.26).

We require counter terms to remove divergences from the loop diagrams contributing to the relevant form factor (shown in figure 5.2). There will be counter terms coming from the conventional EOMS ChPT Lagrangian ($\mathcal{L}^{\mathrm{EOMS}}$), and also counter terms from the baryon-number-violating Lagrangian ($\mathcal{L}^{\not{B}}$). However, only

the lowest order contribution to $\mathcal{L}^{\not B}$ ($\mathcal{L}_0^{\not B}$ shown in eq. (5.27)) has been calculated. For this work we have determined the terms in the higher-order Lagrangian that are relevant to our calculation.

We are interested in vertices that allow an off-shell baryon to decay into a lepton, or into a lepton and meson. This means the terms in the higher-order Lagrangian will be similar to those in eq. (5.27) but will contain the construct χ

$$\chi = 2B_0(s + ip). \tag{5.30}$$

The terms in $\mathcal{L}_0^{\not B}$ transform under $\mathrm{SU}(3)_L \otimes \mathrm{SU}(3)_R$ as

$$uBu \to LuBuR^\dagger \tag{5.31}$$

$$u^\dagger B u^\dagger \to R u^\dagger B u^\dagger L^\dagger \tag{5.32}$$

$$uBu^\dagger \to LuBu^\dagger L^\dagger \tag{5.33}$$

$$u^\dagger B u \to R u^\dagger B u R^\dagger \tag{5.34}$$

and we wish the terms in the higher order Lagrangian to have the same transformation properties. There are only three ways to include χ and maintain the correct transformation properties

$$uBu\mathrm{Tr}(\chi) \to LuBuR^\dagger \mathrm{Tr}(\chi) \tag{5.35}$$

$$uB\chi u \to LuB\chi uR^\dagger \tag{5.36}$$

$$u\chi Bu \to Lu\chi BuR^\dagger \tag{5.37}$$

with similar expressions for the three remaining constructs $u^\dagger B u^\dagger$, $uBu^\dagger$ and $u^\dagger Bu$. This tells us that there will be three LECs based on terms proportional to α in eq. (5.27) that we shall call α_{1-3} and three LECs based on terms proportional to

β that we shall call β_{1-3}.

The higher-order Lagrangian will contain terms of the form

$$\begin{aligned}
\mathcal{L}_1^{\not B} = \alpha_1 \sum_{d=1}^{2} \Big[& C_d^{(1)} \left(e_{dL} \mathrm{Tr}(\mathcal{F}_1 u B_L u) \mathrm{Tr}(\chi) - \nu_{dL} \mathrm{Tr}(\mathcal{F}_2 u B_L u) \mathrm{Tr}(\chi) \right) \\
& + \tilde{C}_d^{(1)} \left(e_{dL} \mathrm{Tr}(\mathcal{F}_3 u B_L u) \mathrm{Tr}(\chi) - \nu_{dL} \mathrm{Tr}(\mathcal{F}_4 u B_L u) \mathrm{Tr}(\chi) \right) \\
& + C_d^{(2)} e_{dR} \mathrm{Tr}(\mathcal{F}_1 u^\dagger B_R u^\dagger) \mathrm{Tr}(\chi) + \tilde{C}_d^{(2)} e_{dR} \mathrm{Tr}(\mathcal{F}_3 u^\dagger B_R u^\dagger) \mathrm{Tr}(\chi) \\
& + \tilde{C}_d^{(5)} \nu_{dL} \mathrm{Tr}(\mathcal{F}_5 u B_L u) \mathrm{Tr}(\chi) \Big] \\
+ \alpha_2 \sum_{d=1}^{2} \Big[& C_d^{(1)} \left(e_{dL} \mathrm{Tr}(\mathcal{F}_1 u B_L \chi u) - \nu_{dL} \mathrm{Tr}(\mathcal{F}_2 u B_L \chi u) \right) \\
& + \tilde{C}_d^{(1)} \left(e_{dL} \mathrm{Tr}(\mathcal{F}_3 u B_L \chi u) - \nu_{dL} \mathrm{Tr}(\mathcal{F}_4 u B_L \chi u) \right) \\
& + C_d^{(2)} e_{dR} \mathrm{Tr}(\mathcal{F}_1 u^\dagger B_R \chi u^\dagger) + \tilde{C}_d^{(2)} e_{dR} \mathrm{Tr}(\mathcal{F}_3 u^\dagger B_R \chi u^\dagger) \\
& + \tilde{C}_d^{(5)} \nu_{dL} \mathrm{Tr}(\mathcal{F}_5 u B_L \chi u) \Big] + \cdots
\end{aligned} \tag{5.38}$$

where the ellipses will include terms proportional to α_3 and β_{1-3}.

The divergences of the loop contributions to the form factors $W_0^{(i)}$ due to diagrams vi-xi, in figure 5.2 will have the same structure as the LECs α_{1-3} and β_{1-3} and this tells us the pattern the LECs will enter. We found that we were able to write the divergences, $W_{0,\infty}^{(i)}$, of $W_0^{(4-6)}$ in terms of those of $W_0^{(1-3)}$ as

$$W_{0,\infty}^{(4)} = \sqrt{2} W_{0,\infty}^{(1)} + W_{0,\infty}^{(3)} \tag{5.39}$$

$$W_{0,\infty}^{(5)} = W_{0,\infty}^{(3)} - W_{0,\infty}^{(2)} \tag{5.40}$$

$$W_{0,\infty}^{(6)} = \sqrt{\frac{1}{3}} W_{0,\infty}^{(1)} + \sqrt{\frac{2}{3}} W_{0,\infty}^{(3)}. \tag{5.41}$$

The divergences proportional to α and β both have the same form.

The terms from the conventional third order EOMS Lagrangian that are relevant for this work are

$$\begin{aligned}\mathcal{L}^{(3)} = {} & h_{38}\mathrm{Tr}(\bar{B}u^\mu\gamma_5\gamma_\mu B\chi_+) + h_{39}\mathrm{Tr}(\bar{B}\chi_+\gamma_5\gamma_\mu Bu^\mu) \\ & + h_{40}\mathrm{Tr}(\bar{B}u^\mu\gamma_5\gamma_\mu B)\mathrm{Tr}(\chi_+) + h_{41}\mathrm{Tr}(\bar{B}\gamma_5\gamma_\mu Bu^\mu)\mathrm{Tr}(\chi_+) \\ & + h_{43}\mathrm{Tr}(\bar{B}\gamma_5\gamma_\mu B\{u^\mu,\chi_+\}) + h_{44}\mathrm{Tr}(\bar{B}\{u^\mu,\chi_+\}\gamma_5\gamma_\mu B) + \cdots .\end{aligned} \tag{5.42}$$

These are the same LECs used in the previous chapter, so we shall use the values we arrived at in chapter 4 based on the $\mathcal{O}(p^3)$ no-decuplet fit that excluded the lattice data (shown in table 4.10).

The loop diagrams that need to be calculated are shown in figure 5.2. Our results for these diagrams are shown in the appendix in eqs (C.14–C.25), and the expressions for the form factors are shown in eqs (C.26–C.37).

Although we shall not be directly calculating the proton lifetime in this work, it would be instructive to see how the matrix elements we shall be calculating relate to the physically observable proton lifetime. The Lagrangian we are using contains several parameters that are not known, the Wilson coefficients C_d^i and $\tilde{C}_d^i$ and the two LECs α and β. The Wilson coefficients can be predicted by various GUT models and can depend on unknown parameters such as the mass of a hypothetical X boson; we shall not be trying to predict them in this work. The parameters α and β are also not known, however as there is lattice data for the hadronic matrix elements, eqs (5.21–5.26), which does not depend on the Wilson coefficients, we can determine α and β by fitting our results to the lattice data. The amplitude for a left handed proton decaying into a pion at tree level is given by

$$\mathcal{M} = \frac{1}{\sqrt{2}F_\pi}\bar{u}_e P_L(\alpha C^{(1)} + \beta C^{(3)})(1 + D + F)u_p \tag{5.43}$$

and so the lifetime is

$$\Gamma(p_L \to \pi^0 e^+) = \frac{m_N}{32\pi^2 F_\pi^2} \left((\alpha C^{(1)} + \beta C^{(3)})(1 + D + F)\right)^2 . \tag{5.44}$$

For the process $p \to \pi^0 e^+$ the parts of the matrix element proportional to α and β are the same, however this is not generally true for other processes. Hadronic matrix elements can be used in conjunction with GUTs to predict the proton lifetime [154, 155]. Calculating the matrix element to a higher precision allows for more accurate tests of GUTs.

As there are no results in the literature to compare our result to, we have used the same method developed in the previous chapter, using a combination of FORM and Mathematica, to ensure our results are as reliable as possible.

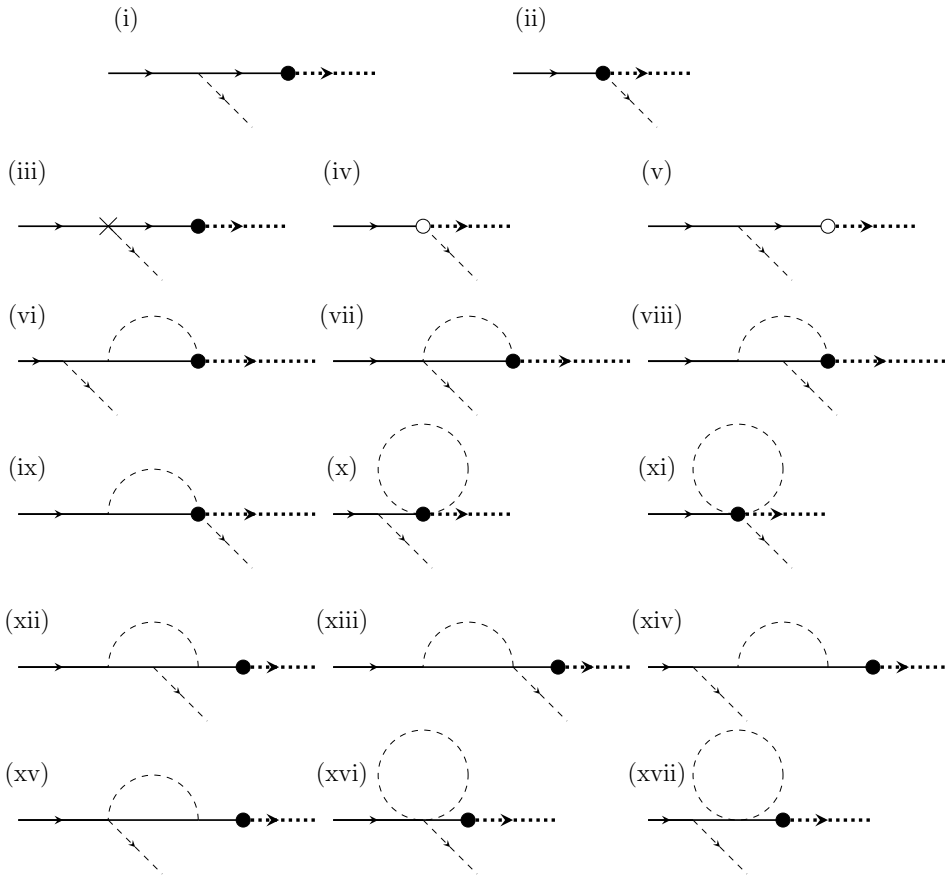

Figure 5.2: Loop diagrams calculated for this work. Solid lines are baryons, dashed lines are mesons and dotted lines are leptons. Vertices from the lowest order baryon-number-violating Lagrangian are depicted with a solid blob, and vertices from the next order baryon-number-violating Lagrangian are an empty blob. The cross denotes a vertex from the third order EOMS ChPT Lagrangian. We have not shown diagrams contributing to wavefunction renormalisation, although we have included these in our calculations.

5.5 Lattice results

There are currently two approaches to calculating hadronic matrix elements relevant to proton decay on the lattice, known as the direct and indirect method.

The direct method involves calculating matrix elements for a baryon decaying into a meson on the lattice. These three-point functions are calculated at unphysical quark mass, so the results must be extrapolated to the physical quark masses. These results can then be combined with predictions of the Wilson coefficients and used to estimate the proton lifetime. The most recent results of baryon decay from LQCD using the direct method are by Aoki et al. [156].

Although the direct method can produce results without any knowledge of the ChPT LECs, performing a linear extrapolation to the chiral limit is physically unrealistic. Many other parameters calculated on the lattice do not show simple linear dependence with the light quark mass, and chiral extrapolations are routinely done with the help of results from ChPT.

The indirect method involves calculating matrix elements for a baryon decaying into the hadronic vacuum (i.e. nucleon $\rightarrow$ lepton). Although this process is unphysical, it only involves two-point calculations on the lattice and is therefore computationally less intensive than the direct method. the proton-to-vacuum matrix elements are proportional to the low energy constants α and β. This is seen by noting that we can calculate the matrix element for a baryon to decay into the vacuum by taking the baryon-violating Lagrangian with meson fields set to $u = u^\dagger = 1$. The constants α and β can be calculated from two-point functions for proton decay on the lattice. Once these have been calculated, matrix elements for a baryon decaying into a meson can be calculated using ChPT. Previous studies using the indirect method have relied on tree-level ChPT results [153, 157]. As the matrix elements involve the full SU(3) meson octet it is unclear whether or not higher-order corrections to the matrix elements are significant.

Using the quenched approximation, results of the relevant form factor for several nucleon decays were presented using both the direct and indirect method by Aoki et al. [153]. The two methods gave results that were roughly comparable, although the indirect method tended to give results that were larger than the direct method. Values of the LECs α and β were $-0.015(1)$ GeV^3 and $0.014(1)$ GeV^3 respectively, with pion masses in the range $0.450 < M_\pi < 0.738$ GeV.

Later lattice work on proton decay by Tsutsui et al. [158] looked at the effect of scale-setting on the lattice by using three different values of the lattice parameter in the range $a^{-1} \sim 2-3$ GeV. The same gauge and quark actions that were used in [153] were also used in [158]. It was shown that when the physical scale is set by the nucleon mass, the scaling violation is minimised, and smaller values of the LECs were obtained with $\alpha = -0.0090(09)(+5-19)$ GeV^3 and $\beta = 0.0096(09)(+6-20)$ GeV^3 [158].

The first results of calculating proton-decay matrix elements with domain wall fermions also investigated the effects of the quenched approximation [152]. Quenched and unquenched results for the direct and indirect method were found to be in good agreement, with $|\alpha| \sim |\beta| \sim 0.01$ GeV^3. It was found that results for the matrix elements using the direct and indirect method were no longer compatible however, with the decay $p \to \pi^0$ differing by a factor of two. Aoki et al. suggested that the indirect method was suffering due to a lack of higher order terms from ChPT [152].

The indirect method was looked at again in [157] where results for the LECs were $\alpha = -0.0112(25)$ GeV^3 and $\beta = 0.0120(26)$ GeV^3. The most recent results using the direct method [156] show good agreement between the relevant form factors calculated using the direct and indirect methods, but did not determine values of α and β.

Currently, the lattice results for proton decay matrix elements with the lowest

pion mass are from Aoki et al. [156], with $0.329 < M_\pi \text{ (GeV)} < 0.672$, where they considered six different matrix elements, eqs (5.21–5.26). Each matrix elements has a different form for quark-level $\mathcal{O}^{\text{RL}}$ and $\mathcal{O}^{\text{LL}}$ operators (they will be proportional to the LECs α and β respectively). Aoki et al. presented results for the relevant form factor W_0 for each of these matrix elements [156].

We shall use the results from Aoki et al. [156] to fit a third order EOMS ChPT expression to determine the parameters α and β.

5.6 Fitting parameters

The parameters not being varied in our fit have been set as $m_N = 0.94$ GeV, $F = 0.0924$ GeV, $D_0 = 0.78$ and $F_0 = 0.48$. We have taken the values of D_0 and F_0 from section 4.6 table 4.10. Where we have expressions involving the K or η mass, we write them as before in terms of the pion mass using the relations

$$M_\pi^2 = 2B_0 m_s \tag{5.45}$$

$$M_K^2 = B_0(m + m_s) = \frac{M_\pi^2}{2} + B_0 m_s \tag{5.46}$$

$$M_\eta^2 = \frac{2B_0}{3}(m + 2m_s) = \frac{M_\pi^2}{3} + \frac{4B_0 m_s}{3} \tag{5.47}$$

where m is the light quark mass in the isospin limit and m_s is the strange quark mass as we did in the previous chapter. The product of the strange quark mass and chiral condensate $B_0 m_s$ is set to 0.23 GeV^2, as it was in the previous chapter. As the values of the pion masses used by Aoki et al. are rather large [156] ($M_\pi = 0.33$, 0.48, 0.56, and 0.67 GeV) we shall only fit our expression to the two lowest masses.

For diagrams with three propagators, such as figure 5.2 (viii) and (xii), we

have used analytic results for three-point scalar functions from 't Hooft and Veltman [159], which we have amended to conform with the EOMS renormalisation scheme. The expressions for three propagator diagrams require the function $\lambda(M_\phi^2, m_N^2, q^2) > 0$, where

$$\lambda(M_\phi^2, m_N^2, q^2) = (M_\phi^2 - m_N^2 - q^2)^2 - 4m_N^2 q^2, \tag{5.48}$$

with q^2 being the lepton momentum. This constraint is to ensure the masses of the particles in the final state are less than or equal to the nucleon mass. When we include SU(3) loops in our expression, there are some lattice data points for which $\lambda < 0$, so we must ignore these results in our fits involving K and η loops; however we have included them in our fits that only include pion loops.

The proton lifetime is an observable quantity, and so has no scale dependence. However, the form factors we are looking at in this work are not directly observable, and so we must choose a renormalisation scale. Much of the lattice data concerning proton decay [156] is renormalized at the scale $\mu = 2$ GeV, and so we have used this as the renormalisation scale for our work. It is more usual for EOMS ChPT results to be renormalized at the scale $\mu = m_N$, however conversion factors for lattice results to change the scale from $\mu = 1/a$ to $\mu = 2$ GeV have already been calculated, whilst those for $\mu = 1/a$ to $\mu = m_N$ have not, so we chose to use the existing lattice scaling factors and set $\mu = 2$ GeV in our results.

The LECs we are varying in our fits are α and β, the parameters from the baryon violating Lagrangian, eq. (5.27), and the LECs α_i and β_i from the higher-order baryon violating Lagrangian.

In the previous chapter we used an augmented χ^2 parameter to ensure that loop contributions did not dominate our fit. We found that to be less of a problem with this work, however we again employed an augmented χ^2 in a similar fashion

to the SU(2) fits of the previous chapter. The augmented χ^2 we used for this work was

$$\chi^2_{\text{aug}} = \chi^2 + \sum_{i=1}^{6} \left(\frac{A_i}{R_i} \right)^2 \tag{5.49}$$

where A_i represents the six LECs α_{1-3} and β_{1-3}, and we used a prior of $R_i = 2$.

5.7 Results using EOMS ChPT

In this section we show the results of our one loop calculation of the relevant form factors $W_0^{(i)}$ using EOMS BChPT for each of the matrix elements shown in eqs (5.21–5.26). Our result will have several undetermined LECs which we shall constrain by matching our expression to lattice data from Aoki et al. [156]. We shall show the results of only including pion loops, and of including the entire mesons octet (π, K and η loops). We shall refer to these two cases as pion loops and octet loops. The pion loop case is not strictly physical, as there are form factors with octet particles in the final states, however we included these results to obtain an insight into the importance of K and η loops in this work.

For each set of initial and final particles, the relevant form factor W_0 will have contributions from left and right handed operators ($\mathcal{O}^{\text{RL}}$ and $\mathcal{O}^{\text{LL}}$), meaning there will be a part proportional to α and a part proportional to β. On the lattice these parts are calculated independently. We have paired the form factors proportional to α and β in our plots.

Taking into account pion loop contributions only, we constrained the free parameters in our expression (eqs (C.26–C.37), with K and η loops not included) by matching to lattice data. The parameters that we arrived at are shown in table 5.3, and we have plotted the relevant form factors at the lowest two values of the pion mass as a function of the lepton momentum in figure 5.3.

For octet loops our results are shown in figure 5.4. We are forced to omit data

with a squared lepton mass $q^2 < -0.1$ due to the constraint of eq. (5.48). Again, we ensured that our results for the form factors were normalised so that they reproduced the tree level results in the chiral limit. The parameters we arrived at are shown in table 5.3, and we have plotted our results in figure 5.4.

To establish errors in the values of α and β we re-sampled our data set using a method similar to the jackknife technique. This method involves taking a sample of size n and performing statistical analysis on all possible samples of size $n-1$. We extended this technique by allowing the sample size to vary between two and six, and shall refer to the technique as the augmented jackknife. We took all possible combinations of two or more matrix elements and performed a χ^2 fit. We have plotted the values of α and β against the reduced χ^2 in figure 5.5. We can see that although there is quite a range in the values of reduced χ^2 (varying between 0 and 5), the variation in α and β is small across the entire range of χ^2 values. This suggests that the values of α and β are not sensitive to any individual data set, even though we match some data sets better than others. The average values and errors based on the standard deviation of α using pion loops and octet loops are $-0.008(1)$ GeV^3 and $-0.008(5)$ GeV^3 respectively. For β, we find the values to be $0.008(2)$ GeV^3 and $0.008(6)$ GeV^3 for pion loops and octet loops respectively. These values are summarised in table 5.2. From the graphs shown in figure 5.5, and from the errors in α and β quoted above, we can see that the standard deviations of our octet loop results are larger than those of the pion loop results.

Taking the zero-lepton-momentum limit we can see how the form factor $W_0(q^2 = 0)$ varies for each decay with pion mass (figure 5.6). We also show the $q^2 = 0$ extractions and chiral extrapolations from ref. [156], but they were not used to constrain our results. We have also included the values of the relevant form factors, W_0, at the chiral limit as calculated by Aoki et al. [156]. Again, these values were not used in our fits.

The percentage contribution to each form factor from loop corrections, calculated as the total loop and LEC contribution divided by the tree level contribution at the physical pion mass and $q^2 = 0$ is shown in table 5.4.

	pion loops	octet loops
α GeV^3	$-0.008(1)$	$-0.008(5)$
β GeV^3	0.008(2)	0.008(6)

Table 5.2: Average values of α and β along with associated error based on the data shown in figure 5.6.

	pion loops	octet loops
α GeV^3	$-0.007(3)$	$-0.007(2)$
β GeV^3	0.007(3)	0.007(2)
α_1 GeV^1	$-0.11(21)$	$-0.11(19)$
α_2 GeV^1	0.11(14)	0.11(14)
α_3 GeV^1	0.13(13)	0.13(12)
β_1 GeV^1	$-0.01(17)$	$-0.01(21)$
β_2 GeV^1	$-0.04(17)$	$-0.04(14)$
β_3 GeV^1	0.00(17)	0.00(13)
χ^2/d.o.f.	135/57	114/49

Table 5.3: The parameters that were minimized, and their values, when including only pion loops and when including pion, K and η loops. The parameters were obtained by minimizing χ^2 and using lattice data from Aoki et al [156].

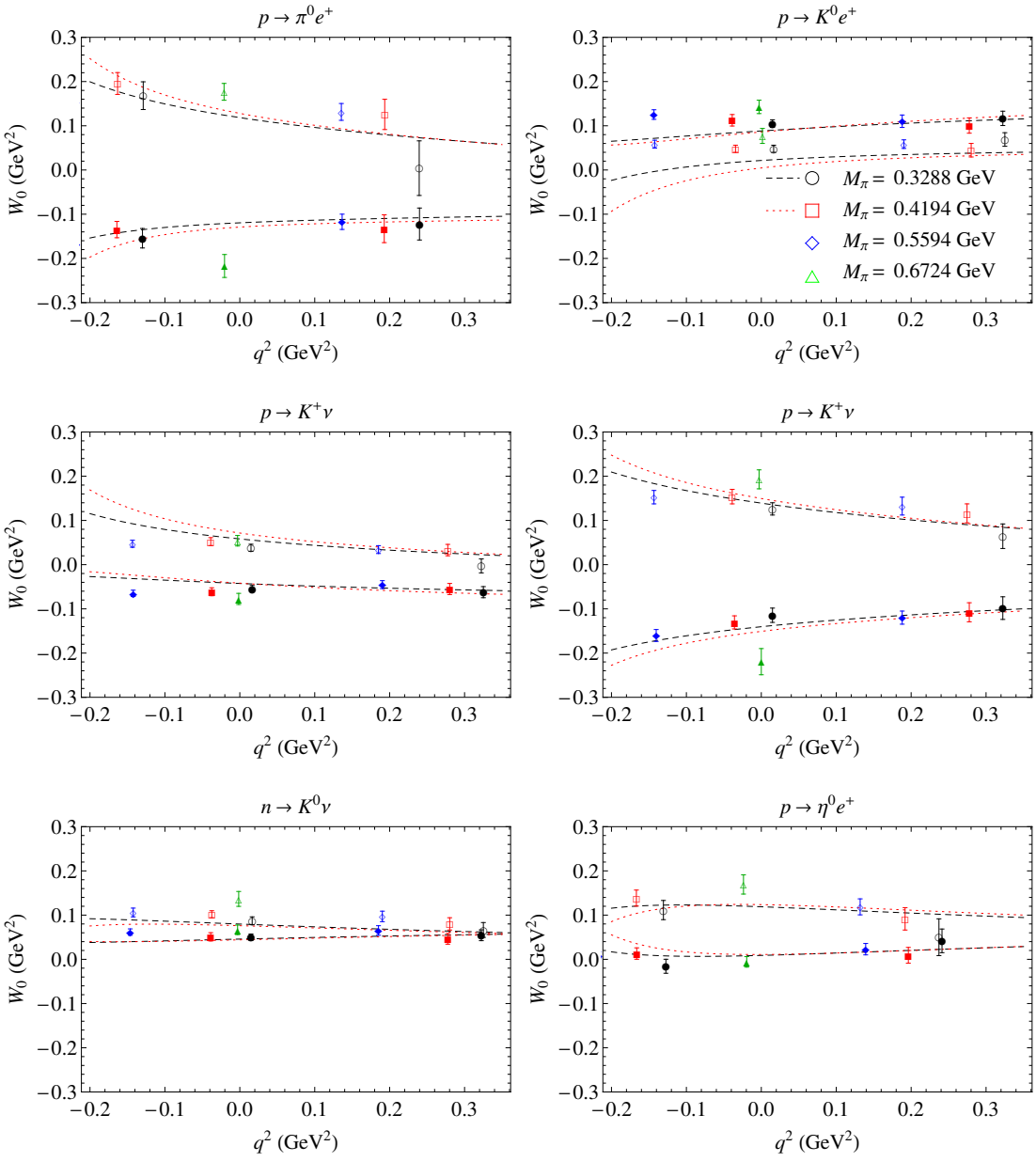

Figure 5.3: Our expression for the relevant form factor, W_0, plotted against lepton momentum, q^2, ignoring K and η loops. We have matched our expression to lattice results from Aoki et al. [156]. There is lattice data at four different pion masses and two different lepton momenta for each pion mass also shown. Filled (open) symbols denote right (left) handed operators. We have only used the lightest two pion masses in our fit ($M_\pi = 0.33$ GeV, black circles, and $M_\pi = 0.42$ GeV, red squares). We have shown the rest of the data although it has not been used to constrain our expression. The black dashed line is our fit to the lowest mass pion data ($M_\pi = 0.33$ GeV) and the red dotted line is our fit to the next lightest pion mass data ($M_\pi = 0.42$ GeV).

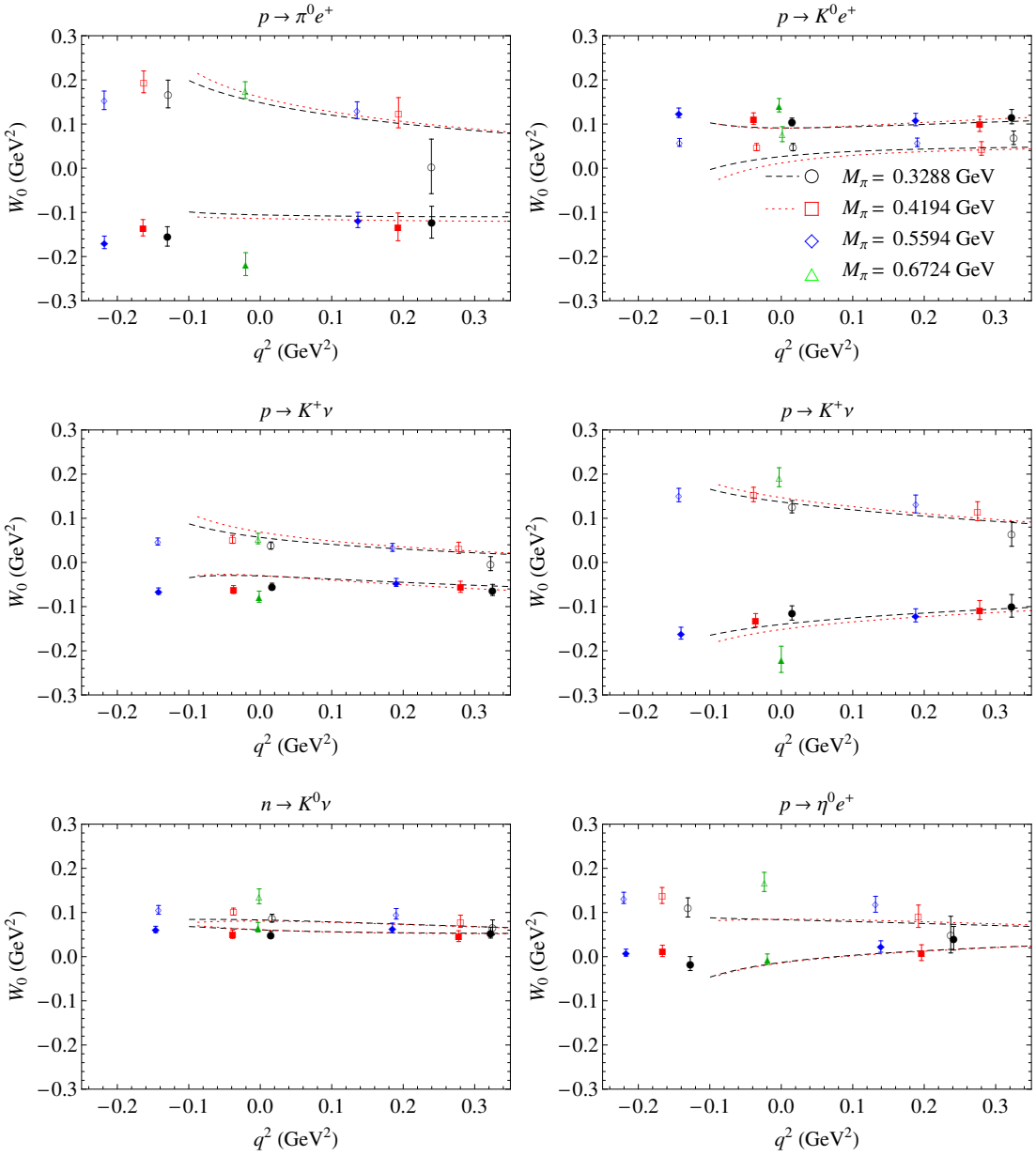

Figure 5.4: Our expression for the relevant form factor, W_0, plotted against lepton momentum, q^2, including K and η loops. Notation is the same as that in figure 5.3.

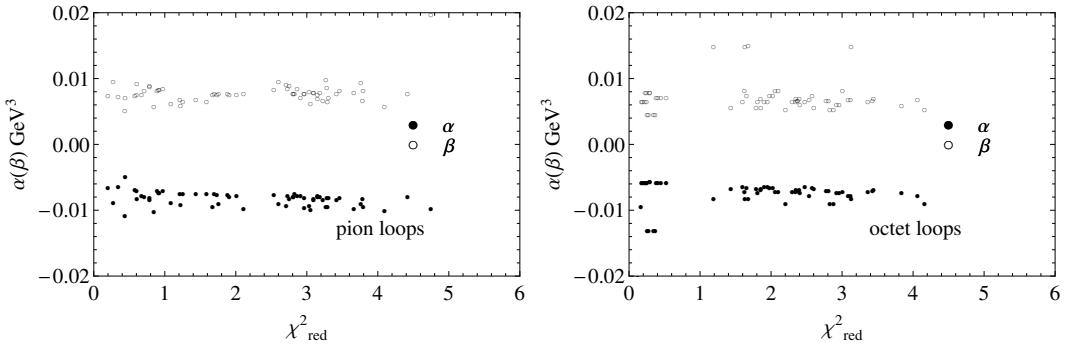

Figure 5.5: We show the minimised values of α and β along with the reduced χ^2 value for every combination of relevant form factors. Filled circles show the value of α and empty circles show the value of β. The left hand plot is only including pion loops, and the right hand plot is pion, K and η loops.

	$p \to \pi^0$	$p \to K^0$	$p \to K^+$	$p \to K^+$	$n \to K^0$	$p \to \eta$
pion loops, $\mathcal{O}^{\mathrm{RL}}$	14.0	13.3	> 100	22.1	> 100	25.1
pion loops, $\mathcal{O}^{\mathrm{LL}}$	14.0	1.9	> 100	22.1	> 100	24.0
octet loops, $\mathcal{O}^{\mathrm{RL}}$	14.0	29.1	> 100	35.7	> 100	> 100
octet loops, $\mathcal{O}^{\mathrm{LL}}$	63.3	19.7	> 100	39.7	> 100	5.0

Table 5.4: Percentage correction to the form factor W_0 at the physical pion mass due to third order corrections. Form factors proportional to α are marked $\mathcal{O}^{\mathrm{RL}}$ in the table. Form factors proportional to β are marked $\mathcal{O}^{\mathrm{LL}}$ in the table.

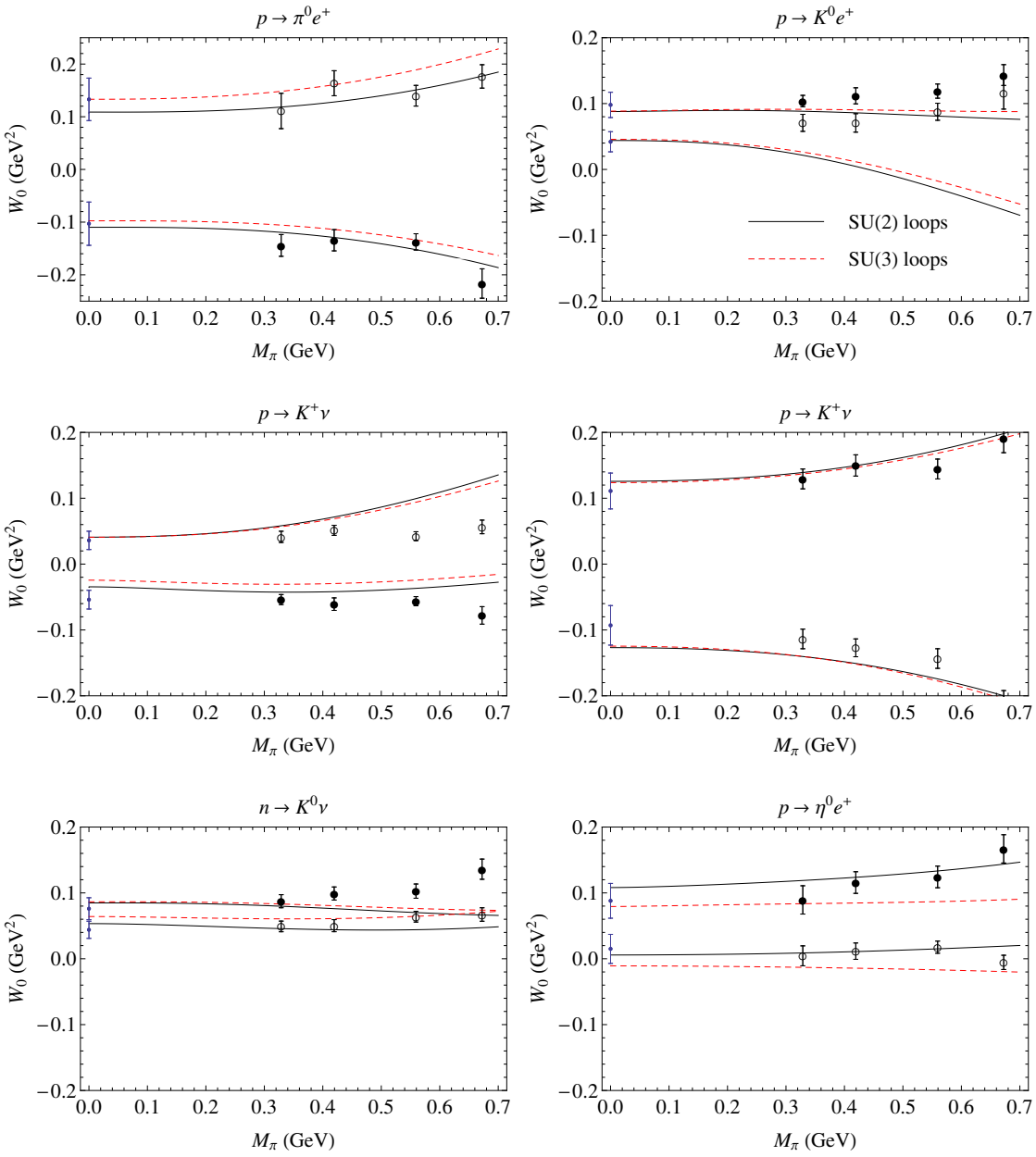

Figure 5.6: Relevant form factors W_0 at $q^2 = 0$ plotted against pion mass. We have shown results for pion loops (solid black lines) and octet loops (red dashed lines). We have included the data points at $q^2 = 0$ from Aoki et al. [156] (filled and empty black circles) and the values obtained by Aoki et al. [156] by linear extrapolation to the chiral limit (blue dots), although we have not used these data points for our fit. In most cases the chiral limit from ref. [156] and our chiral limit values agree.

5.8 Discussion

We have calculated the first order loop corrections for proton decay matrix elements using EOMS BChPT. There are two free parameters α and β from the leading-order baryon-number-violating Lagrangian, eq. (5.27), and there are also six LECs from the next-to-leading-order baryon-number-violating Lagrangian to be constrained, α_{1-3} and β_{1-3}. Currently, the best lattice data on proton decay has been produced by Aoki et al. [156], and we have performed a fit using their data to constrain the free parameters in our expression.

When we only include pion loop corrections (figure 5.3), we see that the curves for the two pion masses show similar q^2 dependence. Some of the lattice data have particularly small error bars (particularly $p \to K^+\nu$ and $n \to K^0\nu$ near $q^2 = 0$), and our fitting scheme will favour these points. We can see that our fit to $W_0^{(2)}$ (top right graph, figure 5.3) at $q^2 < 0$ is not good. For the remaining form factors our fit to the lattice data is quite good. It is important to note that the lattice data for $W_0^{(1)}$ has very large error bars at $q^2 > 0$, and for the form factor proportional to β (our fit to the empty symbols) we do not match the lattice data. This is particularly important when use octet loops, as we are forced to exclude data with $q^2 < -0.1$ and our fit to $W_0^{(1)}$ is based entirely on the data we do not match well in the pion loop only case.

Our results with octet loops are broadly similar to those including only pion loops (see figure 5.4). Our match to $W_0^{(2)}$ is better when octet loops are included. We can see that for $W_0^{(1)}$ (figure 5.4 top left) our curve does not pass close to the only lowest mass data point (black empty circle). This was the only data point we could include at this pion mass and we do not match it. Extrapolating the curve by eye towards the data we could not fit to, it appears that our expression would not match the lattice data.

The other form factor with data for $q^2 < -0.1$ that had to be omitted from the

fit was $W_0^{(6)}$ (see figure 5.4 bottom right). For this process, we fit the available data quite well. However it is apparent from the plot that our fit is not approaching the lattice data for $q^2 < 0$.

The LECs we varied to achieve our fit (shown in table 5.3) are very similar for the pion loop and octet loop case. We again note that the pion loop results are not particularly physical, but are used to help gauge the effect of K and η loops. The fact that the LECs are almost identical between the two fits suggests that K and η loops are not having an excessively large impact. We can also see that our fit is also slightly improved when including octet loops, which suggests that the loop corrections are small and the perturbative series is converging well.

Looking at our chiral extrapolation in figure 5.6 we can see that the pion loop and octet loop are in good agreement with each other. Results differ slightly for $W_0^{(1)}$ and $W_0^{(6)}$. This is most likely due to us having less data to fit our octet loop expression to. If there were more data available to use in our fit it is likely that the fits using pion loops and octet loops would be closer. We can also see that our curve is within the error bars for the extrapolated values of the form factors from the lattice data. The fact that a simple chiral extrapolation matches our third order chiral extrapolation suggests that loop effects are not small. The curves show very little variation with pion mass below $M_\pi \sim 0.2$ GeV, and for $W_0^{(5)}$ and $W_0^{(6)}$ there is little dependence on pion mass over the entire range $0 \leqslant M_\pi \leqslant 0.7$ GeV.

Calculating the percentage contribution due to loops at $M_\pi = M_\pi^{\text{phys}}$ (see table 5.4), the third order correction is generally high if the form factor is very close to 0. The octet loop fits have a larger contribution from the loops which can be attributed to the larger masses of the K and η compared to the pion.

We have also performed an augmented jackknife analysis on our results. We calculated χ^2 for every combination of two or more matrix elements and plotted the results against the reduced χ^2 values in figure 5.5. We can see that there

is some spread in the values of α and β, but the approximate relationship $\alpha \sim -\beta$ is generally respected by the results. We have used the mean and standard deviation of these results to predict our values of $\alpha = -0.008(5)$ GeV^3 and $\beta = 0.008(6)$ GeV^3. We have used the results using octet loops and not pion loops. These values of α and β are in agreement with the previous quoted values of $\alpha = -0.01122 \pm 0.0012_{\text{stat}} \pm 0.0022_{\text{syst}}$ GeV^3 and $\beta = 0.0120 \pm 0.0013_{\text{stat}} \pm 0.0023_{\text{syst}}$ GeV^3 from Aoki et al. [157].

These previous values of α and β were calculated using two point correlators on the lattice and then performing a simple linear extrapolation to the chiral limit. If we look at the extrapolation and ignore the data for the two heaviest light quark masses, it appears that the extrapolation would produce lower values of α and β, although they would still be within the error bars of our fit.

5.9 Conclusion

We have calculated one loop corrections to the matrix elements for proton decay using EOMS BChPT. Our expression contains the free parameters α and β, along with several other LECs that we constrained using LQCD data from Aoki et al. [156]. We performed a fit to an equation that only contained pion loop corrections, and to an equation that contained octet loop corrections. When we use corrections from the entire meson octet, we have to omit a small amount of lattice data as it lies outside the range of our expression.

For both pion loops and octet loops, we found values of α of $-0.007(3)$ GeV^3 and $-0.007(2)$ GeV^3 respectively, and for β we found $0.007(3)$ GeV^3 and $0.007(2)$ GeV^3 respectively. These values are slightly lower than previous results of α and β from LQCD by Aoki et al. [157] of $\alpha = -0.0112(25)$ GeV^3 and β=0.0120(26) GeV^3. All results were normalized at a scale $\mu = 2$ GeV.

For our final values of α and β we have used the average and standard deviation from the octet loop fits shown in figure 5.5 based on an augmented jackknife analysis. This gives us $\alpha = -0.008(5)$ GeV^3 and $\beta = 0.008(6)$ GeV^3.

In general there is very little dependence on whether pion loops or octet loops are used, as seen most clearly in our plots showing the variation of the form factors with M_π in figure 5.6. The difference noted in the case of the form factors $W_0^{(1)}$ and $W_0^{(6)}$ are due to data being excluded from the octet loop fit. It appears that the match between lattice and ChPT is best for the form factors $W_0^{(4)}$ and $W_0^{(5)}$. Our worst match is to the $W_0^{(2)}$ lattice data, although our chiral limit values are in agreement with those of Aoki et al. [157]. There is almost no dependence on the pion mass for $W_0^{(5)}$ and $W_0^{(6)}$, which suggests that lattice extrapolations for these form factors could be achieved with minimal input from ChPT.

It would be interesting to see if lattice data over a wider range of lepton momentum values is in agreement with our expressions for the form factors.

Chapter 6

Conclusions

In this thesis we have presented work on the axial coupling constant and the lifetime of the proton. For both of these pieces of work we have used lattice data to constrain any free parameters and also to compare the variation with M_π in lattice QCD and ChPT.

Work on the axial coupling constant is shown in chapter 4. Using SU(3) EOMS ChPT we calculated, up to $\mathcal{O}(p^4)$, the axial coupling constant for the baryon octet. We investigated the effect of including the decuplet explicitly, and also studied the HB limit, the effect of omitting $\mathcal{O}(p^4)$ corrections, and the SU(2) limit (which restricts us to studying only the axial coupling constant of the nucleon). To constrain the free parameters in our expression, we performed an augmented χ^2 fit to a combination of lattice data and experimental data. The majority of the lattice data was for the axial coupling constant of the nucleon.

Our best fit to the data was our $\mathcal{O}(p^4)$ EOMS expression with no decuplet contributions. However, to achieve this fit we had to allow some of the $\mathcal{O}(p^4)$ LECs to vary as free parameters (d_{1-3}). The $\mathcal{O}(p^4)$ contribution was quite large, and we also had to employ an augmented χ^2 fit as a regular fit would result in very unphysical values of the LECs.

Although the $\mathcal{O}(p^4)$ contributions with no decuplet were large, we found that the $\mathcal{O}(p^4)$ contributions that come from including the decuplet were very small. We set the $\mathcal{O}(p^4)$ decuplet contributions to 0 because of this.

We found that the lattice data for g_A^{pn} and the experimental data for the baryon axial coupling constants cannot be easily matched with a $\mathcal{O}(p^4)$ expression. The experimental data alone, however, can be matched very well with only a simple first order ChPT expression. We therefore conclude that the running of g_A^{pn} with M_π as calculated on the lattice cannot be matched well using ChPT up to order $\mathcal{O}(p^4)$. The ChPT perturbative series also has large contributions at high order. There is also some evidence that the lattice data is very sensitive to finite size effects, which could explain why the lower mass lattice data for g_A^{pn} is not in agreement with the well known experimental value.

Work on the proton lifetime is shown in chapter 5. We were not trying to calculate the lifetime of the proton, instead we were trying to constrain two LECs, α and β, that appear in the baryon-number-violating Lagrangian. To predict the proton lifetime additional parameters, known as Wilson coefficients, are required and ChPT cannot be used to calculate them.

We used EOMS ChPT to calculate the hadronic contribution to six matrix elements. The matrix elements can be split into two form factors known as the relevant and irrelevant form factor. The irrelevant one is suppressed by a power of the lepton mass and can therefore be ignored. We matched our expression to lattice data for the relevant form factor at varying final-state lepton energy q^2. The baryon-number-violating Lagrangian has only been calculated to leading order, and we required counter-terms from a higher order term in the Lagrangian. We showed that there are in total only six relevant structures for this calculation. We were able to determine how these LECs entered our expression by noting that the divergences in $W_0^{(4-6)}$ could be expressed in terms of the divergences contained

in $W_0^{(1-3)}$. For the LECs required from the third order EOMS Lagrangian we used the values obtained in chapter 4.

For work on proton decay we again used an augmented χ^2 to ensure the LECs were of natural order (of order $\mathcal{O}(1)$). We calculated two expressions, one with only pion loop contributions and one with pion, kaon and eta loop contributions. We refer to these as pion loop and octet loop expressions respectively. Our results were only valid in a finite range of parameter space, and for our octet loop expressions we were forced to omit some of the lattice data as it was not in a physically realistic area of parameter space. We should note that our pion loop results are not particularly realistic, and we only use them to try to quantify the impact octet loops have on our fit. The lattice data was calculated at four pion masses, ranging from 0.33 GeV to 0.67 GeV over a range of final lepton momentum $-0.2 < q^2 < 0.35$. We only included lattice data in our fit at the two lowest pion masses, $M_\pi = 0.33$ GeV and $M_\pi = 0.42$ GeV. We also showed our chiral extrapolation at $q^2 = 0$ and compared this with the extrapolation performed by Aoki et al. that did not use higher order ChPT.

Generally our match to the lattice data was fair. The form factor $W_0^{(2)}$ (the process $p \to K^0 e^+$) was our worst match, although surprisingly the chiral extrapolation of Aoki et al. agreed with our extrapolation at the chiral limit, but not for $M_\pi > 0$. We found the difference between pion loops and octet loops was small, with the LECs α_{1-3} and β_{1-3} being nearly identical in each case.

To establish values of α and β we re-sampled the lattice data set using a technique based on jackknife analysis that we termed an "augmented jackknife" analysis. We took all combinations of two or more matrix elements and performed a fit to the reduced data set. We used the average and standard deviation of these results to determine our values of α and β. We found that, for our pion loop expression, $\alpha = -0.008(1)$ GeV^2 and $\beta = 0.008(2)$ GeV^3. For our octet

loop expression we found $\alpha = -0.008(5)$ GeV^2 and $\beta = 0.008(6)$ GeV^3. These values are in agreement with previous determinations found in the literature that rely on a chiral extrapolation based only on tree level terms. Our results for the chiral limit values of the form factors are also in good agreement with previous determinations based only on first order ChPT.

Throughout this thesis we have used a combination of lattice QCD and ChPT results to investigate the properties of nucleons. We have seen that lattice QCD and ChPT do not agree well for g_A^{pn}, most likely due to a combination of large $\mathcal{O}(p^4)$ effects from ChPT and the impact of finite size effects on lattice results. The convergence of SU(3) ChPT is an important issue due to the relatively heavy kaon and eta, and we have shown that the expression for g_A does not appear to be converging at $\mathcal{O}(p^4)$. Caution may be needed when using ChPT to calculate finite size effects on the lattice. If the ChPT expression is not convergent, the finite size calculations are likely to be inaccurate.

We have also seen that, for calculating baryon decay matrix elements, a chiral extrapolation including higher-order terms leads us to the same results for α and β as a linear extrapolation. The effects of chiral loops are small in this case.

It is important to maintain an open dialogue between ChPT and lattice QCD to help test the validity of both approaches.

Appendices

Appendix A

Anatomy of a calculation

There are several methods of solving Feynman diagrams, in this section I shall outline the method used for the calculations presented in this thesis.

The general method used is known as Passarino Veltman decomposition [160]. It is a method that allows us to write a tensor integral in terms of a combination of scalar integrals.

For calculations with two propagators and one external momentum (for example zero momentum transfer form factor calculations) all expressions can be written in terms of the two basic integrals

$$\int \frac{d^4k}{(2\pi F)^4} \frac{1}{k^2 - M^2} \tag{A.1}$$

$$\int \frac{d^4k}{(2\pi F)^4} \frac{1}{(p-k)^2 - m^2} \frac{1}{k^2 - M^2}. \tag{A.2}$$

Throughout this work, we have regularised all integrals using dimensional regularisation. The first integral, eq. (A.1), is often referred to as a tadpole, as it naturally emerges from diagrams with a single propagator in the loop, which loosely resemble a tadpole. Any tadpole diagram can be rescaled to be put in the same form as eq. (A.1). More complicated tensor integrals (with two propagators), can always

be written in terms of the two scalar integrals, eqs (A.1) and (A.2). The idea of Passarino–Veltman decomposition is to note what rank of tensor the integral is, and then construct a tensor of the same rank using combinations of available four vectors and the metric tensor. For example, if we had an integral with $k^\mu k^\nu k^\rho$ in the numerator and the only other momenta in our problem was p^μ, the only ways to write a tensor of rank three would be

$$\begin{array}{ccc} g^{\mu\nu}p^\rho & g^{\mu\rho}p^\nu & g^{\nu\rho}p^\mu \\ & p^\mu p^\nu p^\rho & \end{array} \tag{A.3}$$

so we know our result must be in terms of these tensors. We can therefore write

$$\int \frac{d^4k}{(2\pi F)^4} \frac{k^\mu k^\nu k^\rho}{((p-k)^2 - m^2)(k^2 - M^2)} = g^{[\mu\nu}p^{\rho]} I_1^3 + p^\mu p^\nu p^\rho I_2^3 \tag{A.4}$$

where I_1^3 and I_2^3 are the solutions to the rank three tensor integral and we have used the notation

$$g^{[\mu\nu}p^{\rho]} = g^{\mu\nu}p^\rho + g^{\mu\rho}p^\nu + g^{\nu\rho}p^\mu. \tag{A.5}$$

Using the notation $k^{\mu_1\mu_2\cdots\mu_n} = k^{\mu_1}k^{\mu_2}\cdots k^{\mu_n}$, a general rank n tensor integral given by

$$\begin{aligned} \int \frac{d^4k}{(2\pi F)^4} \frac{k^{\mu_1\mu_2\cdots\mu_n}}{(k^2 - M_\pi^2)((p-k)^2 - m^2)} &= g^{[\mu_1\mu_2}\cdots g^{\mu_{n-1}\mu_n]} I_1^n \\ &+ g^{[\mu_1\mu_2}\cdots p^{\mu_{n-1}\mu_n]} I_2^n \\ &+ \cdots + p^{\mu_1\cdots\mu_n} I^n_{\frac{n+2}{2}} \end{aligned} \tag{A.6}$$

there will be $(n+2)/2$ solutions for even n and $(n+1)/2$ solutions for odd n.

To solve eq. (A.6) we can multiply both sides by $g_{\mu_1\mu_2}$ and use the substitution

$$k^2 = (k^2 - M_\pi^2) + M_\pi^2 \tag{A.7}$$

to express the left hand side in terms of tensors of lower rank. We can also multiply eq. (A.6) by p_{μ_1} and use the substitution

$$p \cdot k = \frac{1}{2}\left((k^2 - M_\pi^2) - ((p-k)^2 - m^2) + (p^2 - m^2 + M_\pi^2)\right). \tag{A.8}$$

It is useful to know the contraction of an arbitrary tensor with $g_{\mu\nu}$ and p_μ. In d dimensions we have

$$\begin{aligned} g_{\mu_1\mu_2} g^{[\mu_1\mu_2} \cdots p^{\mu_{n-m}\cdots\mu_n]} &= (d+n+m-1)\, g^{[\mu_3\mu_4} \cdots p^{\mu_{n-m}\cdots\mu_n]} \\ &\quad + p^2 g^{[\mu_3\mu_4} \cdots p^{\mu_{n-m+2}\cdots\mu_n]} \end{aligned} \tag{A.9}$$

where we can set $m = -1$ if there are no factors of p^{μ_i} present, and

$$\begin{aligned} p_{\mu_1} g^{[\mu_1\mu_2} \cdots p^{\mu_{n-m}\cdots\mu_n]} &= (m+2) g^{[\mu_2\mu_3} \cdots p^{\mu_{n-m-1}\cdots\mu_n]} \\ &\quad + p^2 g^{[\mu_2\mu_3} \cdots p^{\mu_{n-m+1}\cdots\mu_n]} \end{aligned} \tag{A.10}$$

for m even or odd. We can count the number of terms in eqs (A.9) and (A.10) using

$$N = \left(\frac{1}{(n/2)!}\binom{n}{2}\binom{n-2}{2}\cdots\binom{2}{2}\right)\binom{n+m}{m} \tag{A.11}$$

if there are $n/2$ factors of $g^{\mu\nu}$ and m factors of p^μ (in this notation n must always be even). Taking eq. (A.6) and setting $l = n$ (with n even) and contracting both sides with $g_{\mu_1\mu_2}$ after collecting together terms that have the same tensor structure, we have

$$(d+n-2)I_1^n + p^2 I_2^n = M_\pi^2 I_1^{n-2} + \frac{(d-1)!!\, m_N^{n-2}}{(d+n-4)!!}\Delta_\pi(m_N^2) \tag{A.12}$$

$$(d+n)I_2^n + p^2 I_3^n = M_\pi^2 I_2^{n-2} + \frac{(d-1)!!\, m_N^{n-4}}{(d+n-6)!!}\Delta_\pi(m_N^2) \tag{A.13}$$

$$\vdots$$

$$(d+n+2l-4)I_l^n + p^2 I_{l+1}^n = M_\pi^2 I_l^{n-2} + \frac{(d-1)!!\, m_N^{n-2l}}{(d+n-2l-2)!!}\Delta_\pi(m_N^2) \tag{A.14}$$

$$\vdots$$

$$(d+n+n-4)I_{\frac{n}{2}}^n + p^2 I_{\frac{n+2}{2}}^n = M_\pi^2 I_{\frac{n}{2}}^{n-2} + \Delta_\pi(m_N^2) \tag{A.15}$$

where we have used the double factorial $n!! = n(n-2)(n-4)\cdots$.

Similarly we can contract with p_{μ_1}

$$I_1^n + p^2 I_2^n = \frac{1}{2}\left(\Omega^2 I_1^{n-1} + \frac{(d-1)!!\, m_N^{n-2}}{(d+n-4)!!}\Delta_\pi(m_N^2)\right) \tag{A.16}$$

$$3I_2^n + p^2 I_3^n = \frac{1}{2}\left(\Omega^2 I_2^{n-1} + \frac{(d-1)!!\, m_N^{n-4}}{(d+n-6)!!}\Delta_\pi(m_N^2)\right) \tag{A.17}$$

$$\vdots$$

$$(2l-1)I_l^n + p^2 I_{l+1}^n = \frac{1}{2}\left(\Omega^2 I_l^{n-1} + \frac{(d-1)!!\, m_N^{n-2l}}{(d+n-2l-2)!!}\Delta_\pi(m_N^2)\right) \tag{A.18}$$

$$\vdots$$

$$(n-1)I_{\frac{n}{2}}^n + p^2 I_{\frac{n+2}{2}}^n = \frac{1}{2}\left(\Omega^2 I_{\frac{n}{2}}^{n-1} + \Delta_\pi(m_N^2)\right) \tag{A.19}$$

where we have used $\Omega^2 = p^2 - m^2 + M_\pi^2$. Solving the two simultaneous equations, eqns (A.18) and (A.18), we get

$$I_l^n = \frac{1}{2(d-3+n)}\Big(2M_\pi^2 I_l^{n-2} - \Omega^2 I_l^{n-1} + \frac{(d-1)!!\, m_N^{n-2l}}{(d+n-2l-2)!!}\Delta_\pi(m_N^2)\Big) \tag{A.20}$$

$$\begin{aligned} I_{l+1}^n = \frac{1}{2p^2(d-3+n)}\Big(&2(1-2l)M_\pi^2 I_l^{n-2} + (d+n+2l-4)\Omega^2 I_l^{n-1} \\ &+ (d+n-2m-2)\frac{(d-1)!!\, m_N^{n-2l}}{(d+n-2l-2)!!}\Delta_\pi(m_N^2)\Big) \end{aligned} \tag{A.21}$$

These equations are valid for $l \leqslant n/2$.

We can repeat the process for an odd rank tensor in eq. (A.6). Setting $l = n+1$

with n even we have

$$I_l^{n+1} = \frac{1}{2(d-2+n)}\Big(2M_\pi^2 I_l^{n-1} - \Omega^2 I_{l+1}^n + \frac{(d-2)!!\, m_N^{n-2l+2}}{(d+n-2l-2)!!}\Delta_\pi(m_N^2)\Big) \tag{A.22}$$

$$\begin{aligned} I_{l+1}^{n+1} = \frac{1}{2p^2(d-2+n)}\Big(&- 4lM_\pi^2 I_l^{n-1} + (d+n-2l-2)\Omega^2 I_{l+1}^{n-1} \\ &+ (d+n-2l-2)\frac{(d-2)!!\, m_N^{n-2l+2}}{(d+n-2l-3)!!}\Delta_\pi(m_N^2)\Big) \end{aligned} \tag{A.23}$$

for $0 < l \leqslant n/2$ and $n > 1$. For odd tensor integrals we also have the extra relationship (for $n > 1$)

$$I_1^{n+1} = \frac{(d-2)!!}{2p^2(d+n-2)!!}\left((m_N^n\Delta_\pi(m_N^2) - M_\pi^n\Delta(M_\pi^2)\right) + \frac{\Omega^2}{2p^2}I_{n+1}^n. \tag{A.24}$$

The presence of the extra relation allows for some redundancy in how expressions with an odd number of tensors can be expressed in terms of the I_i^ns, although the different expressions will be identical when expressed solely in terms of $\Delta_\pi(M^2)$ and I_1^0.

The presence of the double factorial means that the recursion relations cannot be easily solved, and we have not found a simple expression for an arbitrary I_i^n in terms of $\Delta_\pi(M^2)$ and I_0, which are given by

$$\Delta_\pi(M^2) = 2LM^2 - \frac{M^2(\alpha-1)}{16\pi^2} + \frac{M^2}{16\pi^2}\log\left(\frac{M^2}{\mu^2}\right) \tag{A.25}$$

$$\begin{aligned} I_1^0 = 2L - \frac{\alpha}{16\pi^2} + \frac{\Omega^2}{32\pi^2p^2}\log\left(\frac{M^2}{m^2}\right) \\ + \frac{1}{16\pi^2}\log\left(\frac{m^2}{\mu^2}\right) + \frac{mM\sqrt{1-\frac{\Omega^4}{4m^2M^2}}}{8\pi^2p^2}\arccos\left(-\frac{\Omega^2}{2mM}\right) \end{aligned} \tag{A.26}$$

where we can choose $\alpha = 1, 2$ depending on our choice of renormalisation scheme. Throughout this thesis we have used the modified minimal subtraction scheme, $\overline{\text{MS}}$ corresponding to $\alpha = 2$ in order to subtract the divergent parts of loop integrals.

The parameter L is given by

$$L = \frac{\mu^{d-4}}{16\pi^2}\left(\frac{1}{d-4} - \frac{1}{2}(\log(4\pi) - \gamma + 1)\right) \tag{A.27}$$

and γ is the Euler–Mascheroni constant, $\gamma = 0.577\cdots$.

For the calculations in this thesis, the program FORM was used to perform simplifications to the Dirac algebra and to express results in terms of the integrals I_i^j described in this appendix. To study the analytical form of the functions encountered in this work, and to plot them, the software package Mathematica was used.

The extension for an arbitrary number of propagators can be found in work by Denner [161].

Appendix B

Expressions for g_A calculation

We can write the axial coupling constant as

$$\begin{aligned} g_{ij} = T_{ij} + A_{ij} &+ \sum_{\phi}^{\pi K \eta} \left(B_T^{\phi} \alpha_{ij}^{\phi} + B_{L1}^{\phi} \beta_{ij}^{\phi} + B_{L2}^{\phi} \gamma_{ij}^{\phi} + D_{L1}^{\phi} \delta_{ij}^{\phi} + D_{L2}^{\phi} \varepsilon_{ij}^{\phi} \right) \\ &+ \sum_{\phi}^{\pi K \eta} \left(B_{L3}^{\phi} \rho_{ij}^{\phi} + B_{L4}^{\phi} \sigma_{ij}^{\phi} + B_{L5}^{\phi} \tau_{ij}^{\phi} \right) \\ &+ \sum_{\phi}^{\pi K \eta} \left(D_{L4A}^{\phi} \kappa_{ij}^{\phi} + D_{L4B}^{\phi} \lambda_{ij}^{\phi} + D_{L5A}^{\phi} \mu_{ij}^{\phi} + D_{L5B}^{\phi} \nu_{ij}^{\phi} \right). \end{aligned} \tag{B.1}$$

For the SU(2) expression, we only use $\phi = \pi$ in eq. (B.1) and note that the SU(2) version of $B_0 A_{pn}$ is given by $4d_{16}M_\pi^2$. The expressions for the integrals can be found in appendix A, and we have used

$$I_i^{j\prime}(m^2, M_\phi^2) = \frac{\partial}{\partial m^2} I_i^j(m^2, M_\phi^2) \tag{B.2}$$

$$K_i^j(m_\Delta^2, m_N^2, M_\phi^2) = \frac{1}{m_\Delta - m_N} \Big(I_i^j(m_\Delta^2, M_\phi^2) - I_i^j(m_N^2, M_\phi^2) \Big). \tag{B.3}$$

The loop functions are given by

$$B_T^\phi = \Delta_\pi(M_\phi^2) \tag{B.4}$$

$$B_{L1}^\phi = -\Delta_\pi(M_\phi^2) - 2M_N^2 I_1^1(m_N^2, M_\phi^2) \tag{B.5}$$

$$\begin{aligned} B_{L2}^\phi = \Delta_\pi(M_\phi^2) + 4M_N^2\Big(& I_1^1(m_N^2, M_\phi^2) + (d-2)I_1^{2\prime}(m_N^2, M_\phi^2) \\ & + M_N^2 I_2^{2\prime}(m_N^2, M_\phi^2)\Big) \end{aligned} \tag{B.6}$$

$$\begin{aligned} D_{L1}^\phi = \frac{d-2}{M_\Delta^2(d-1)}\Big(& 4M_N^3(M_\Delta + M_N)K_1^2(m_\Delta^2, m_N^2, M_\phi^2) \\ & - 4M_N^3(M_\Delta + 2M_N)K_1^3(m_\Delta^2, m_N^2, M_\phi^2) \\ & - M_N^4 K_2^5(m_\Delta^2, m_N^2, M_\phi^2) \\ & + M_N^3(M_\Delta + 5M_N)K_2^4(m_\Delta^2, m_N^2, M_\phi^2) \\ & - M_N^2(d+4)K_1^5(m_\Delta^2, m_N^2, M_\phi^2) \\ & + M_N(M_\Delta(2+d) + M_N(8+3d))K_1^4(m_\Delta^2, m_N^2, M_\phi^2)\Big) \end{aligned} \tag{B.7}$$

$$\begin{aligned} D_{L2}^\phi = \frac{M_N^2(d-3)(d-2)(d+1)}{M_\Delta^3(d-1)^2}\Big(& M_N^3(M_\Delta + M_N)^2 I_1^{2\prime}(m_\Delta^2, M_\phi^2) \\ & - M_N^3(M_\Delta + M_N)(\Delta + 3M_N)I_1^{3\prime}(m_\Delta^2, M_\phi^2) \\ & + M_N^4(2M_\Delta + 3M_N)I_2^{4\prime}(m_\Delta^2, M_\phi^2) - M_N^3(d+4)I_1^{5\prime}(m_\Delta^2, M_\phi^2) \\ & + M_N^2(2M_\Delta(d+1) + M_N(d+4))I_1^{4\prime}(m_\Delta^2, M_\phi^2) \\ & - M_N^5 I_2^{5\prime}(m_\Delta^2, M_\phi^2)\Big) \end{aligned} \tag{B.8}$$

$$B_{L3}^\phi = 2M_N I_1^2(m_N^2, M_\phi^2) \tag{B.9}$$

$$B_{L4}^\phi = 2M_N^2\left(I_1^2(m_N^2, M_\phi^2) + M_N^2 I_2^2(m_N^2, M_\phi^2)\right) \tag{B.10}$$

$$B_{L5}^\phi = 4M_N\left((1-d)I_1^2(m_N^2, M_\phi^2) - M_N^2 I_2^2(m_N^2, M_\phi^2)\right) \tag{B.11}$$

$$
\begin{aligned}
D^{\phi}_{L4A} = & \frac{(d-2)(d+1)M_N\left(M_\Delta - M_N\right)}{d-1} I_1^2(m_\Delta^2, M_\phi^2) \\
& + \frac{(d-2)M_N^2\left(3M_\Delta - \mathrm{dM}_N\right)}{(d-1)M_\Delta} I_1^3(m_\Delta^2, M_\phi^2) \\
& + \frac{d\left(d^2-4\right)M_N}{(d-1)M_\Delta} I_1^4(m_\Delta^2, M_\phi^2) + \frac{(d-2)dM_N^2}{(d-1)M_\Delta} I_2^4(m_\Delta^2, M_\phi^2)
\end{aligned} \tag{B.12}
$$

$$
\begin{aligned}
D^{\phi}_{L4B} = & -\frac{(d-3)(d-2)M_N\left(M_\Delta - M_N\right)}{d-1} I_1^2(m_\Delta^2, M_\phi^2) \\
& + \frac{(d-2)M_N^2\left((d-2)M_N + 3M_\Delta\right)}{(d-1)M_\Delta} I_1^3(m_\Delta^2, M_\phi^2) \\
& - \frac{(d-2)^2 M_N}{(d-1)M_\Delta}\left((d+2)I_1^4(m_\Delta^2, M_\phi^2) + M_N^2 I_2^4(m_\Delta^2, M_\phi^2)\right)
\end{aligned} \tag{B.13}
$$

$$
\begin{aligned}
D^{\phi}_{L5A} = & -\frac{(d-5)(d-2)M_N\left(M_\Delta - M_N\right)}{d-1} I_1^2(m_\Delta^2, M_\phi^2) \\
& - \frac{(d-2)M_N^2\left(dM_N + M_\Delta\right)}{(d-1)M_\Delta} I_1^3(m_\Delta^2, M_\phi^2) \\
& + \frac{d\left(d^2-4\right)M_N}{(d-1)M_\Delta} I_1^4(m_\Delta^2, M_\phi^2) + \frac{(d-2)dM_N^3}{(d-1)M_\Delta} I_2^4(m_\Delta^2, M_\phi^2)
\end{aligned} \tag{B.14}
$$

$$
\begin{aligned}
D^{\phi}_{L5B} = & -\frac{(d-2)(3d-7)M_N\left(M_\Delta - M_N\right)}{d-1} I_1^2(m_\Delta^2, M_\phi^2) \\
& + \frac{(d-2)M_N^2\left((d-2)M_N - M_\Delta\right)}{(d-1)M_\Delta} I_1^3(m_\Delta^2, M_\phi^2) \\
& - \frac{(d-2)^2 M_N}{(d-1)M_\Delta}\left((d+2)I_1^4(m_\Delta^2, M_\phi^2) + M_N^2 I_2^4(m_\Delta^2, M_\phi^2)\right)
\end{aligned} \tag{B.15}
$$

and the wavefunction renormalisation diagrams are given by (noting that $p^2 = \not{p}^2$)

$$
\begin{aligned}
Z^{\phi}_{N,ij} = & 1 - \frac{\partial}{\partial \not{p}}\Big(\not{p}(p^2 - M_N^2) I_1^1(m_N^2, M_\phi^2) - (\not{p} + M_N) d I_1^2(m_N^2, M_\phi^2) \\
& - (\not{p} + M_N) p^2 I_2^2(m_N^2, M_\phi^2)\Big)
\end{aligned} \tag{B.16}
$$

$$
Z^{\phi}_{\Delta,ij} = 1 - \frac{\partial}{\partial \not{p}}\Big(\frac{(d-2)p^2}{M_\Delta^2}(\not{p} I_1^3(m_\Delta^2, M_\phi^2) - (M_\Delta + \not{p}) I_1^2(m_\Delta^2, M_\phi^2))\Big). \tag{B.17}
$$

The coefficients of eq. (B.1) are given in the following equations and tables.

$$
\begin{array}{lll}
T_{pn} = D_0 + F_0 & T_{\Lambda p} = -\frac{D_0+3F_0}{\sqrt{6}} & T_{\Sigma^- \Lambda} = \sqrt{\frac{2}{3}} D_0 \\
T_{\Sigma^- n} = D_0 - F_0 & T_{\Xi^- \Lambda} = -\frac{D_0-3F_0}{\sqrt{6}} & T_{\Xi^0 \Sigma^+} = D_0 + F_0 \\
T_{\Sigma^+ \Sigma^+} = 2F_0 & T_{\Xi^0 \Xi^0} = F_0 - D_0 &
\end{array}
\tag{B.18}
$$

$$
\begin{aligned}
A_{pn} = \frac{8}{3}\Big(& \left(h_{38} + 3h_{40} + 2h_{44}\right) B_0 \left(2m + m_s\right) \\
& - 2\left(h_{38} - h_{44}\right) B_0 \left(m - m_s\right) \Big)
\end{aligned}
\tag{B.19}
$$

$$
\begin{aligned}
A_{\Lambda p} = \frac{4}{3}\sqrt{\frac{2}{3}}\Big(& \left(h_{39} - 2h_{38} - 6h_{40} + 3h_{41} + 2h_{43} - 4h_{44}\right) B_0 \left(2m + m_s\right) \\
& + \left(4h_{38} + h_{39} - h_{43} + 2h_{44}\right) B_0 \left(m - m_s\right) \Big)
\end{aligned}
\tag{B.20}
$$

$$
\begin{aligned}
A_{\Lambda \Sigma^-} = \frac{4}{3}\sqrt{\frac{2}{3}}\Big(& \left(h_{38} + h_{39} + 3h_{40} + 3h_{41} + 2h_{43} + 2h_{44}\right) B_0 \left(2m + m_s\right) \\
& + \left(h_{38} + h_{39} + 2\left(h_{43} + h_{44}\right)\right) B_0 \left(m - m_s\right) \Big)
\end{aligned}
\tag{B.21}
$$

$$
\begin{aligned}
A_{\Sigma^- n} = \frac{8}{3}\Big(& \left(h_{39} + 3h_{41} + 2h_{43}\right) B_0 \left(2m + m_s\right) \\
& + \left(h_{39} - h_{43}\right) B_0 \left(m - m_s\right) \Big)
\end{aligned}
\tag{B.22}
$$

$$
\begin{aligned}
A_{\Xi^- \Lambda} = \frac{4}{3}\sqrt{\frac{2}{3}}\Big(& \left(h_{38} - 2h_{39} + 3h_{40} - 6h_{41} - 4h_{43} + 2h_{44}\right) B_0 \left(2m + m_s\right) \\
& + \left(h_{38} + 4h_{39} + 2h_{43} - h_{44}\right) B_0 \left(m - m_s\right) \Big)
\end{aligned}
\tag{B.23}
$$

$$
\begin{aligned}
A_{\Xi^0 \Sigma^+} = \frac{8}{3}\Big(& \left(h_{38} + 3h_{40} + 2h_{44}\right) B_0 \left(2m + m_s\right) \\
& + \left(h_{38} - h_{44}\right) B_0 \left(m - m_s\right) \Big)
\end{aligned}
\tag{B.24}
$$

$$
\begin{aligned}
A_{\Sigma^+ \Sigma^+} = \frac{4}{3}\sqrt{2}\Big(& \left(h_{38} - h_{39} + 3h_{40} - 3h_{41} - 2h_{43} + 2h_{44}\right) B_0 \left(2m + m_s\right) \\
& + \left(h_{38} - h_{39} - 2h_{43} + 2h_{44}\right) B_0 \left(m - m_s\right) \Big)
\end{aligned}
\tag{B.25}
$$

$$
\begin{aligned}
A_{\Xi^0 \Xi^0} = \frac{4}{3}\sqrt{2}\Big(& - \left(h_{39} + 3h_{41} + 2h_{43}\right) B_0 \left(2m + m_s\right) \\
& + 2\left(h_{39} - h_{43}\right) B_0 \left(m - m_s\right) \Big)
\end{aligned}
\tag{B.26}
$$

α^{ϕ}_{np}	$-2(D_0+F_0)$	$-D_0-F_0$	0
β^{ϕ}_{np}	$-\frac{1}{4}(D_0+F_0)^3$	$-\frac{1}{3}(D_0-F_0)(D_0^2+3F_0^2)$	$\frac{1}{12}(D_0-3F_0)^2(D_0+F_0)$
γ^{ϕ}_{np}	$-2D_0-2F_0$	$-D_0-F_0$	0
δ^{ϕ}_{np}	$-\frac{4}{3}C_A^2(D_0+F_0)$	$-\frac{1}{6}C_A^2(3D_0+F_0)$	0
ε^{ϕ}_{np}	$-\frac{10}{9}HC_A^2$	$-\frac{2}{9}HC_A^2$	0
ρ^{ϕ}_{np}	$-4(b_1+b_2+b_3+2b_4)$ $\times(D_0+F_0)$	$-\frac{4}{3}(3b_1(5D_0-3F_0)$ $+b_2(7F_0-9D_0))$ $+3b_3(D_0+F_0)$	$-\frac{4}{3}(3b_1-b_2+b_3)$ $\times(3D_0-F_0)$
σ^{ϕ}_{np}	0	0	0
τ^{ϕ}_{np}	$-2(d_1+d_2)(D_0+F_0)$	$\frac{1}{3}d_1(F_0-3D_0)$ $+\frac{1}{4}(d_3(F_0-D_0)$ $-4d_2(D_0+F_0))$	0
κ^{ϕ}_{np}	$-\frac{5}{6}f_4C_A$	$-\frac{1}{24}(f_1+5f_4)C_A$	0
λ^{ϕ}_{np}	$\frac{1}{6}(f_3-2f_2)C_A$	$\frac{1}{24}(f_3-f_2)C_A$	0
μ^{ϕ}_{np}	0	$-\frac{1}{24}(f_1+f_4)C_A$	0
ν^{ϕ}_{np}	$\frac{1}{3}f_2C_A$	$\frac{1}{24}(f_2-f_3)C_A$	0

Table B.1: Coefficients that occur in eq. (B.1) for the axial decay $n \to p$. The second, third and fourth columns show the contribution from pion loops, kaon loops and eta loops respectively.

$\alpha^{\phi}_{\Lambda p}$	$\frac{1}{4}\sqrt{\frac{3}{2}}(D_0+3F_0)$	$\frac{1}{2}\sqrt{\frac{3}{2}}(D_0+3F_0)$	$\frac{1}{4}\sqrt{\frac{3}{2}}(D_0+3F_0)$
$\beta^{\phi}_{\Lambda p}$	$\frac{1}{2}\sqrt{\frac{3}{2}}D_0(D_0^2-F_0^2)$	$-\frac{1}{6\sqrt{6}}(D_0-3F_0)(5D_0^2-9F_0^2)$	$-\frac{1}{6\sqrt{6}}D_0(D_0^2-9F_0^2)$
$\gamma^{\phi}_{\Lambda p}$	$\sqrt{\frac{3}{32}}(D_0+3F_0)$	$\frac{1}{2}\sqrt{\frac{3}{2}}(D_0+3F_0)$	$\frac{1}{2}\sqrt{\frac{3}{2}}D_0-\frac{1}{4}\sqrt{\frac{3}{2}}(D_0-3F_0)$
$\delta^{\phi}_{\Lambda p}$	$\sqrt{\frac{3}{32}}C_A^2(5D_0+F_0)$	$\frac{3}{4\sqrt{6}}C_A^2(D_0+F_0)$	0
$\varepsilon^{\phi}_{\Lambda p}$	$\sqrt{\frac{2}{3}}HC_A^2$	$\frac{1}{\sqrt{6}}HC_A^2$	0
$\rho^{\phi}_{\Lambda p}$	$\sqrt{\frac{3}{2}}((3b_1-b_2+3b_3)\times(D_0+F_0)+2(b_1-3b_2+b_3)F_0)$	$\frac{1}{3}\sqrt{\frac{2}{3}}(27b_1(5D_0-F_0)+3(b_3+4b_4)(3D_0+F_0)+b_2(37F_0-33D_0))$	$\frac{1}{\sqrt{6}}(9b_1-11b_2-3b_3)\times(D_0-F_0)$
$\sigma^{\phi}_{\Lambda p}$	$\sqrt{\frac{3}{2}}((3b_5+b_6+3b_7)\times(D_0+F_0)+2(b_5-b_6+b_7)F_0)$	$\sqrt{\frac{2}{3}}(4b_6F_0-(3b_5+b_6+3b_7)(3D_0+F_0))$	$\sqrt{\frac{3}{2}}(3b_5+b_6+3b_7)\times(D_0-F_0)$
$\tau^{\phi}_{\Lambda p}$	$\sqrt{\frac{3}{32}}(d_1(D_0+3F_0)+d_2(3D_0+F_0)-2d_3F_0)$	$\frac{2}{4\sqrt{6}}d_1(3D_0+5F_0)+6d_2(3D_0+F_0)+3d_3(D_0+F_0)$	$\frac{1}{4\sqrt{6}}d_1(3D_0+F_0)+3d_2(3D_0+F_0)+2d_3F_0$
$\kappa^{\phi}_{\Lambda p}$	$-\frac{1}{8}\sqrt{\frac{3}{2}}\,(f_1-3f_4)\,C_A$	$\frac{1}{4}\sqrt{\frac{3}{2}}f_4C_A$	0
$\lambda^{\phi}_{\Lambda p}$	$\frac{1}{8}\sqrt{\frac{3}{2}}\,(f_2-f_3)\,C_A$	$-\frac{1}{4\sqrt{6}}f_3C_A$	0
$\mu^{\phi}_{\Lambda p}$	0	$-\frac{1}{8}\sqrt{\frac{3}{2}}\,(f_1+f_4)\,C_A$	0
$\nu^{\phi}_{\Lambda p}$	$\frac{1}{\sqrt{6}}f_3C_A$	$-\frac{1}{8\sqrt{6}}\,(3f_2+f_3)\,C_A$	0

Table B.2: Coefficients that occur in eq. (B.1) for the axial decay $\Lambda \to p$. The second, third and fourth columns show the contribution from pion loops, kaon loops and eta loops respectively.

$\alpha^{\phi}_{\Sigma^-\Lambda}$	$-2\sqrt{\frac{2}{3}}D_0$	$-\sqrt{\frac{2}{3}}D_0$	0
$\beta^{\phi}_{\Sigma^-\Lambda}$	$\frac{1}{3}\sqrt{\frac{2}{3}}D_0(D_0^2-6F_0^2)$	$\frac{1}{\sqrt{6}}D_0(F_0^2-D_0^2)$	$-\frac{1}{3}\sqrt{\frac{2}{3}}D_0^3$
$\gamma^{\phi}_{\Sigma^-\Lambda}$	$-2\sqrt{\frac{2}{3}}D_0$	$-2\frac{2}{\sqrt{6}}D_0$	0
$\delta^{\phi}_{\Sigma^-\Lambda}$	$-\frac{1}{6\sqrt{6}}C_A^2(D_0+6F_0)$	$-\frac{1}{3}\sqrt{\frac{2}{3}}C_A^2(2D_0+3F_0)$	$-\frac{1}{2\sqrt{6}}D_0C_A^2$
$\varepsilon^{\phi}_{\Sigma^-\Lambda}$	$-\frac{1}{3}\sqrt{\frac{2}{3}}HC_A^2$	$-\frac{1}{3\sqrt{6}}HC_A^2$	0
$\rho^{\phi}_{\Sigma^-\Lambda}$	$\frac{8}{3}\sqrt{\frac{2}{3}}(3b_1-7b_2-3b_4)F_0$	$-4\sqrt{\frac{2}{3}}(3b_3D_0$ $-(b_1+b_2)F_0)$	0
$\sigma^{\phi}_{\Sigma^-\Lambda}$	$8\sqrt{\frac{2}{3}}(b_6D_0-(b_5+b_7)F_0)$	$-8\sqrt{\frac{2}{3}}(b_6D_0-(b_5+b_7)F_0)$	0
$\tau^{\phi}_{\Sigma^-\Lambda}$	$-\frac{1}{2\sqrt{6}}(8d_1D_0$ $+(8d_2+3d_3)F_0)$	$\frac{1}{\sqrt{6}}((d_3-2d_2)F_0$ $-2d_1D_0)$	$\frac{1}{\sqrt{6}}d_3F_0$
$\kappa^{\phi}_{\Sigma^-\Lambda}$	0	$-\frac{1}{4\sqrt{6}}(f_1+4f_4)C_A$	$-\frac{1}{4\sqrt{6}}(f_1+f_4)C_A$
$\lambda^{\phi}_{\Sigma^-\Lambda}$	$\frac{1}{6\sqrt{6}}(f_3-3f_2)C_A$	$-\frac{1}{12\sqrt{6}}(3f_2+2f_3)C_A$	0
$\mu^{\phi}_{\Sigma^-\Lambda}$	$-\frac{1}{4\sqrt{6}}(f_1+f_4)C_A$	$-\frac{1}{4\sqrt{6}}(f_1+f_4)C_A$	0
$\nu^{\phi}_{\Sigma^-\Lambda}$	$\frac{1}{2\sqrt{6}}(f_2+f_3)C_A$	$\frac{1}{4\sqrt{6}}(f_2+f_3)C_A$	0

Table B.3: Coefficients that occur in eq. (B.1) for the axial decay $\Sigma^- \to \Lambda$. The second, third and fourth columns show the contribution from pion loops, kaon loops and eta loops respectively.

$\alpha^{\phi}_{\Sigma^- n}$	$\frac{3}{4}(F_0 - D_0)$	$-\frac{3}{2}(D_0 - F_0)$	$-\frac{3}{4}(D_0 - F_0)$
$\beta^{\phi}_{\Sigma^- n}$	$\frac{1}{6}(2D_0^2F_0 - 3D_0F_0^2$ $-D_0^3 - 6F_0^3)$	$-\frac{1}{6}(D_0 + F_0)(D_0^2 + 3F_0^2)$	$-\frac{1}{6}D_0(D_0-3F_0)(D_0-F_0)$
$\gamma^{\phi}_{\Sigma^- n}$	$-\frac{3}{4}(D_0 - F_0)$	$-\frac{3}{2}(D_0 - F_0)$	$-\frac{3}{4}(D_0 - F_0)$
$\delta^{\phi}_{\Sigma^- n}$	$-\frac{1}{6}C_A^2(D_0 + 5F_0)$	$-\frac{1}{12}C_A^2(D_0 + 5F_0)$	$\frac{1}{12}C_A^2(D_0 - 3F_0)$
$\varepsilon^{\phi}_{\Sigma^- n}$	$\frac{2}{9}HC_A^2$	$\frac{1}{9}HC_A^2$	0
$\rho^{\phi}_{\Sigma^- n}$	$b_2(-9D_0 - \frac{17F_0}{3})$ $+b_3(F_0 - 5D_0)$ $+b_1(19D_0 + 9F_0)$	$-2(3b_3 - 4b_4)(D_0 - F_0)$ $+2b_1(7D_0 + F_0)$ $-\frac{2}{3}b_2(3D_0 + 13F_0)$	$\frac{1}{3}(3b_1-b_2-b_3)(3D_0+F_0)$
$\sigma^{\phi}_{\Sigma^- n}$	$b_5(F_0 - 5D_0)$ $+b_7(F_0 - 5D_0)$ $+\frac{5}{3}b_6(3D_0 + F_0)$	$2b_5(D_0 - F_0)$ $-2b_7(F_0 - D_0)$ $-\frac{2}{3}b_6(3D_0 + F_0)$	$(b_5 - b_6 + b_7)(3D_0 + F_0)$
$\tau^{\phi}_{\Sigma^- n}$	$\frac{1}{12}(9d_2(D_0 - F_0)$ $+d_1(F_0 - 9D_0))$	$\frac{1}{12}(18d_2(D_0 - F_0)$ $+3d_3(D_0 + F_0)$ $-2d_1(9D_0 - 5F_0))$	$-\frac{3}{4}(d_1 - d_2)(D_0 - F_0)$
$\kappa^{\phi}_{\Sigma^- n}$	$-\frac{1}{12}(f_1 + f_4)C_A$	$-\frac{1}{12}(4f_1 + f_4)C_A$	$-\frac{1}{24}(f_1 + f_4)C_A$
$\lambda^{\phi}_{\Sigma^- n}$	$\frac{1}{12}(f_2 - f_3)C_A$	$-\frac{1}{12}(4f_2 + f_3)C_A$	$-\frac{1}{24}(3f_2 + f_3)C_A$
$\mu^{\phi}_{\Sigma^- n}$	$-\frac{1}{3}(f_1 + f_4)C_A$	$-\frac{1}{8}(f_1 + f_4)C_A$	0
$\nu^{\phi}_{\Sigma^- n}$	$\frac{1}{3}(f_2 + 2f_3)C_A$	$\frac{1}{24}(f_2 + 3f_3)C_A$	0

Table B.4: Coefficients that occur in eq. (B.1) for the axial decay $\Sigma \to n$. The second, third and fourth columns show the contribution from pion loops, kaon loops and eta loops respectively.

$\alpha^{\phi}_{\Xi^-\Lambda}$	$\frac{1}{4}\sqrt{\frac{3}{2}}(D_0-3F_0)$	$\frac{1}{2}\sqrt{\frac{3}{2}}(D_0-3F_0)$	$\frac{1}{4}\sqrt{\frac{3}{2}}(D_0-3F_0)$
$\beta^{\phi}_{\Xi^-\Lambda}$	$\frac{1}{2}\sqrt{\frac{3}{2}}D_0(D_0^2-F_0^2)$	$-\frac{1}{6\sqrt{6}}(D_0+3F_0)$ $\times(5D_0^2-9F_0^2)$	$-\frac{1}{6\sqrt{6}}D_0(D_0^2-9F_0^2)$
$\gamma^{\phi}_{\Xi^-\Lambda}$	$\frac{1}{4}\sqrt{\frac{3}{2}}(D_0-3F_0)$	$\frac{1}{2}\sqrt{\frac{3}{2}}(D_0-3F_0)$	$\frac{1}{4}\sqrt{\frac{3}{2}}(D_0-3F_0)$
$\delta^{\phi}_{\Xi^-\Lambda}$	$\frac{1}{4\sqrt{6}}C_A^2(3F_0-D_0)$	$-\frac{1}{4}\sqrt{\frac{3}{2}}C_A^2(D_0-F_0)$	$-\frac{1}{2\sqrt{6}}D_0C_A^2$
$\varepsilon^{\phi}_{\Xi^-\Lambda}$	$-\frac{1}{\sqrt{6}}HC_A^2$	$-\frac{1}{\sqrt{6}}HC_A^2$	0
$\rho^{\phi}_{\Xi^-\Lambda}$	$\sqrt{\frac{3}{2}}(b_2(D_0-7F_0)$ $+b_3(3D_0-5F_0)$ $+b_1(5F_0-3D_0))$	$\sqrt{\frac{2}{3}}((b_3-4b_4)(3D_0-F_0)$ $-9b_1(5D_0+F_0)$ $+b_2(11D_0+\frac{37}{3}F_0))$	$-\frac{1}{\sqrt{6}}(9b_1-11b_2+3b_3)$ $\times(D_0+F_0)$
$\sigma^{\phi}_{\Xi^-\Lambda}$	$\sqrt{\frac{3}{2}}((3b_5-b_6+3b_7)$ $\times(D_0-F_0)$ $-2(b_5+b_6+b_7)F_0)$	$\sqrt{\frac{2}{3}}(4b_6F_0$ $-(3b_5-b_6+3b_7)$ $\times(3D_0-F_0))$	$\sqrt{\frac{3}{2}}(3b_5-b_6+3b_7)$ $\times(D_0+F_0)$
$\tau^{\phi}_{\Xi^-\Lambda}$	$\frac{1}{4}\sqrt{\frac{3}{2}}(d_1(D_0-3F_0)$ $+d_2(F_0-3D_0)$ $-2d_3F_0)$	$\frac{1}{2\sqrt{6}}(d_1(3D_0-5F_0)$ $+d_2(3F_0-9D_0)$ $+2d_3F_0)$	$-\frac{1}{4\sqrt{6}}(d_1-3d_2-d_3)$ $\times(F_0-3D_0)$
$\kappa^{\phi}_{\Xi^-\Lambda}$	$\frac{1}{8}\sqrt{\frac{3}{2}}f_1C_A$	$\frac{1}{8}\sqrt{\frac{3}{2}}\,(f_1-f_4)\,C_A$	$\frac{1}{8\sqrt{6}}\,(f_1-2f_4)\,C_A$
$\lambda^{\phi}_{\Xi^-\Lambda}$	$\frac{1}{8\sqrt{6}}\,(2f_3-3f_2)\,C_A$	$\frac{1}{8}\sqrt{\frac{3}{2}}\,(f_2+f_3)\,C_A$	$\frac{1}{8}\sqrt{\frac{3}{2}}f_2C_A$
$\mu^{\phi}_{\Xi^-\Lambda}$	$\frac{1}{8}\sqrt{\frac{3}{2}}\,(f_1+f_4)\,C_A$	$\frac{1}{2\sqrt{6}}\,(f_1+f_4)\,C_A$	0
$\nu^{\phi}_{\Xi^-\Lambda}$	$-\frac{1}{8}\sqrt{\frac{3}{2}}\,(f_2+3f_3)\,C_A$	$-\frac{1}{2\sqrt{6}}f_3C_A$	0

Table B.5: Coefficients that occur in eq. (B.1) for the axial decay $\Xi^- \to \Lambda$. The second, third and fourth columns show the contribution from pion loops, kaon loops and eta loops respectively.

$\alpha^{\phi}_{\Xi^0\Sigma^+}$	$-\frac{3}{4}(D_0+F_0)$	$-\frac{3}{2}(D_0+F_0)$	$-\frac{3}{4}(D_0+F_0)$
$\beta^{\phi}_{\Xi^0\Sigma^+}$	$\frac{1}{6}(-2D_0^2F_0-3D_0F_0^2$ $-D_0^3+6F_0^3)$	$-\frac{1}{6}(D_0-F_0)(D_0^2+3F_0^2)$	$-\frac{1}{6}D_0(D_0+F_0)(D_0+3F_0)$
$\gamma^{\phi}_{\Xi^0\Sigma^+}$	$-\frac{3}{4}(D_0+F_0)$	$-\frac{3}{2}(D_0+F_0)$	$\frac{1}{4}(-D_0-3F_0)-\frac{D_0}{2}$
$\delta^{\phi}_{\Xi^0\Sigma^+}$	$-\frac{1}{6}C_A^2(2D_0+F_0)$	$-\frac{1}{12}C_A^2(15D_0+13F_0)$	$-\frac{3}{12}C_A^2(D_0+F_0)$
$\varepsilon^{\phi}_{\Xi^0\Sigma^+}$	$-\frac{2}{9}HC_A^2$	$-\frac{7}{9}HC_A^2$	$-\frac{1}{3}HC_A^2$
$\rho^{\phi}_{\Xi^0\Sigma^+}$	$b_1(9F_0-19D_0)$ $+b_2(9D_0-\frac{17F_0}{3})$ $-b_3(5D_0+F_0)$	$2b_1(F_0-7D_0)$ $+b_2(2D_0-\frac{26}{3}F_0)$ $-2(3b_3+4b_4)(D_0+F_0)$	$\frac{1}{3}(3b_1-b_2+b_3)(F_0-3D_0)$
$\sigma^{\phi}_{\Xi^0\Sigma^+}$	$-b_5(5D_0+F_0)$ $+b_6(\frac{5}{3}F_0-5D_0)$ $-b_7(5D_0+F_0)$	$2b_5(D_0+F_0)$ $+b_6(2D_0-\frac{2}{3}F_0)$ $+2b_7(D_0+F_0)$	$(b_5+b_6+b_7)(3D_0-F_0)$
$\tau^{\phi}_{\Xi^0\Sigma^+}$	$\frac{1}{12}(-d_1(9D_0+F_0)$ $+9d_2(D_0+F_0)$ $-3d_3(D_0-F_0))$	$\frac{1}{6}(-d_1(9D_0+5F_0)$ $-9d_2(D_0+F_0))$	$-\frac{3}{4}(d_1+d_2)(D_0+F_0)$
$\kappa^{\phi}_{\Xi^0\Sigma^+}$	$\frac{1}{24}(f_1-6f_4)C_A$	$-\frac{1}{24}(f_1+15f_4)C_A$	$-\frac{1}{24}(f_1+4f_4)C_A$
$\lambda^{\phi}_{\Xi^0\Sigma^+}$	$-\frac{1}{24}f_2C_A$	$\frac{1}{24}(3f_3-5f_2)C_A$	$\frac{1}{24}(2f_3-3f_2)C_A$
$\mu^{\phi}_{\Xi^0\Sigma^+}$	$-\frac{1}{12}(f_1+f_4)C_A$	0	$\frac{1}{24}(f_1+f_4)C_A$
$\nu^{\phi}_{\Xi^0\Sigma^+}$	$\frac{1}{12}(f_2-f_3)C_A$	$\frac{1}{6}f_2C_A$	$\frac{1}{24}(3f_2+f_3)C_A$

Table B.6: Coefficients that occur in eq. (B.1) for the axial decay $\Xi^0 \to \Sigma^+$. The second, third and fourth columns show the contribution from pion loops, kaon loops and eta loops respectively.

$\alpha^{\phi}_{\Sigma^-\Sigma^0}$	$-2\sqrt{2}F_0$	$-\sqrt{2}F_0$	0
$\beta^{\phi}_{\Sigma^-\Sigma^0}$	$\frac{1}{3}\sqrt{2}F_0(3F_0^2-2D_0^2)$	$\frac{1}{\sqrt{2}}F_0(F_0^2-D_0^2)$	$\frac{1}{3}\sqrt{2}D_0^2F_0$
$\gamma^{\phi}_{\Sigma^-\Sigma^0}$	$-2\sqrt{2}F_0$	$-\sqrt{2}F_0$	0
$\delta^{\phi}_{\Sigma^-\Sigma^0}$	$-\frac{1}{3\sqrt{2}}C_A^2(D_0+F_0)$	$-\frac{1}{3\sqrt{2}}C_A^2(3D_0-F_0)$	$-\frac{1}{3\sqrt{2}}D_0C_A^2$
$\varepsilon^{\phi}_{\Sigma^-\Sigma^0}$	$-\frac{1}{9\sqrt{2}}HC_A^2$	$-\frac{11}{9\sqrt{2}}HC_A^2$	$-\frac{1}{3\sqrt{2}}HC_A^2$
$\rho^{\phi}_{\Sigma^-\Sigma^0}$	$8\sqrt{2}(3b_1-b_2+b_4)D_0$	$4\sqrt{2}((3b_1-b_2)D_0+b_3F_0)$	$\frac{8}{3}\sqrt{2}b_3F_0$
$\sigma^{\phi}_{\Sigma^-\Sigma^0}$	0	0	0
$\tau^{\phi}_{\Sigma^-\Sigma^0}$	$\frac{1}{6\sqrt{2}}(24d_2D_0+3d_3D_0$ $+8d_1F_0)$	$\sqrt{2}(d_2D_0+d_1F_0)$	0
$\kappa^{\phi}_{\Sigma^-\Sigma^0}$	$-\frac{1}{12\sqrt{2}}(f_1-2f_4)C_A$	$-\frac{1}{4\sqrt{2}}(f_1-2f_4)C_A$	$-\frac{1}{12\sqrt{2}}(f_1-2f_4)C_A$
$\lambda^{\phi}_{\Sigma^-\Sigma^0}$	$-\frac{1}{12\sqrt{2}}f_2C_A$	$\frac{1}{12\sqrt{2}}(f_2-4f_3)C_A$	$-\frac{1}{12\sqrt{2}}f_3C_A$
$\mu^{\phi}_{\Sigma^-\Sigma^0}$	$-\frac{1}{12\sqrt{2}}(f_1+f_4)C_A$	$-\frac{1}{4\sqrt{2}}(f_1+f_4)C_A$	$-\frac{1}{12\sqrt{2}}(f_1+f_4)C_A$
$\nu^{\phi}_{\Sigma^-\Sigma^0}$	$\frac{1}{12\sqrt{2}}(f_2+f_3)C_A$	$-\frac{1}{12\sqrt{2}}(f_2-7f_3)C_A$	$\frac{1}{6\sqrt{2}}f_3C_A$

Table B.7: Coefficients that occur in eq. (B.1) for the axial decay $\Sigma^- \to \Sigma^0$. The second, third and fourth columns show the contribution from pion loops, kaon loops and eta loops respectively.

$\alpha^{\phi}_{\Xi^-\Xi^0}$	$2F_0 - 2D_0$	$F_0 - D_0$	0
$\beta^{\phi}_{\Xi^-\Xi^0}$	$-\frac{1}{4}(D_0 - F_0)^3$	$-\frac{1}{3}(D_0 + F_0)(D_0^2 + 3F_0^2)$	$\frac{1}{12}(D_0 - F_0)(D_0 + 3F_0)^2$
$\gamma^{\phi}_{\Xi^-\Xi^0}$	$2F_0 - 2D_0$	$F_0 - D_0$	0
$\delta^{\phi}_{\Xi^-\Xi^0}$	$\frac{1}{6}C_A^2(D_0 - F_0)$	$-\frac{1}{6}C_A^2(D_0 + 5F_0)$	$-\frac{1}{6}C_A^2(D_0 + 3F_0)$
$\varepsilon^{\phi}_{\Xi^-\Xi^0}$	$-\frac{1}{18}HC_A^2$	$\frac{2}{9}HC_A^2$	$\frac{1}{6}HC_A^2$
$\rho^{\phi}_{\Xi^-\Xi^0}$	$4(b_1 + b_2 - b_3 + 2b_4)$ $\times(D_0 - F_0)$	$\frac{4}{3}(3b_1(5D_0 + 3F_0)$ $-b_2(9D_0 + 7F_0)$ $+3b_3(F_0 - D_0))$	$\frac{4}{3}(3b_1 - b_2 - b_3)(3D_0 + F_0)$
$\sigma^{\phi}_{\Xi^-\Xi^0}$	0	0	0
$\tau^{\phi}_{\Xi^-\Xi^0}$	$-2(d_1 - d_2)(D_0 - F_0)$	$-\frac{1}{3}d_1(3D_0 + F_0)$ $+d_2(D_0 - F_0)$ $+\frac{1}{4}d_3(D_0 + F_0)$	0
$\kappa^{\phi}_{\Xi^-\Xi^0}$	$-\frac{1}{12}f_1 C_A$	$-\frac{1}{24}(7f_1 + 3f_4)\,C_A$	$-\frac{1}{12}(f_1 + f_4)\,C_A$
$\lambda^{\phi}_{\Xi^-\Xi^0}$	$-\frac{1}{6}f_2 C_A$	$-\frac{1}{24}(5f_2 + 3f_3)\,C_A$	$-\frac{1}{12}f_3 C_A$
$\mu^{\phi}_{\Xi^-\Xi^0}$	$-\frac{1}{12}(f_1 + f_4)\,C_A$	$-\frac{7}{24}(f_1 + f_4)\,C_A$	$-\frac{1}{12}(f_1 + f_4)\,C_A$
$\nu^{\phi}_{\Xi^-\Xi^0}$	$\frac{1}{6}(f_2 + f_3)\,C_A$	$\frac{1}{24}(5f_2 + 11f_3)\,C_A$	$\frac{1}{6}f_3 C_A$

Table B.8: Coefficients that occur in eq. (B.1) for the axial decay $\Xi^- \to \Xi^0$. The second, third and fourth columns show the contribution from pion loops, kaon loops and eta loops respectively.

$\alpha^{\phi}_{\Sigma^+\Sigma^+}$	$-4F_0$	$-2F_0$	0
$\beta^{\phi}_{\Sigma^+\Sigma^+}$	$\frac{2}{3}F_0(3F_0^2-2D_0^2)$	$F_0^3-D_0^2F_0$	$\frac{2}{3}D_0^2F_0$
$\gamma^{\phi}_{\Sigma^+\Sigma^+}$	$-4F_0$	$-2F_0$	0
$\delta^{\phi}_{\Sigma^+\Sigma^+}$	$-\frac{1}{3}C_A^2(D_0+F_0)$	$-\frac{1}{3}C_A^2(3D_0-F_0)$	$-\frac{1}{3}D_0C_A^2$
$\varepsilon^{\phi}_{\Sigma^+\Sigma^+}$	$-\frac{1}{9}HC_A^2$	$-\frac{11}{9}HC_A^2$	$-\frac{1}{3}HC_A^2$
$\rho^{\phi}_{\Sigma^+\Sigma^+}$	$-16(3b_1-b_2+b_4)D_0$	$-8((3b_1-b_2)D_0+b_3F_0)$	$-\frac{16}{3}b_3F_0$
$\sigma^{\phi}_{\Sigma^+\Sigma^+}$	0	0	0
$\tau^{\phi}_{\Sigma^+\Sigma^+}$	$-4d_2D_0-\frac{1}{2}d_3D_0-\frac{4}{3}d_1F_0$	$-2(d_2D_0+d_1F_0)$	0
$\kappa^{\phi}_{\Sigma^+\Sigma^+}$	$\frac{1}{12}(f_1-2f_4)C_A$	$\frac{1}{4}(f_1-2f_4)C_A$	$\frac{1}{12}(f_1-2f_4)C_A$
$\lambda^{\phi}_{\Sigma^+\Sigma^+}$	$\frac{1}{12}f_2C_A$	$-\frac{1}{12}(f_2-4f_3)C_A$	$\frac{1}{12}f_3C_A$
$\mu^{\phi}_{\Sigma^+\Sigma^+}$	$\frac{1}{12}(f_1+f_4)C_A$	$\frac{1}{4}(f_1+f_4)C_A$	$\frac{1}{12}(f_1+f_4)C_A$
$\nu^{\phi}_{\Sigma^+\Sigma^+}$	$-\frac{1}{12}(f_2+f_3)C_A$	$\frac{1}{12}(f_2-7f_3)C_A$	$-\frac{1}{6}f_3C_A$

Table B.9: Coefficients that occur in eq. (B.1) for the axial transition $\Sigma^+ \to \Sigma^+$. The second, third and fourth columns show the contribution from pion loops, kaon loops and eta loops respectively.

$\alpha^{\phi}_{\Xi^0\Xi^0}$	$2(D_0 - F_0)$	$D_0 - F_0$	0
$\beta^{\phi}_{\Xi^0\Xi^0}$	$\frac{1}{4}(D_0 - F_0)^3$	$\frac{1}{3}(D_0 + F_0)(D_0^2 + 3F_0^2)$	$-\frac{1}{12}(D_0 - F_0)(D_0 + 3F_0)^2$
$\gamma^{\phi}_{\Xi^0\Xi^0}$	$2D_0 - 2F_0$	$D_0 - F_0$	0
$\delta^{\phi}_{\Xi^0\Xi^0}$	$-\frac{1}{6}C_A^2(D_0 - F_0)$	$\frac{1}{6}C_A^2(D_0 + 5F_0)$	$\frac{1}{6}C_A^2(D_0 + 3F_0)$
$\varepsilon^{\phi}_{\Xi^0\Xi^0}$	$\frac{1}{18}HC_A^2$	$-\frac{2}{9}HC_A^2$	$-\frac{1}{6}HC_A^2$
$\rho^{\phi}_{\Xi^0\Xi^0}$	$-4(b_1 + b_2 - b_3 + 2b_4)$ $\times(D_0 - F_0)$	$\frac{4}{3}(-3b_1(5D_0 + 3F_0)$ $+b_2(9D_0 + 7F_0)$ $+3b_3(D_0 - F_0))$	$-\frac{4}{3}(3b_1 - b_2 - b_3)$ $\times(3D_0 + F_0)$
$\sigma^{\phi}_{\Xi^0\Xi^0}$	0	0	0
$\tau^{\phi}_{\Xi^0\Xi^0}$	$2(d_1 - d_2)(D_0 - F_0)$	$d_1(D_0 + \frac{F_0}{3})$ $+d_2(F_0 - D_0)$ $-\frac{1}{4}d_3(D_0 + F_0)$	0
$\kappa^{\phi}_{\Xi^0\Xi^0}$	$\frac{1}{12}f_1C_A$	$\frac{1}{24}(7f_1 + 3f_4)C_A$	$\frac{1}{12}(f_1 + f_4)C_A$
$\lambda^{\phi}_{\Xi^0\Xi^0}$	$\frac{1}{6}f_2C_A$	$\frac{1}{24}(5f_2 + 3f_3)C_A$	$\frac{1}{12}f_3C_A$
$\mu^{\phi}_{\Xi^0\Xi^0}$	$\frac{1}{12}(f_1 + f_4)C_A$	$\frac{7}{24}(f_1 + f_4)C_A$	$\frac{1}{12}(f_1 + f_4)C_A$
$\nu^{\phi}_{\Xi^0\Xi^0}$	$-\frac{1}{6}(f_2 + f_3)C_A$	$-\frac{1}{24}(5f_2 + 11f_3)C_A$	$-\frac{1}{6}f_3C_A$

Table B.10: Coefficients that occur in eq. (B.1) for the axial transition $\Xi^0 \to \Xi^0$. The second, third and fourth columns show the contribution from pion loops, kaon loops and eta loops respectively.

Appendix C

Expressions for baryon decay calculations

In this appendix we show the relevant equations for our work on proton decay. We have used a slightly different notation to the previous appendix, where K here refers to a three point function, whereas in the previous appendix it referred to the difference between two different two point functions. The two loop functions I_i^j are shown as a recurrence relation in appendix A. The symbol Li_2 refers to the polylogarithm function which is defined as

$$\mathrm{Li}_n(z) = \sum_{k=1}^{\infty} \frac{z^k}{k^n}. \tag{C.1}$$

This can be seen as a generalisation of the power series of the logarithm function, as for $n = 1$ we have

$$\mathrm{Li}_1(z) = -\ln(1-z). \tag{C.2}$$

The explicit formula for the form factors we have calculated are given in eqs (C.26)–(C.37).

The functions K_{0-2} are the solution to the integrals

$$K_0(q^2,m^2,M^2) = \int \frac{d^4k}{(2\pi F)^4}\frac{1}{(k^2-M^2)((p-k)^2-m^2)((p-q-k)^2-m^2)}\bigg|_{p^2=m^2} \tag{C.3}$$

$$p^\mu K_1(q^2,m^2,M^2) + q^\mu K_2(q^2,m^2,M^2) = \int \frac{d^4k}{(2\pi F)^4}\frac{k^\mu}{(k^2-M^2)((p-k)^2-m^2)((p-q-k)^2-m^2)}\bigg|_{p^2=m^2} \tag{C.4}$$

and can be written in closed form as

$$\begin{aligned}
K_0(q^2,m^2,M^2) = \frac{1}{16\pi^2}\frac{1}{\sqrt{B_1}}\Bigg(&- 2\mathrm{ReLi}_2\left(\frac{A_1+M^2\sqrt{B_1}}{A_1-\sqrt{B_1}\sqrt{C_1}}\right)\\
&+ 2\mathrm{ReLi}_2\left(\frac{A_1+(M^2-m^2)\sqrt{B_1}}{A_1-\sqrt{B_1}\sqrt{C_1}}\right)\\
&+ 2\mathrm{ReLi}_2\left(\frac{2M^2(A_1+\sqrt{B_1}(M^2-2m^2))}{D_1}\right)\\
&+ 2\mathrm{ReLi}_2\left(-\frac{M^2(-A_1-A_2+2\sqrt{B_1}(m^2-2M^2+q^2))}{D_1}\right)\\
&+ \mathrm{Li}_2\left(\frac{A_1+M^2\sqrt{B_1}}{(\sqrt{B_1}-m^2+M^2-q^2)(m^2+2M^2-q^2)}\right)\\
&+ \mathrm{Li}_2\left(\frac{(A_1+M^2\sqrt{B_1})q^2}{(\sqrt{B_1}-m^2+M^2-q^2)((m^2-M^2)^2-M^2m^2)}\right)\\
&- \mathrm{Li}_2\left(\frac{E_1+\sqrt{B_1}(m^2-M^2+q^2)}{2q^2(m^2+2M^2-q^2)}\right)\\
&- \mathrm{Li}_2\left(\frac{E_1+\sqrt{B_1}(m^2-M^2+q^2)}{2(m^2+M^2)^2-2m^2q^2}\right)\Bigg)
\end{aligned} \tag{C.5}$$

$$\begin{aligned}
K_1(q^2,m^2,M^2) = &\frac{q^2-2M^2q^2+2M^2m^2-M^4-m^4}{m^4+(M^2-q^2)^2-2m^2(M^2+q^2)}K_0(q^2,m^2,M^2)\\
&+\frac{m^2-M^2+q^2}{4m^2q^2-(m^2-M^2+q^2)^2}I_1^0(m^2,M^2,m^2)\\
&+\frac{M^2-m^2+q^2}{m^4+(M^2-q^2)^2-2m^2(M^2+q^2)}I_1^0(M^2,m^2,m^2)
\end{aligned}$$

$$+\frac{2q^2}{m^4+(M^2-q^2)^2-2m^2(M^2+q^2)}I_1^0(q^2,M^2,m^2) \tag{C.6}$$

$$\begin{aligned}K_2(q^2,m^2,M^2) &= \frac{2m^4+M^2(q^2-M^2)-m^2(M^2+2q^2)}{mN^4+(M^2-q^2)^2-2mN^2(M^2+q^2)}K_0(m^2,q^2,M^2)\\ &+\frac{m^2-M^2+q^2}{4m^2q^2-(m^2-M^2+q^2)^2}I_1^0(q^2,M^2,m^2)\\ &+\frac{m^2+M^2-q^2}{m^4+(M^2-q^2)^2-2m^2(M^2+q^2)}I_1^0(M^2,m^2,m^2)\\ &+\frac{2m^2}{m^4+(M^2-q^2)^2-2m^2(M^2+q^2)}I_1^0(m^2,M^2,m^2)\end{aligned} \tag{C.7}$$

with

$$\begin{aligned}A_1 &= M^4-2m^4+m^2M^2\\ A_2 &= 2q^4-5M^2q^2-2m^2q^2-3M^2m^2+3M^4\\ B_1 &= (m^2+M^2-q^2)^2-4m^2M^2\\ C_1 &= M^2(M^2-4m^2)\\ D_1 &= \sqrt{B_1}(\sqrt{C_1}(M^2+m^2-q^2)+M^2(3M^2-3m^2-q^2))\\ &\quad +M^2(M^2+m^2-q^2)(3M^2-3m^2-q^2)\\ &\quad +\sqrt{C_1}((m^2-M^2)^2-2q^2(M^2+m^2)+q^4)\\ E_1 &= (m^2-M^2)^2+2M^2q^2-q^4.\end{aligned} \tag{C.8}$$

These expressions simplify for $q^2=0$ to

$$\begin{aligned}K_0(0,m^2,M^2) = -\frac{1}{8\pi^2(M^2-m^2)}\Bigg(&-\mathrm{ReLi}_2\left(\frac{2m^2}{2m^2+M^2+M\sqrt{M^2-4m^2}}\right)\\ &+\mathrm{ReLi}_2\left(\frac{4m^2}{2m^2+M^2+M\sqrt{M^2-4m^2}}\right)\\ &+\mathrm{ReLi}_2\left(\frac{2M^2}{3M^2-M\sqrt{M^2-4m^2}}\right)\end{aligned}$$

$$- \mathrm{ReLi}_2\left(\frac{4M^2}{3M^2 - M\sqrt{M^2-4m^2}}\right)\Bigg) \tag{C.9}$$

$$K_1(0,m^2,M^2) = -K_0(0,m^2,M^2) + \frac{1}{M^2-m^2}\Big(I_1^0(p^2,M^2,m^2)\big|_{p^2=m^2} - I_1^0(p^2,m^2,m^2)\big|_{p^2=M^2}\Big) \tag{C.10}$$

$$\begin{aligned} K_2(0,m^2,M^2) = {} & \frac{2m^2+M^2}{m^2-M^2}K_0(0,m^2,M^2) - \frac{1}{m^2-M^2}I_1^0(0,M^2,m^2) \\ & + \frac{1}{(m^2-M^2)^2}\Big(2m^2\ I_1^0(p^2,M^2,m^2)\big|_{p^2=m^2} \\ & - (M^2+m^2)\ I_1^0(p^2,m^2,m^2)\big|_{p^2=M^2}\Big). \end{aligned} \tag{C.11}$$

It is useful to expand the operator $u\partial_\mu u^\dagger$ in terms of ϕ fields so we get

$$u^\dagger\partial_\mu u + u\partial_\mu u^\dagger = \frac{2q_i}{2!F^2}[\phi_j,\phi_i] - \frac{2q_i}{4!F^4}q_i[\phi_l,[\phi_k,[\phi_j,\phi_i]]] + \ldots \tag{C.12}$$

$$u^\dagger\partial_\mu u - u\partial_\mu u^\dagger = \frac{2iq_i}{F}\phi_i - \frac{2iq_i}{3!F^2}[\phi_k,[\phi_j,\phi_i]] + \ldots \tag{C.13}$$

with the repeated index i summed over and values of $i,j,\ldots$ in the range $[0,n]$ with n the number of fields ϕ.

The loop diagrams are given by

$$\mathcal{M}_1 = -\Delta_\pi(M_\phi^2) \tag{C.14}$$

$$\mathcal{M}_2 = (-\Delta_\pi(M_\phi^2) - 2m_N^2 I_1^1(m_N^2,M_\phi^2,m_N^2))\gamma_5 \tag{C.15}$$

$$\begin{aligned} \mathcal{M}_3 = {} & 4m_N^2\left(q^2 - \frac{m_N^2 - M_\phi^2 + q^2}{2}\right)K_2(m_N^2,q^2,M_\phi^2) \\ & - 2m_N^2M_\phi^2K_0(m_N^2,q^2,M_\phi^2) + (q^2-m_N^2)I_1^0(q^2,M_\phi^2,m_N^2) \\ & - q^2I_1^1(q^2,M_\phi^2,m_N^2) + 2m_N^2I_1^1(m_N^2,M_\phi^2,M_\phi^2) \\ & - 2m_N^2I_1^0(M_{\mathrm{final}}^2,m_N^2,m_N^2) \end{aligned} \tag{C.16}$$

$$\mathcal{M}_4 = \Delta_\pi(M_\phi^2) \tag{C.17}$$

$$\mathcal{M}_5 = \left(1 - \frac{m_N^2 - M_\phi^2 + q^2}{q^2 - m_N^2}\right) \Delta_\pi(M_\phi^2) \tag{C.18}$$

$$\mathcal{M}_6 = \frac{m_N^2 + q^2}{m_N^2 - q^2} \Delta_\pi(M_\phi^2)\gamma_5 \tag{C.19}$$

$$\mathcal{M}_7 = 0 \tag{C.20}$$

$$\begin{aligned}\mathcal{M}_8 = {} & q^2 \frac{q^2 + 3m_N^2}{m_N^2 - q^2} I_1^1(q^2, M_\phi^2, m_N^2)\gamma_5 \\ & + \frac{(q^2 + m_N^2)^2 + 4m_N^2 q^2}{(q^2 - m_N^2)^2}(dI_1^2(q^2, M_\phi^2, m_N^2) + q^2 I_2^2(q^2, M_\phi^2, m_N^2))\gamma_5\end{aligned} \tag{C.21}$$

$$\begin{aligned}\mathcal{M}_9 = {} & \Bigg(\frac{q^2 + m_N^2}{q^2 - m_N^2}\Delta_\pi(M_\phi^2) - (q^2 + m_N^2) I_1^0(q^2, M_\phi^2, m_N^2) \\ & + 2\frac{q^2(q^2 + m_N^2)}{q^2 - m_N^2} I_1^1(q^2, M_\phi^2, m_N^2) \\ & - \frac{q^2 + m_N^2}{q^2 - m_N^2}(dI_1^2(q^2, M_\phi^2, m_N^2) + q^2 I_2^2(q^2, M_\phi^2, m_N^2))\Bigg)\gamma_5\end{aligned} \tag{C.22}$$

$$\begin{aligned}\mathcal{M}_{10} = {} & \Bigg(\frac{m_N^2 + q^2}{m_N^2 - q^2}\Delta_\pi(M_\phi^2) + 2\frac{m_N^2(m_N^2 - 3q^2)}{q^2 - m_N^2} I_1^0(M_{\text{final}}^2, m_N^2, m_N^2) \\ & + (m_N^2 + q^2) I_1^0(q^2, M_\phi^2, m_N^2) - q^2 I_1^1(q^2, M_\phi^2, m_N^2) \\ & - \frac{2m_N^2 M_\phi^2(m_N^2 + 3q^2)}{q^2 - m_N^2} K_0(m_N^2, q^2, M_\phi^2) \\ & + 4m_N^2(q^2 + \frac{m_N^2 - M_\phi^2 + q^2}{2}) K_2(m_N^2, q^2, M_\phi^2)\Bigg)\gamma_5\end{aligned} \tag{C.23}$$

$$\begin{aligned}\mathcal{M}_{11} = {} & \frac{q^2 + m_N^2}{q^2 - m_N^2}\big(dI_1^2(q^2, M_\phi^2, m_N^2) + q^2 I_2^2(q^2, M_\phi^2, m_N^2)\big) \\ & - q^2 I_1^1(q^2, M_\phi^2, m_N^2)\end{aligned} \tag{C.24}$$

$$\begin{aligned}\mathcal{M}_{12} = {} & \frac{2m_N^2}{q^2 - m_N^2} I_1^1(m_N^2, M_\phi^2, m_N^2) \\ & - 2\frac{m_N^2}{q^2 - m_N^2}(dI_1^2(q^2, M_\phi^2, m_N^2) + m_N^2 I_2^2(q^2, M_\phi^2, m_N^2)).\end{aligned} \tag{C.25}$$

The following equations show the relevant form factor for each matrix element studied in chapter 5. For our octet loop results, the full equation is used, and for the pion loop results, we take all the $\mathcal{M}_i(M_K^2)$ and $\mathcal{M}_i(M_\eta^2)$ to be zero.

$$
\begin{aligned}
\frac{W_0^{(1)}}{\alpha} = &\Big(\frac{1}{\sqrt{2}F_\pi} - \frac{(D+F)(m_N^2+q^2)}{\sqrt{2}F_\pi(q^2-m_N^2)}\Big)\Big(1 + \frac{3(D+F)^2}{16F_\pi^2}\mathcal{M}_{\rm wv}(M_\pi^2) + \frac{\alpha_1}{\alpha}\Big) \\
&+ \frac{q^2+m_N^2}{q^2-m_N^2}\frac{B_0\left(h_{38}m_s + h_{40}\left(m_s+2m\right) + 2h_{44}m\right)}{\sqrt{2}F_\pi} \\
&- \frac{1}{2\sqrt{2}F_\pi^3}\mathcal{M}_1(M_\pi^2) - \frac{(D+F)}{4\sqrt{2}F_\pi^3}\mathcal{M}_2(M_\pi^2) - \frac{(D+F)^2}{2\sqrt{2}F_\pi^3}\mathcal{M}_3(M_\pi^2) \\
&- \frac{1}{4\sqrt{2}F_\pi^3}\mathcal{M}_4(M_\pi^2) + \frac{\sqrt{2}(D+F)}{3F_\pi^3}\mathcal{M}_5(M_\pi^2) + \frac{3(D+F)}{4\sqrt{2}F_\pi^3}\mathcal{M}_6(M_\pi^2) \\
&- \frac{3(D+F)^3}{2\sqrt{2}F_\pi^3}\mathcal{M}_8(M_\pi^2) - \frac{(D+F)}{\sqrt{2}F_\pi^3}\mathcal{M}_9(M_\pi^2) + \frac{(D+F)^3}{2\sqrt{2}F_\pi^3}\mathcal{M}_{10}(M_\pi^2) \\
&+ \frac{3(D+F)^2}{2\sqrt{2}F_\pi^3}\mathcal{M}_{11}(M_\pi^2) - \frac{(D+F)}{\sqrt{2}F_\pi^3}\mathcal{M}_{12}(M_\pi^2) \\
&+ \Big(\frac{1}{\sqrt{2}F_\pi} - \frac{(D+F)(m_N^2+q^2)}{\sqrt{2}F_\pi(q^2-m_N^2)}\Big)\frac{5D^2-6DF+9F^2}{24F_\pi^2}\mathcal{M}_{\rm wv}(M_K^2) \\
&- \frac{1}{4\sqrt{2}F_\pi^3}\mathcal{M}_1(M_K^2) - \frac{\sqrt{2}(D^2-2DF+3F^2)}{3F_\pi^3}\mathcal{M}_3(M_K^2) \\
&- \frac{1}{6\sqrt{2}F_\pi^3}\mathcal{M}_4(M_K^2) + \frac{(D+F)}{3\sqrt{2}F_\pi^3}\mathcal{M}_5(M_K^2) + \frac{3(D+F)}{2\sqrt{2}F_\pi^3}\mathcal{M}_6(M_K^2) \\
&- \frac{(5D^3-D^2F+3DF^2+9F^3)}{3\sqrt{2}F_\pi^3}\mathcal{M}_8(M_K^2) - \frac{(D+F)}{2\sqrt{2}F_\pi^3}\mathcal{M}_9(M_K^2) \\
&+ \frac{\sqrt{2}(D-F)(D^2+3F^2)}{3F_\pi^3}\mathcal{M}_{10}(M_K^2) + \frac{(5D-3F)(D+F)}{3\sqrt{2}F_\pi^3}\mathcal{M}_{11}(M_K^2) \\
&- \frac{(D+F)}{2\sqrt{2}F_\pi^3}\mathcal{M}_{12}(M_K^2) \\
&+ \Big(\frac{1}{\sqrt{2}F_\pi} - \frac{(D+F)(m_N^2+q^2)}{\sqrt{2}F_\pi(q^2-m_N^2)}\Big)\frac{5D^2-6DF+9F^2}{24F_\pi^2} \\
&- \frac{(D-3F)}{12\sqrt{2}F_\pi^3}\mathcal{M}_2(M_\eta^2) + \frac{(D-3F)(D+F)}{6\sqrt{2}F_\pi^3}\mathcal{M}_3(M_\eta^2) \\
&- \frac{1}{36\sqrt{2}F_\pi^3}\mathcal{M}_4(M_\eta^2) + \frac{(D+F)}{12\sqrt{2}F_\pi^3}\mathcal{M}_6(M_\eta^2) - \frac{(D-3F)^2(D+F)}{6\sqrt{2}F_\pi^3}\mathcal{M}_8(M_\eta^2) \\
&- \frac{(D-3F)^2(D+F)}{6\sqrt{2}F_\pi^3}\mathcal{M}_{10}(M_\eta^2) + \frac{(D-3F)(D+F)}{6\sqrt{2}F_\pi^3}\mathcal{M}_{11}(M_\eta^2)
\end{aligned}
\tag{C.26}
$$

$$
\begin{aligned}
\frac{W_0^{(1)}}{\beta} = &\Big(\frac{1}{\sqrt{2}F_\pi} - \frac{1(D+F)(m_N^2+q^2)}{\sqrt{2}F_\pi(q^2-m_N^2)}\Big)\Big(1+\frac{3(D+F)^2}{16F_\pi^2}\mathcal{M}_{\rm wv}(M_\pi^2)+\frac{\beta_1}{\beta}\Big)\\
&+\frac{q^2+m_N^2}{q^2-m_N^2}\frac{B_0\left(h_{38}m_s+h_{40}\left(m_s+2m\right)+2h_{44}m\right)}{\sqrt{2}F_\pi}\\
&-\frac{1}{2\sqrt{2}F_\pi^3}\mathcal{M}_1(M_\pi^2)-\frac{(D+F)}{4\sqrt{2}F_\pi^3}\mathcal{M}_2(M_\pi^2)-\frac{(D+F)^2}{2\sqrt{2}F_\pi^3}\mathcal{M}_3(M_\pi^2)\\
&-\frac{1}{4\sqrt{2}F_\pi^3}\mathcal{M}_4(M_\pi^2)+\frac{\sqrt{2}(D+F)}{3F_\pi^3}\mathcal{M}_5(M_\pi^2)+\frac{3(D+F)}{4\sqrt{2}F_\pi^3}\mathcal{M}_6(M_\pi^2)\\
&-\frac{3(D+F)^3}{2\sqrt{2}F_\pi^3}\mathcal{M}_8(M_\pi^2)-\frac{(D+F)}{\sqrt{2}F_\pi^3}\mathcal{M}_9(M_\pi^2)+\frac{(D+F)^3}{2\sqrt{2}F_\pi^3}\mathcal{M}_{10}(M_\pi^2)\\
&+\frac{3(D+F)^2}{2\sqrt{2}F_\pi^3}\mathcal{M}_{11}(M_\pi^2)-\frac{(D+F)}{\sqrt{2}F_\pi^3}\mathcal{M}_{12}(M_\pi^2)\\
&+\Big(\frac{1}{\sqrt{2}F_\pi} - \frac{1(D+F)(m_N^2+q^2)}{\sqrt{2}F_\pi(q^2-m_N^2)}\Big)\frac{5D^2-6DF+9F^2}{24F_\pi^2}\mathcal{M}_{\rm wv}(M_K^2)\\
&-\frac{1}{4\sqrt{2}F_\pi^3}\mathcal{M}_1(M_K^2)-\frac{\sqrt{2}\left(D^2-2DF+3F^2\right)}{3F_\pi^3}\mathcal{M}_3(M_K^2)\\
&-\frac{1}{6\sqrt{2}F_\pi^3}\mathcal{M}_4(M_K^2)+\frac{(D+F)}{3\sqrt{2}F_\pi^3}\mathcal{M}_5(M_K^2)+\frac{3(D+F)}{2\sqrt{2}F_\pi^3}\mathcal{M}_6(M_K^2)\\
&-\frac{(5D^3-D^2F+3DF^2+9F^3)}{3\sqrt{2}F_\pi^3}\mathcal{M}_8(M_K^2)\\
&-\frac{(D+F)}{2\sqrt{2}F_\pi^3}\mathcal{M}_9(M_K^2)+\frac{\sqrt{2}(D-F)\left(D^2+3F^2\right)}{3F_\pi^3}\mathcal{M}_{10}(M_K^2)\\
&+\frac{(5D-3F)(D+F)}{3\sqrt{2}F_\pi^3}\mathcal{M}_{11}(M_K^2)-\frac{(D+F)}{2\sqrt{2}F_\pi^3}\mathcal{M}_{12}(M_K^2)\\
&+\Big(\frac{1}{\sqrt{2}F_\pi} - \frac{1(D+F)(m_N^2+q^2)}{\sqrt{2}F_\pi(q^2-m_N^2)}\Big)\frac{5D^2-6DF+9F^2}{24F_\pi^2}\\
&-\frac{(D-3F)}{12\sqrt{2}F_\pi^3}\mathcal{M}_2(M_\eta^2)+\frac{(D-3F)(D+F)}{6\sqrt{2}F_\pi^3}\mathcal{M}_3(M_\eta^2)\\
&-\frac{1}{36\sqrt{2}F_\pi^3}\mathcal{M}_4(M_\eta^2)+\frac{(D+F)}{12\sqrt{2}F_\pi^3}\mathcal{M}_6(M_\eta^2)-\frac{(D-3F)^2(D+F)}{6\sqrt{2}F_\pi^3}\mathcal{M}_8(M_\eta^2)\\
&-\frac{(D-3F)^2(D+F)}{6\sqrt{2}F_\pi^3}\mathcal{M}_{10}(M_\eta^2)+\frac{(D-3F)(D+F)}{6\sqrt{2}F_\pi^3}\mathcal{M}_{11}(M_\eta^2)
\end{aligned}
\tag{C.27}
$$

$$
\begin{aligned}
\frac{W_0^{(2)}}{\alpha} = &\Big(\frac{(D-F)(m_N^2+q^2)}{F_\pi(q^2-m_N^2)} - \frac{1}{F_\pi}\Big)\Big(1 + \frac{3(D+F)^2}{16F_\pi^2}\mathcal{M}_{\rm wv}(M_\pi^2) + \frac{\alpha_2}{\alpha}\Big) \\
&- \frac{q^2+m_N^2}{q^2-m_N^2}\frac{B_0\left(h_{43}\left(m_s+m\right)+h_{41}\left(m_s+2m\right)+h_{39}m\right)}{F_\pi} \\
&+ \frac{1}{4F_\pi^3}\mathcal{M}_1(M_\pi^2) - \frac{3(D+F)}{2F_\pi^3}\mathcal{M}_2(M_\pi^2) + \frac{(D+F)(D+3F)}{3F_\pi^3}\mathcal{M}_3(M_\pi^2) \\
&+ \frac{3}{4F_\pi^3}\mathcal{M}_4(M_\pi^2) - \frac{(D-F)}{4F_\pi^3}\mathcal{M}_5(M_\pi^2) - \frac{(D-F)}{F_\pi^3}\mathcal{M}_6(M_\pi^2) \\
&+ \frac{2(D-F)(D^2+6F^2)}{3F_\pi^3}\mathcal{M}_8(M_\pi^2) + \frac{(D-2F)}{2F_\pi^3}\mathcal{M}_9(M_\pi^2) \\
&- \frac{(D+F)(D^2-3DF+6F^2)}{3F_\pi^3}\mathcal{M}_{10}(M_\pi^2) \\
&- \frac{2D(D-F)}{3F_\pi^3}\mathcal{M}_{11}(M_\pi^2) + \frac{(D+F)}{4F_\pi^3}\mathcal{M}_{12}(M_\pi^2) \\
&+ \Big(\frac{(D-F)(m_N^2+q^2)}{F_\pi(q^2-m_N^2)} - \frac{1}{F_\pi}\Big)\frac{5D^2-6DF+9F^2}{24F_\pi^2}\mathcal{M}_{\rm wv}(M_K^2) \\
&+ \frac{1}{4F_\pi^3}\mathcal{M}_1(M_K^2) - \frac{2D}{3F_\pi^3}\mathcal{M}_2(M_K^2) + \frac{(D^2+3F^2)}{3F_\pi^3}\mathcal{M}_3(M_K^2) \\
&+ \frac{5}{6F_\pi^3}\mathcal{M}_4(M_K^2) - \frac{(D-F)}{2F_\pi^3}\mathcal{M}_5(M_K^2) - \frac{(D-F)}{F_\pi^3}\mathcal{M}_6(M_K^2) \\
&+ \frac{2(D-F)(D^2+F^2)}{F_\pi^3}\mathcal{M}_8(M_K^2) + \frac{(D-F)}{2F_\pi^3}\mathcal{M}_9(M_K^2) \\
&- \frac{(D+F)(D^2+3F^2)}{3F_\pi^3}\mathcal{M}_{10}(M_K^2) \\
&- \frac{2D(D-F)}{F_\pi^3}\mathcal{M}_{11}(M_K^2) + \frac{(D-F)}{F_\pi^3}\mathcal{M}_{12}(M_K^2) \\
&+ \Big(\frac{(D-F)(m_N^2+q^2)}{F_\pi(q^2-m_N^2)} - \frac{1}{F_\pi}\Big)\frac{5D^2-6DF+9F^2}{24F_\pi^2} \\
&+ \frac{1}{4F_\pi^3}\mathcal{M}_1(M_\eta^2) + \frac{(D-3F)(D-F)}{3F_\pi^3}\mathcal{M}_3(M_\eta^2) + \frac{1}{36F_\pi^3}\mathcal{M}_4(M_\eta^2) \\
&- \frac{(D-F)}{4F_\pi^3}\mathcal{M}_5(M_\eta^2) - \frac{(D-F)}{3F_\pi^3}\mathcal{M}_6(M_\eta^2) + \frac{2D^2(D-F)}{3F_\pi^3}\mathcal{M}_8(M_\eta^2) \\
&+ \frac{D}{2F_\pi^3}\mathcal{M}_9(M_\eta^2) - \frac{D(D-3F)(D-F)}{3F_\pi^3}\mathcal{M}_{10}(M_\eta^2) \\
&- \frac{2D(D-F)}{3F_\pi^3}\mathcal{M}_{11}(M_\eta^2) + \frac{(D-3F)}{4F_\pi^3}\mathcal{M}_{12}(M_\eta^2)
\end{aligned}
\tag{C.28}
$$

$$
\begin{aligned}
\frac{W_0^{(2)}}{\beta} = &\Big(\frac{(D-F)\,(m_N^2+q^2)}{F_\pi\,(q^2-m_N^2)}+\frac{1}{F_\pi}\Big)\Big(1+\frac{3(D+F)^2}{16F_\pi^2}\mathcal{M}_{\rm wv}(M_\pi^2)+\frac{\beta_2}{\beta}\Big)\\
&-\frac{q^2+m_N^2}{q^2-m_N^2}\frac{B_0\,(h_{43}\,(m_s+m)+h_{41}\,(m_s+2m)+h_{39}m)}{F_\pi}\\
&-\frac{1}{2F_\pi^3}\mathcal{M}_1(M_\pi^2)+\frac{3(D+F)}{2F_\pi^3}\mathcal{M}_2(M_\pi^2)-\frac{2(D-F)(D+F)}{F_\pi^3}\mathcal{M}_3(M_\pi^2)\\
&-\frac{3}{4F_\pi^3}\mathcal{M}_4(M_\pi^2)-\frac{(D-F)}{4F_\pi^3}\mathcal{M}_5(M_\pi^2)-\frac{2(D-F)}{F_\pi^3}\mathcal{M}_6(M_\pi^2)\\
&+\frac{2(D-F)(D^2+6F^2)}{3F_\pi^3}\mathcal{M}_8(M_\pi^2)+\frac{(D-2F)}{2F_\pi^3}\mathcal{M}_9(M_\pi^2)\\
&-\frac{(D+F)(D^2-3DF+6F^2)}{3F_\pi^3}\mathcal{M}_{10}(M_\pi^2)\\
&-\frac{4F(D-F)}{F_\pi^3}\mathcal{M}_{11}(M_\pi^2)+\frac{(D+F)}{4F_\pi^3}\mathcal{M}_{12}(M_\pi^2)\\
&+\Big(\frac{(D-F)\,(m_N^2+q^2)}{F_\pi\,(q^2-m_N^2)}+\frac{1}{F_\pi}\Big)\frac{5D^2-6DF+9F^2}{24F_\pi^2}\mathcal{M}_{\rm wv}(M_K^2)\\
&-\frac{1}{4F_\pi^3}\mathcal{M}_1(M_K^2)+\frac{2F}{F_\pi^3}\mathcal{M}_2(M_K^2)+\frac{(D^2+3F^2)}{3F_\pi^3}\mathcal{M}_3(M_K^2)\\
&-\frac{5}{6F_\pi^3}\mathcal{M}_4(M_K^2)-\frac{(D-F)}{2F_\pi^3}\mathcal{M}_5(M_K^2)-\frac{(D-F)}{F_\pi^3}\mathcal{M}_6(M_K^2)\\
&+\frac{2(D-F)(D^2+F^2)}{F_\pi^3}\mathcal{M}_8(M_K^2)+\frac{(D-F)}{2F_\pi^3}\mathcal{M}_9(M_K^2)\\
&-\frac{(D+F)(D^2+3F^2)}{3F_\pi^3}\mathcal{M}_{10}(M_K^2)\\
&-\frac{2F(D-F)}{F_\pi^3}\mathcal{M}_{11}(M_K^2)+\frac{(D-F)}{F_\pi^3}\mathcal{M}_{12}(M_K^2)\\
&+\Big(\frac{(D-F)\,(m_N^2+q^2)}{F_\pi\,(q^2-m_N^2)}+\frac{1}{F_\pi}\Big)\frac{5D^2-6DF+9F^2}{24F_\pi^2}\\
&-\frac{(D-3F)}{3F_\pi^3}\mathcal{M}_2(M_\eta^2)-\frac{13}{36F_\pi^3}\mathcal{M}_4(M_\eta^2)-\frac{(D-F)}{4F_\pi^3}\mathcal{M}_5(M_\eta^2)\\
&+\frac{2D^2(D-F)}{3F_\pi^3}\mathcal{M}_8(M_\eta^2)+\frac{D}{2F_\pi^3}\mathcal{M}_9(M_\eta^2)-\frac{D(D-3F)(D-F)}{3F_\pi^3}\mathcal{M}_{10}(M_\eta^2)\\
&+\frac{(D-3F)}{4F_\pi^3}\mathcal{M}_{12}(M_\eta^2)
\end{aligned}
\tag{C.29}
$$

$$
\begin{aligned}
\frac{W_0^{(3)}}{\alpha} = & \Big(\frac{2D\,(m_N^2+q^2)}{3F_\pi\,(q^2-m_N^2)}\Big)\Big(1+\frac{3(D+F)^2}{16F_\pi^2}\mathcal{M}_{\rm wv}(M_\pi^2)+\frac{\alpha_3}{\alpha}\Big) \\
& -\frac{q^2+m_N^2}{q^2-m_N^2}\Big(\frac{h_{38}B_0m_s+h_{39}B_0m}{3F_\pi} \\
& \quad +\frac{(h_{40}+h_{41})B_0(2m+m_s)}{3F_\pi}+\frac{(h_{43}+h_{44})B_0(m+m_s)}{3F_\pi}\Big) \\
& -\frac{1}{4F_\pi^3}\mathcal{M}_1(M_\pi^2)+\frac{(5D-3F)(D+F)}{3F_\pi^3}\mathcal{M}_3(M_\pi^2) \\
& -\frac{D}{6F_\pi^3}\mathcal{M}_5(M_\pi^2)-\frac{(D+F)}{F_\pi^3}\mathcal{M}_6(M_\pi^2) \\
& +\frac{2\,(D^3+D^2F+3DF^2-3F^3)}{3F_\pi^3}\mathcal{M}_8(M_\pi^2)-\frac{F}{2F_\pi^3}\mathcal{M}_9(M_\pi^2) \\
& -\frac{(D+F)\,(2D^2-3DF+3F^2)}{3F_\pi^3}\mathcal{M}_{10}(M_\pi^2) \\
& -\frac{4D(D+2F)}{3F_\pi^3}\mathcal{M}_{11}(M_\pi^2)+\frac{(D+F)}{2F_\pi^3}\mathcal{M}_{12}(M_\pi^2) \\
& +\Big(\frac{2D\,(m_N^2+q^2)}{3F_\pi\,(q^2-m_N^2)}\Big)\frac{5D^2-6DF+9F^2}{24F_\pi^2}\mathcal{M}_{\rm wv}(M_K^2) \\
& -\frac{1}{4F_\pi^3}\mathcal{M}_1(M_K^2)+\frac{(D-F)}{2F_\pi^3}\mathcal{M}_2(M_K^2) \\
& +\frac{(D^2-F^2)}{F_\pi^3}\mathcal{M}_3(M_K^2)-\frac{D}{3F_\pi^3}\mathcal{M}_5(M_K^2)-\frac{(D-3F)}{3F_\pi^3}\mathcal{M}_6(M_K^2) \\
& +\frac{2\,(5D^3-3D^2F+9DF^2+9F^3)}{9F_\pi^3}\mathcal{M}_8(M_K^2)+\frac{(D+F)}{2F_\pi^3}\mathcal{M}_9(M_K^2) \\
& +\frac{(D^3-9D^2F-9DF^2+9F^3)}{9F_\pi^3}\mathcal{M}_{10}(M_K^2) \\
& -\frac{2D(D-3F)}{3F_\pi^3}\mathcal{M}_{11}(M_K^2)+\frac{(D-F)}{2F_\pi^3}\mathcal{M}_{12}(M_k^2) \\
& +\Big(\frac{2D\,(m_N^2+q^2)}{3F_\pi\,(q^2-m_N^2)}\Big)\frac{5D^2-6DF+9F^2}{24F_\pi^2} \\
& +\frac{2D(D-3F)}{9F_\pi^3}\mathcal{M}_3(M_\eta^2)-\frac{D}{6F_\pi^3}\mathcal{M}_5(M_\eta^2)-\frac{2D}{9F_\pi^3}\mathcal{M}_6(M_\eta^2) \\
& +\frac{4D^3}{9F_\pi^3}\mathcal{M}_8(M_\eta^2)+\frac{D}{2F_\pi^3}\mathcal{M}_9(M_\eta^2)-\frac{D(D-3F)^2}{9F_\pi^3}\mathcal{M}_{10}(M_\eta^2) \\
& -\frac{2D(D-3F)}{9F_\pi^3}\mathcal{M}_{11}(M_\eta^2)
\end{aligned}
\tag{C.30}
$$

$$
\begin{aligned}
\frac{W_0^{(3)}}{\beta} = & \Big(\frac{2D\,(m_N^2+q^2)}{3F_\pi\,(q^2-m_N^2)}\Big)\Big(1+\frac{3(D+F)^2}{16F_\pi^2}\mathcal{M}_{\rm wv}(M_\pi^2)+\frac{\beta_3}{\beta}\Big) \\
& -\frac{q^2+m_N^2}{q^2-m_N^2}\Big(\frac{h_{38}B_0m_s+h_{39}B_0m}{3F_\pi} \\
& \quad +\frac{(h_{40}+h_{41})B_0(2m+m_s)}{3F_\pi}+\frac{(h_{43}+h_{44})B_0(m+m_s)}{3F_\pi}\Big) \\
& -\frac{1}{4F_\pi^3}\mathcal{M}_1(M_\pi^2)+\frac{(F-D)(D+F)}{F_\pi^3}\mathcal{M}_3(M_\pi^2)-\frac{D}{6F_\pi^3}\mathcal{M}_5(M_\pi^2) \\
& -\frac{(D-F)}{F_\pi^3}\mathcal{M}_6(M_\pi^2)+\frac{2(D^3+D^2F+3DF^2-3F^3)}{3F_\pi^3}\mathcal{M}_8(M_\pi^2) \\
& -\frac{F}{2F_\pi^3}\mathcal{M}_9(M_\pi^2)-\frac{(D+F)(2D^2-3DF+3F^2)}{3F_\pi^3}\mathcal{M}_{10}(M_\pi^2) \\
& -\frac{2F(D-F)}{F_\pi^3}\mathcal{M}_{11}(M_\pi^2)+\frac{(D+F)}{2F_\pi^3}\mathcal{M}_{12}(M_\pi^2) \\
& +\Big(\frac{2D\,(m_N^2+q^2)}{3F_\pi\,(q^2-m_N^2)}\Big)\frac{5D^2-6DF+9F^2}{24F_\pi^2}\mathcal{M}_{\rm wv}(M_K^2) \\
& +\frac{1}{4F_\pi^3}\mathcal{M}_1(M_K^2)+\frac{(D-F)}{2F_\pi^3}\mathcal{M}_2(M_K^2)+\frac{(3D^2-3F^2)}{3F_\pi^3}\mathcal{M}_3(M_K^2) \\
& -\frac{D}{3F_\pi^3}\mathcal{M}_5(M_K^2)-\frac{(D+F)}{F_\pi^3}\mathcal{M}_6(M_K^2) \\
& +\frac{2(5D^3-3D^2F+9DF^2+9F^3)}{9F_\pi^3}\mathcal{M}_8(M_K^2) \\
& +\frac{(D+F)}{2F_\pi^3}\mathcal{M}_9(M_K^2)+\frac{(D^3-9D^2F-9DF^2+9F^3)}{9F_\pi^3}\mathcal{M}_{10}(M_K^2) \\
& -\frac{2F(D+F)}{F_\pi^3}\mathcal{M}_{11}(M_K^2)+\frac{(D-F)}{2F_\pi^3}\mathcal{M}_{12}(M_K^2) \\
& +\Big(\frac{2D\,(m_N^2+q^2)}{3F_\pi\,(q^2-m_N^2)}\Big)\frac{5D^2-6DF+9F^2}{24F_\pi^2} \\
& -\frac{D}{6F_\pi^3}\mathcal{M}_5(M_\eta^2)+\frac{4D^3}{9F_\pi^3}\mathcal{M}_8(M_\eta^2)+\frac{D}{2F_\pi^3}\mathcal{M}_9(M_\eta^2) \\
& -\frac{D(D-3F)^2}{9F_\pi^3}\mathcal{M}_{10}(M_\eta^2)
\end{aligned}
\tag{C.31}
$$

$$
\begin{aligned}
\frac{W_0^{(4)}}{\alpha} = &\Big(\frac{1}{F_\pi} - \frac{(D+3F)\,(m_N^2+q^2)}{3F_\pi\,(q^2-m_N^2)}\Big)\Big(1 + \frac{3(D+F)^2}{16F_\pi^2}\mathcal{M}_{\rm wv}(M_\pi^2) + \frac{\sqrt{2}\alpha_1+\alpha_3}{\alpha}\Big)\\
&\frac{q^2+m_N^2}{q^2-m_N^2}\Big(\frac{2h_{38}B_0m_s - h_{39}B_0m}{3F_\pi}\\
&- \frac{(h_{41}-2h_{40})\,B_0\,(2m+m_s)}{3F_\pi} - \frac{(h_{43}-2h_{44})\,B_0\,(m+m_s)}{3F_\pi}\Big)\\
&+ \frac{(D+3F)}{12F_\pi^3}\mathcal{M}_5(M_\pi^2) - \frac{2D^2(D+3F)}{3F_\pi^3}\mathcal{M}_8(M_\pi^2) + \frac{D}{2F_\pi^3}\mathcal{M}_9(M_\pi^2)\\
&- \frac{D(F-D)(D+F)}{F_\pi^3}\mathcal{M}_{10}(M_\pi^2) - \frac{3(D+F)}{4F_\pi^3}\mathcal{M}_{12}(M_\pi^2)\\
&+ \Big(\frac{1}{F_\pi} - \frac{(D+3F)\,(m_N^2+q^2)}{3F_\pi\,(q^2-m_N^2)}\Big)\frac{5D^2-6DF+9F^2}{24F_\pi^2}\mathcal{M}_{\rm wv}(M_K^2)\\
&- \frac{3}{4F_\pi^3}\mathcal{M}_1(M_K^2) + \frac{(5D^2-9F^2)}{3F_\pi^3}\mathcal{M}_3(M_K^2) - \frac{1}{3F_\pi^3}\mathcal{M}_4(M_K^2)\\
&+ \frac{(D+3F)}{6F_\pi^3}\mathcal{M}_5(M_K^2) + \frac{(D+3F)}{3F_\pi^3}\mathcal{M}_6(M_K^2)\\
&- \frac{2\,(D^3+3D^2F+9DF^2+27F^3)}{9F_\pi^3}\mathcal{M}_8(M_K^2)\\
&- \frac{(D+3F)}{2F_\pi^3}\mathcal{M}_9(M_K^2) + \frac{(-5D^3+15D^2F+9DF^2-27F^3)}{9F_\pi^3}\mathcal{M}_{10}(M_K^2)\\
&+ \frac{2D(D+3F)}{3F_\pi^3}\mathcal{M}_{11}(M_K^2)\\
&+ \Big(\frac{1}{F_\pi} - \frac{(D+3F)\,(m_N^2+q^2)}{3F_\pi\,(q^2-m_N^2)}\Big)\frac{5D^2-6DF+9F^2}{24F_\pi^2}\\
&- \frac{1}{2F_\pi^3}\mathcal{M}_1(M_\eta^2) + \frac{(D-3F)}{6F_\pi^3}\mathcal{M}_2(M_\eta^2) + \frac{2(D-3F)(D+3F)}{9F_\pi^3}\mathcal{M}_3(M_\eta^2)\\
&- \frac{1}{9F_\pi^3}\mathcal{M}_4(M_\eta^2) + \frac{(D+3F)}{12F_\pi^3}\mathcal{M}_5(M_\eta^2) + \frac{4(D+3F)}{9F_\pi^3}\mathcal{M}_6(M_\eta^2)\\
&- \frac{2D^2(D+3F)}{9F_\pi^3}\mathcal{M}_8(M_\eta^2) - \frac{D}{2F_\pi^3}\mathcal{M}_9(M_\eta^2) - \frac{D(D-3F)(D+3F)}{9F_\pi^3}\mathcal{M}_{10}(M_\eta^2)\\
&+ \frac{4D(D+3F)}{9F_\pi^3}\mathcal{M}_{11}(M_\eta^2) + \frac{(D-3F)}{4F_\pi^3}\mathcal{M}_{12}(M_\eta^2)
\end{aligned}
\tag{C.32}
$$

$$
\begin{aligned}
\frac{W_0^{(4)}}{\beta} = &\Big(\frac{1}{F_\pi} - \frac{(D+3F)\,(m_N^2+q^2)}{3F_\pi\,(q^2-m_N^2)}\Big)\Big(1 + \frac{3(D+F)^2}{16F_\pi^2}\mathcal{M}_{\rm wv}(M_\pi^2) + \frac{\sqrt{2}\beta_1+\beta_3}{\beta}\Big)\\
&\frac{q^2+m_N^2}{q^2-m_N^2}\Big(\frac{2h_{38}B_0m_s - h_{39}B_0m}{3F_\pi}\\
&- \frac{(h_{41}-2h_{40})\,B_0\,(2m+m_s)}{3F_\pi} - \frac{(h_{43}-2h_{44})\,B_0\,(m+m_s)}{3F_\pi}\Big)\\
&- \frac{(-D-3F)}{12F_\pi^3}\mathcal{M}_5(M_\pi^2) - \frac{2D^2(D+3F)}{3F_\pi^3}\mathcal{M}_8(M_\pi^2) + \frac{D}{2F_\pi^3}\mathcal{M}_9(M_\pi^2)\\
&- \frac{D(F-D)(D+F)}{F_\pi^3}\mathcal{M}_{10}(M_\pi^2) - \frac{3(D+F)}{4F_\pi^3}\mathcal{M}_{12}(M_\pi^2)\\
&+ \Big(\frac{1}{F_\pi} - \frac{(D+3F)\,(m_N^2+q^2)}{3F_\pi\,(q^2-m_N^2)}\Big)\frac{5D^2-6DF+9F^2}{24F_\pi^2}\mathcal{M}_{\rm wv}(M_K^2)\\
&- \frac{3}{4F_\pi^3}\mathcal{M}_1(M_K^2) + \frac{(9F^2-5D^2)}{3F_\pi^3}\mathcal{M}_3(M_K^2) - \frac{1}{3F_\pi^3}\mathcal{M}_4(M_K^2)\\
&- \frac{(-D-3F)}{6F_\pi^3}\mathcal{M}_5(M_K^2) - \frac{(-D-3F)}{F_\pi^3}\mathcal{M}_6(M_K^2)\\
&+ \frac{2\,(-D^3-3D^2F-9DF^2-27F^3)}{9F_\pi^3}\mathcal{M}_8(M_K^2)\\
&+ \frac{(-D-3F)}{2F_\pi^3}\mathcal{M}_9(M_K^2) + \frac{(-5D^3+15D^2F+9DF^2-27F^3)}{9F_\pi^3}\mathcal{M}_{10}(M_K^2)\\
&- \frac{2F(-D-3F)}{F_\pi^3}\mathcal{M}_{11}(M_K^2)\\
&+ \Big(\frac{1}{F_\pi} - \frac{(D+3F)\,(m_N^2+q^2)}{3F_\pi\,(q^2-m_N^2)}\Big)\frac{5D^2-6DF+9F^2}{24F_\pi^2}\\
&+ \frac{(D-3F)}{6F_\pi^3}\mathcal{M}_2(M_\eta^2) - \frac{1}{9F_\pi^3}\mathcal{M}_4(M_\eta^2) - \frac{(-D-3F)}{12F_\pi^3}\mathcal{M}_5(M_\eta^2)\\
&+ \frac{2D^2(-D-3F)}{9F_\pi^3}\mathcal{M}_8(M_\eta^2) - \frac{D}{2F_\pi^3}\mathcal{M}_9(M_\eta^2)\\
&- \frac{D(D-3F)(D+3F)}{9F_\pi^3}\mathcal{M}_{10}(M_\eta^2)\\
&+ \frac{(D-3F)}{4F_\pi^3}\mathcal{M}_{12}(M_\eta^2)
\end{aligned}
\tag{C.33}
$$

$$
\begin{aligned}
\frac{W_0^{(5)}}{\alpha} = &\Big(\frac{1}{F_\pi} - \frac{(D-3F)\,(m_N^2+q^2)}{3F_\pi\,(q^2-m_N^2)}\Big)\Big(1+\frac{3(D+F)^2}{16F_\pi^2}\mathcal{M}_{\rm wv}(M_\pi^2)+\frac{\alpha_3-\alpha_2}{\alpha}\Big)\\
&\frac{q^2+m_N^2}{q^2-m_N^2}\Big(\frac{2mB_0h_{39}-B_0h_{38}m_s}{3F_\pi}\\
&+\frac{B_0\,(2h_{43}-h_{44})\,(m+m_s)}{3F_\pi}+\frac{B_0\,(-h_{40}+2h_{41})\,(2m+m_s)}{3F_\pi}\Big)\\
&-\frac{1}{2F_\pi^3}\mathcal{M}_1(M_\pi^2)+\frac{3(D+F)}{2F_\pi^3}\mathcal{M}_2(M_\pi^2)+\frac{(D+F)(4D-6\alpha F)}{3F_\pi^3}\mathcal{M}_3(M_\pi^2)\\
&-\frac{3}{4F_\pi^3}\mathcal{M}_4(M_\pi^2)+\frac{(D-3F)}{12F_\pi^3}\mathcal{M}_5(M_\pi^2)-\frac{2F}{F_\pi^3}\mathcal{M}_6(M_\pi^2)\\
&-\frac{2F(-2D^2+3DF-3F^2)}{3F_\pi^3}\mathcal{M}_8(M_\pi^2)+\frac{(F-D)}{2F_\pi^3}\mathcal{M}_9(M_\pi^2)\\
&-\frac{(D+F)(D^2-3F^2)}{3F_\pi^3}\mathcal{M}_{10}(M_\pi^2)-\frac{2D(D+5F)}{3F_\pi^3}\mathcal{M}_{11}(M_\pi^2)\\
&+\frac{(D+F)}{4F_\pi^3}\mathcal{M}_{12}(M_\pi^2)\\
&+\Big(\frac{1}{F_\pi}-\frac{(D-3F)\,(m_N^2+q^2)}{3F_\pi\,(q^2-m_N^2)}\Big)\frac{5D^2-6DF+9F^2}{24F_\pi^2}\mathcal{M}_{\rm wv}(M_K^2)\\
&-\frac{1}{2F_\pi^3}\mathcal{M}_1(M_K^2)+\frac{(7D-3F)}{6F_\pi^3}\mathcal{M}_2(M_K^2)+\frac{2\,(D^2-3F^2)}{3F_\pi^3}\mathcal{M}_3(M_K^2)\\
&-\frac{5}{6F_\pi^3}\mathcal{M}_4(M_K^2)+\frac{(D-3F)}{6F_\pi^3}\mathcal{M}_5(M_K^2)+\frac{2D}{3F_\pi^3}\mathcal{M}_6(M_K^2)\\
&-\frac{4(2D^3-3D^2F-9F^3)}{9F_\pi^3}\mathcal{M}_8(M_K^2)+\frac{F}{F_\pi^3}\mathcal{M}_9(M_K^2)\\
&+\frac{2(2D^3-3D^2F+9F^3)}{9F_\pi^3}\mathcal{M}_{10}(M_K^2)\\
&+\frac{4D^2}{3F_\pi^3}\mathcal{M}_{11}(M_K^2)-\frac{(D-F)}{2F_\pi^3}\mathcal{M}_{12}(M_K^2)\\
&+\Big(\frac{1}{F_\pi}-\frac{(D-3F)\,(m_N^2+q^2)}{3F_\pi\,(q^2-m_N^2)}\Big)\frac{5D^2-6DF+9F^2}{24F_\pi^2}\\
&-\frac{1}{4F_\pi^3}\mathcal{M}_1(M_\eta^2)-\frac{(D-3F)^2}{9F_\pi^3}\mathcal{M}_3(M_\eta^2)-\frac{1}{36F_\pi^3}\mathcal{M}_4(M_\eta^2)\\
&+\frac{(D-3F)}{12F_\pi^3}\mathcal{M}_5(M_\eta^2)+\frac{(D-3F)}{9F_\pi^3}\mathcal{M}_6(M_\eta^2)-\frac{2D^2(D-3F)}{9F_\pi^3}\mathcal{M}_8(M_\eta^2)\\
&+\frac{2D^2(D-3F)}{9F_\pi^3}\mathcal{M}_{10}(M_\eta^2)+\frac{4D^2}{9F_\pi^3}\mathcal{M}_{11}(M_\eta^2)-\frac{(D-3F)}{4F_\pi^3}\mathcal{M}_{12}(M_\eta^2)
\end{aligned}
\tag{C.34}
$$

$$
\begin{aligned}
\frac{W_0^{(5)}}{\beta} = &\Big(-\frac{(D-3F)\,(m_N^2+q^2)}{3F_\pi\,(q^2-m_N^2)} - \frac{1}{F_\pi}\Big)\Big(1 + \frac{3(D+F)^2}{16F_\pi^2}\mathcal{M}_{\rm wv}(M_\pi^2) + \frac{\beta_3-\beta_2}{\beta}\Big)\\
&\frac{q^2+m_N^2}{q^2-m_N^2}\Big(\frac{2mB_0h_{39}-B_0h_{38}m_s}{3F_\pi}\\
&+ \frac{B_0\,(2h_{43}-h_{44})\,(m+m_s)}{3F_\pi} + \frac{B_0\,(-h_{40}+2h_{41})\,(2m+m_s)}{3F_\pi}\Big)\\
&+ \frac{1}{4F_\pi^3}\mathcal{M}_1(M_\pi^2) - \frac{3(D+F)}{2F_\pi^3}\mathcal{M}_2(M_\pi^2) + \frac{(D-F)(D+F)}{F_\pi^3}\mathcal{M}_3(M_\pi^2)\\
&+ \frac{3}{4F_\pi^3}\mathcal{M}_4(M_\pi^2) + \frac{(D-3F)}{12F_\pi^3}\mathcal{M}_5(M_\pi^2) - \frac{(F-D)}{F_\pi^3}\mathcal{M}_6(M_\pi^2)\\
&- \frac{2F(-2D^2+3DF-3F^2)}{3F_\pi^3}\mathcal{M}_8(M_\pi^2) + \frac{(F-D)}{2F_\pi^3}\mathcal{M}_9(M_\pi^2)\\
&- \frac{(D+F)(D^2-3F^2)}{3F_\pi^3}\mathcal{M}_{10}(M_\pi^2) - \frac{2F(F-D)}{F_\pi^3}\mathcal{M}_{11}(M_\pi^2)\\
&+ \frac{(D+F)}{4F_\pi^3}\mathcal{M}_{12}(M_\pi^2)\\
&+ \Big(-\frac{(D-3F)\,(m_N^2+q^2)}{3F_\pi\,(q^2-m_N^2)} - \frac{1}{F_\pi}\Big)\frac{5D^2-6DF+9F^2}{24F_\pi^2}\mathcal{M}_{\rm wv}(M_K^2)\\
&+ \frac{1}{2F_\pi^3}\mathcal{M}_1(M_K^2) + \frac{(D-5F)}{2F_\pi^3}\mathcal{M}_2(M_K^2) + \frac{(2D^2-6F^2)}{3F_\pi^3}\mathcal{M}_3(M_K^2)\\
&+ \frac{5}{6F_\pi^3}\mathcal{M}_4(M_K^2) + \frac{(D-3F)}{6F_\pi^3}\mathcal{M}_5(M_K^2) - \frac{2F}{F_\pi^3}\mathcal{M}_6(M_K^2)\\
&- \frac{4(2D^3-3D^2F-9F^3)}{9F_\pi^3}\mathcal{M}_8(M_K^2) + \frac{F}{F_\pi^3}\mathcal{M}_9(M_K^2)\\
&+ \frac{2(2D^3-3D^2F+9F^3)}{9F_\pi^3}\mathcal{M}_{10}(M_K^2) - \frac{4F^2}{F_\pi^3}\mathcal{M}_{11}(M_K^2)\\
&- \frac{(D-F)}{2F_\pi^3}\mathcal{M}_{12}(M_K^2)\\
&+ \Big(-\frac{(D-3F)\,(m_N^2+q^2)}{3F_\pi\,(q^2-m_N^2)} - \frac{1}{F_\pi}\Big)\frac{5D^2-6DF+9F^2}{24F_\pi^2}\mathcal{M}_{\rm wv}(M_K^2)\\
&+ \frac{(D-3F)}{3F_\pi^3}\mathcal{M}_2(M_\eta^2) + \frac{13}{36F_\pi^3}\mathcal{M}_4(M_\eta^2) + \frac{(D-3F)}{12F_\pi^3}\mathcal{M}_5(M_\eta^2)\\
&- \frac{2D^2(D-3F)}{9F_\pi^3}\mathcal{M}_8(M_\eta^2) + \frac{2D^2(D-3F)}{9F_\pi^3}\mathcal{M}_{10}(M_\eta^2)\\
&- \frac{(D-3F)}{4F_\pi^3}\mathcal{M}_{12}(M_\eta^2)
\end{aligned}
\tag{C.35}
$$

$$
\begin{aligned}
\frac{W_0^{(6)}}{\alpha} = &\Big(\frac{(D-3F)\,(m_N^2+q^2)}{\sqrt{6}F_\pi\,(q^2-m_N^2)} - \frac{1}{\sqrt{6}F_\pi}\Big)\Big(1 + \frac{3(D+F)^2}{16F_\pi^2}\mathcal{M}_{\rm wv}(M_\pi^2) + \frac{\alpha_1+\sqrt{2}\alpha_3}{\sqrt{3}\alpha}\Big)\\
&\frac{q^2+m_N^2}{q^2-m_N^2}\Big(\frac{2mB_0\,(h_{40}-h_{39}-2h_{41}+h_{42}+h_{44})}{\sqrt{6}F_\pi}\\
&+\frac{(h_{38}+h_{40}-2\,(h_{41}+h_{42}+2h_{43}))\,B_0 m_s}{\sqrt{6}F_\pi}\Big)\\
&-\frac{3\sqrt{\frac{3}{2}}(D+F)}{4F_\pi^3}\mathcal{M}_2(M_\pi^2) - \frac{\sqrt{\frac{3}{2}}(D-3F)(D+F)}{2F_\pi^3}\mathcal{M}_3(M_\pi^2)\\
&+\frac{5}{4\sqrt{6}F_\pi^3}\mathcal{M}_4(M_\pi^2) - \frac{\sqrt{\frac{3}{2}}(D-3F)}{4F_\pi^3}\mathcal{M}_6(M_\pi^2)\\
&+\frac{\sqrt{\frac{3}{2}}(D-3F)(D+F)^2}{2F_\pi^3}\mathcal{M}_8(M_\pi^2) + \frac{\sqrt{\frac{3}{2}}(D-3F)(D+F)^2}{2F_\pi^3}\mathcal{M}_{10}(M_\pi^2)\\
&-\frac{\sqrt{\frac{3}{2}}(D-3F)(D+F)}{2F_\pi^3}\mathcal{M}_{11}(M_\pi^2)\\
&+\Big(\frac{(D-3F)\,(m_N^2+q^2)}{\sqrt{6}F_\pi\,(q^2-m_N^2)} - \frac{1}{\sqrt{6}F_\pi}\Big)\frac{5D^2-6DF+9F^2}{24F_\pi^2}\mathcal{M}_{\rm wv}(M_K^2)\\
&+\frac{\sqrt{\frac{3}{2}}}{4F_\pi^3}\mathcal{M}_1(M_K^2) - \frac{(7D+3F)}{3\sqrt{6}F_\pi^3}\mathcal{M}_2(M_K^2) + \frac{2\sqrt{\frac{2}{3}}D(2D-3F)}{3F_\pi^3}\mathcal{M}_3(M_K^2)\\
&+\frac{\sqrt{\frac{3}{2}}}{2F_\pi^3}\mathcal{M}_4(M_K^2) - \frac{(D-3F)}{\sqrt{6}F_\pi^3}\mathcal{M}_5(M_K^2) - \frac{\sqrt{\frac{3}{2}}(D-3F)}{2F_\pi^3}\mathcal{M}_6(M_K^2)\\
&+\frac{(D-3F)(5D^2-6DF+9F^2)}{3\sqrt{6}F_\pi^3}\mathcal{M}_8(M_K^2) + \frac{\sqrt{\frac{3}{2}}(D-3F)}{2F_\pi^3}\mathcal{M}_9(M_K^2)\\
&-\frac{4\sqrt{\frac{2}{3}}D^2(D-3F)}{3F_\pi^3}\mathcal{M}_{10}(M_K^2) - \frac{(D-3F)(5D-3F)}{3\sqrt{6}F_\pi^3}\mathcal{M}_{11}(M_K^2)\\
&+\frac{\sqrt{\frac{3}{2}}(D-3F)}{2F_\pi^3}\mathcal{M}_{12}(M_K^2)\\
&+\Big(\frac{(D-3F)\,(m_N^2+q^2)}{\sqrt{6}F_\pi\,(q^2-m_N^2)} - \frac{1}{\sqrt{6}F_\pi}\Big)\frac{5D^2-6DF+9F^2}{24F_\pi^2}\\
&-\frac{(D-3F)}{12\sqrt{6}F_\pi^3}\mathcal{M}_2(M_\eta^2) - \frac{(D-3F)^2}{6\sqrt{6}F_\pi^3}\mathcal{M}_3(M_\eta^2) + \frac{1}{36\sqrt{6}F_\pi^3}\mathcal{M}_4(M_\eta^2)\\
&-\frac{(D-3F)}{12\sqrt{6}F_\pi^3}\mathcal{M}_6(M_\eta^2) + \frac{(D-3F)^3}{6\sqrt{6}F_\pi^3}\mathcal{M}_8(M_\eta^2)\\
&+\frac{(D-3F)^3}{6\sqrt{6}F_\pi^3}\mathcal{M}_{10}(M_\eta^2) - \frac{(D-3F)^2}{6\sqrt{6}F_\pi^3}\mathcal{M}_{11}(M_\eta^2)
\end{aligned}
\tag{C.36}
$$

$$
\begin{aligned}
\frac{W_0^{(6)}}{\beta} = &\Big(\frac{(D-3F)\,(m_N^2+q^2)}{\sqrt{6}F_\pi\,(q^2-m_N^2)} + \frac{\sqrt{\frac{3}{2}}}{F_\pi}\Big)\Big(1 + \frac{3(D+F)^2}{16F_\pi^2}\mathcal{M}_{\rm wv}(M_\pi^2) + \frac{\beta_1+\sqrt{2}\beta_3}{\sqrt{3}\beta}\Big)\\
&\frac{q^2+m_N^2}{q^2-m_N^2}\Big(\frac{2mB_0\,(h_{40}-h_{39}-2h_{41}+h_{42}+h_{44})}{\sqrt{6}F_\pi}\\
&+\frac{(h_{38}+h_{40}-2\,(h_{41}+h_{42}+2h_{43}))\,B_0 m_s}{\sqrt{6}F_\pi}\Big)\\
&+\frac{5\sqrt{\frac{3}{2}}(D+F)}{4F_\pi^3}\mathcal{M}_2(M_\pi^2) - \frac{\sqrt{\frac{3}{2}}(D-3F)(D+F)}{2F_\pi^3}(\mathcal{M}_3(M_\pi^2)+\mathcal{M}_{11}(M_\pi^2))\\
&-\frac{7}{4\sqrt{6}F_\pi^3}\mathcal{M}_4(M_\pi^2) - \frac{\sqrt{\frac{3}{2}}(D-3F)}{4F_\pi^3}\mathcal{M}_6(M_\pi^2)\\
&+\frac{\sqrt{\frac{3}{2}}(D-3F)(D+F)^2}{2F_\pi^3}\mathcal{M}_8(M_\pi^2) + \frac{\sqrt{\frac{3}{2}}(D-3F)(D+F)^2}{2F_\pi^3}\mathcal{M}_{10}(M_\pi^2)\\
&+\Big(\frac{(D-3F)\,(m_N^2+q^2)}{\sqrt{6}F_\pi\,(q^2-m_N^2)} + \frac{\sqrt{\frac{3}{2}}}{F_\pi}\Big)\frac{5D^2-6DF+9F^2}{24F_\pi^2}\mathcal{M}_{\rm wv}(M_K^2)\\
&-\frac{3\sqrt{\frac{3}{2}}}{4F_\pi^3}\mathcal{M}_1(M_K^2) - \frac{(D-3F)}{\sqrt{6}F_\pi^3}\mathcal{M}_2(M_K^2) - \frac{2\sqrt{\frac{2}{3}}D^2}{F_\pi^3}\mathcal{M}_3(M_K^2)\\
&-\frac{11}{6\sqrt{6}F_\pi^3}\mathcal{M}_4(M_K^2) - \frac{(D-3F)}{\sqrt{6}F_\pi^3}\mathcal{M}_5(M_K^2) - \frac{\sqrt{\frac{3}{2}}(D-3F)}{2F_\pi^3}\mathcal{M}_6(M_K^2)\\
&+\frac{(D-3F)(5D^2-6DF+9F^2)}{3\sqrt{6}F_\pi^3}\mathcal{M}_8(M_K^2) + \frac{\sqrt{\frac{3}{2}}(D-3F)}{2F_\pi^3}\mathcal{M}_9(M_K^2)\\
&-\frac{4\sqrt{\frac{2}{3}}D^2(D-3F)}{3F_\pi^3}\mathcal{M}_{10}(M_K^2)\\
&-\frac{(D-3F)(9F-3D)}{3\sqrt{6}F_\pi^3}\mathcal{M}_{11}(M_K^2) + \frac{\sqrt{\frac{3}{2}}(D-3F)}{2F_\pi^3}\mathcal{M}_{12}(M_K^2)\\
&+\Big(\frac{(D-3F)\,(m_N^2+q^2)}{\sqrt{6}F_\pi\,(q^2-m_N^2)} + \frac{\sqrt{\frac{3}{2}}}{F_\pi}\Big)\frac{5D^2-6DF+9F^2}{24F_\pi^2}\\
&-\frac{\sqrt{\frac{3}{2}}(D-3F)}{4F_\pi^3}(\mathcal{M}_2(M_\eta^2)+\mathcal{M}_6(M_\eta^2)) + \frac{(D-3F)^2}{2\sqrt{6}F_\pi^3}(\mathcal{M}_3(M_\eta^2)+\mathcal{M}_{11}(M_\eta^2))\\
&-\frac{\sqrt{\frac{3}{2}}}{4F_\pi^3}\mathcal{M}_4(M_\eta^2) + \frac{(D-3F)^3}{6\sqrt{6}F_\pi^3}(\mathcal{M}_8(M_\eta^2)+\mathcal{M}_{10}(M_\eta^2))
\end{aligned}
\tag{C.37}
$$

Bibliography

[1] K.A. Olive and Particle Data Group. Review of particle physics. *Chinese Physics C*, 38(9):090001, 2014.

[2] David J. Gross and Frank Wilczek. Ultraviolet behavior of Non-Abelian gauge theories. *Phys. Rev. Lett.*, 30:1343–1346, Jun 1973.

[3] H. David Politzer. Reliable perturbative results for strong interactions? *Phys. Rev. Lett.*, 30:1346–1349, Jun 1973.

[4] J. D. Bjorken. Asymptotic sum rules at infinite momentum. *Phys. Rev.*, 179:1547–1553, Mar 1969.

[5] Matthew B. Robinson, Karen R. Bland, Gerald B. Cleaver, and Jay R. Dittmann. A simple introduction to particle physics part i - foundations and the standard model. 2008. arXiv:0810.3328.

[6] M. Gell-Mann. A schematic model of baryons and mesons. *Physics Letters*, 8(3):214 – 215, 1964.

[7] F. E. Close. *An introduction to quarks and partons.* Academic Press Inc. (London) Ltd, 1979.

[8] Jean-Marc Richard. An introduction to the quark model. 2012. arXiv:1205.4326.

[9] E. Eichten, K. Gottfried, T. Kinoshita, et al. Spectrum of charmed quark-antiquark bound states. *Phys. Rev. Lett.*, 34:369–372, Feb 1975.

[10] Aneesh V. Manohar. Large N QCD. 1998. arXiv:hep-ph/9802419.

[11] A. Chodos, R. L. Jaffe, K. Johnson, C. B. Thorn, and V. F. Weisskopf. New extended model of hadrons. *Phys. Rev. D*, 9:3471–3495, Jun 1974.

[12] A. Chodos, R. L. Jaffe, K. Johnson, and C. B. Thorn. Baryon structure in the bag theory. *Phys. Rev. D*, 10:2599–2604, Oct 1974.

[13] Atushi Hosaka and Hiroshi Toki. *Quarks, Baryons And Chiral Symmetry.* World Scientific Publishing Co., 2001.

[14] C E DeTar and J F Donoghue. Bag models of hadrons. *Annual Review of Nuclear and Particle Science*, 33(1):235–264, 1983.

[15] Alan Chodos and Charles Thorn. Chiral invariance in a bag theory. *Phys. Rev. D*, 12:2733–2743, Nov 1975.

[16] G.E. Brown and Mannque Rho. The little bag. *Physics Letters B*, 82(2):177 – 180, 1979.

[17] G.E. Brown, Mannque Rho, and Vincent Vento. Little bag dynamics. *Physics Letters B*, 84(4):383 – 388, 1979.

[18] Y. Nambu and G. Jona-Lasinio. Dynamical model of elementary particles based on an analogy with superconductivity. I. *Phys. Rev.*, 122:345–358, Apr 1961.

[19] Y. Nambu and G. Jona-Lasinio. Dynamical model of elementary particles based on an analogy with superconductivity. II. *Phys. Rev.*, 124:246–254, Oct 1961.

[20] U. Vogl and W. Weise. The Nambu and Jona-Lasinio model: Its implications for hadrons and nuclei. *Progress in Particle and Nuclear Physics*, 27(0):195 – 272, 1991.

[21] Dietmar Ebert, Thorsten Feldmann, and Hugo Reinhardt. Extended NJL model for light and heavy mesons without $q - \bar{q}$ thresholds. *Physics Letters B*, 388(1):154 – 160, 1996.

[22] G. Hellstern, R. Alkofer, and H. Reinhardt. Diquark confinement in an extended NJL model. *Nuclear Physics A*, 625(4):697 – 712, 1997.

[23] Manuel E. Carrillo-Serrano, Ian C. Cloet, and Anthony W. Thomas. SU(3)-flavour breaking in octet baryon masses and axial couplings. 2014. arXiv:1409.1653.

[24] G.'t Hooft. A planar diagram theory for strong interactions. *Nuclear Physics B*, 72(3):461 – 473, 1974.

[25] Elizabeth Jenkins. Large-Nc baryons. *Annual Review of Nuclear and Particle Science*, 48(1):81–119, 1998.

[26] Biagio Lucini and Marco Panero. Introductory lectures to large-N QCD phenomenology and lattice results. *Progress in Particle and Nuclear Physics*, 75(0):1 – 40, 2014.

[27] Stefan Scherer and Matthias R. Schindler. *A Primer For Chiral Perturbation Theory*. Springer-Verlag, 2012.

[28] Steven Weinberg. Phenomenological Lagrangians. *Physica A*, 96:327–340, 1979.

[29] J Gasser and H Leutwyler. Chiral perturbation theory to one loop. *Annals of Physics*, 158(1):142 – 210, 1984.

[30] J. Gasser and H. Leutwyler. On the low energy structure of QCD. *Physics Letters B*, 125(4):321 – 324, 1983.

[31] Stefan Scherer. Introduction to chiral perturbation theory. *Adv. Nucl. Phys.*, 27:277–538, 2003.

[32] J Gasser and H Leutwyler. Chiral perturbation theory: Expansions in the mass of the strange quark. *Nuclear Physics B*, 250:465–516, 1985.

[33] J. Gasser, M.E. Sainio, and A. Švarc. Nucleons with chiral loops. *Nuclear Physics B*, 307(4):779 – 853, 1988.

[34] Elizabeth Jenkins and Aneesh V. Manohar. Baryon chiral perturbation theory using a heavy fermion lagrangian. *Physics Letters B*, 255(4):558 – 562, 1991.

[35] Vronique Bernard, Norbert Kaiser, Joachim Kambor, and Ulf-G. Meiner. Chiral structure of the nucleon. *Nuclear Physics B*, 388(2):315 – 345, 1992.

[36] Howard Georgi. An effective field theory for heavy quarks at low energies. *Physics Letters B*, 240(34):447 – 450, 1990.

[37] Véronique Bernard. Chiral perturbation theory and baryon properties. *Progress in Particle and Nuclear Physics*, 60(1):82 – 160, 2008.

[38] T Fuchs, J Gegelia, G Japaridze, and S Scherer. Renormalization of relativistic baryon chiral perturbation theory and power counting. *Physical Review D*, 68:056005, 2003.

[39] T. Becher and H. Leutwyler. Baryon chiral perturbation theory in manifestly lorentz invariant form. *The European Physical Journal C - Particles and Fields*, 9(4):643–671, 1999.

[40] Jose Antonio Oller, Michela Verbeni, and Joaquim Prades. Meson-baryon effective chiral Lagrangians to $\mathcal{O}(q^3)$. *JHEP*, 9:079, 2006.

[41] Nadia Fettes, Ulf-G. Meißner, Martin Mojzis, and Steininger Sven. The chiral effective pion-nucleon lagrangian of order p^4. *Annals of Physics*, 283(2):273 – 307, 2000.

[42] G. Ecker, J. Gasser, A. Pich, and E. De Rafael. The role of resonances in chiral perturbation theory. *Nuclear Physics B*, 321(2):311 – 342, 1989.

[43] John Donoghue, Carlos Ramirez, and German Valencia. Spectrum of QCD and chiral Lagrangians of the strong and weak interactions. *Phys. Rev. D*, 39:1947–1955, Apr 1989.

[44] J. M. Alarcón, J. Martin Camalich, and J. A. Oller. Chiral representation of the πN scattering amplitude and the pion-nucleon sigma term. *Phys. Rev. D*, 85:051503, Mar 2012.

[45] William Rarita and Julian Schwinger. On a theory of particles with half-integral spin. *Phys. Rev.*, 60:61–61, Jul 1941.

[46] Thomas R. Hemmert, Barry R. Holstein, and Joachim Kambor. Heavy baryon chiral perturbation theory with light deltas. *Journal of Physics G: Nuclear and Particle Physics*, 24(10):1831, 1998.

[47] L. S. Geng, J. Martin Camalich, L. Alvarez-Ruso, and M. J. Vicente Vacas. Nucleon-to-Δ axial transition form factors in relativistic baryon chiral perturbation theory. *Phys. Rev. D*, 78:014011, Jul 2008.

[48] V. Pascalutsa. Correspondence of consistent and inconsistent spin-3/2 couplings via the equivalence theorem. *Physics Letters B*, 503(12):85 – 90, 2001.

[49] V Pascalutsa and D Phillips. Effective theory of the $\Delta(1232)$ resonance in Compton scattering off the nucleon. *Physical Review C*, 67:055202, 2003.

[50] Thomas R Hemmert, Barry R Holstein, and Joachim Kambor. Heavy baryon chiral perturbation theory with light deltas. *Journal of Physics G: Nuclear and Particle Physics*, 24(10):1831, 1998.

[51] Steven Weinberg. Pion scattering lengths. *Phys. Rev. Lett.*, 17:616–621, Sep 1966.

[52] Véronique Bernard, Norbert Kaiser, and Ulf-G. Meißner. Chiral corrections to the S-wave pion-nucleon scattering lengths. *Physics Letters B*, 309(34):421 – 425, 1993.

[53] J.M. Alarcón, J. Martin Camalich, and J.A. Oller. Improved description of the πN-scattering phenomenology at low energies in covariant baryon chiral perturbation theory. *Annals of Physics*, 336(0):413 – 461, 2013.

[54] L. Alvarez-Ruso, T. Ledwig, J. Martin Camalich, and M. J. Vicente-Vacas. Nucleon mass and pion-nucleon sigma term from a chiral analysis of lattice qcd data. *Phys. Rev. D*, 88:054507, Sep 2013.

[55] Maxim Mai and Ulf-G. Meißner. New insights into antikaon-nucleon scattering and the structure of the $\Lambda(1405)$. *Nuclear Physics A*, 900(0):51 – 64, 2013.

[56] Yan-Rui Liu and Shi-Lin Zhu. Decuplet contribution to the mesonbaryon scattering lengths. *The European Physical Journal C*, 52(1):177–186, 2007.

[57] Zhan-Wei Liu, Yan-Rui Liu, and Shi-Lin Zhu. Pseudoscalar meson and decuplet baryon scattering lengths. *Phys. Rev. D*, 83:034004, Feb 2011.

[58] Kenneth G. Wilson. Confinement of quarks. *Phys. Rev. D*, 10:2445–2459, Oct 1974.

[59] Michael Creutz. Confinement and the critical dimensionality of Space-Time. *Phys. Rev. Lett.*, 43:553–556, Aug 1979.

[60] Michael Creutz, Laurence Jacobs, and Claudio Rebbi. Experiments with a gauge-invariant ising system. *Phys. Rev. Lett.*, 42:1390–1393, May 1979.

[61] Michael Creutz, Laurence Jacobs, and Claudio Rebbi. Monte carlo study of Abelian lattice gauge theories. *Phys. Rev. D*, 20:1915–1922, Oct 1979.

[62] A. Ukawa. Computational cost of full QCD simulations experienced by CP-PACS and JLQCD collaborations. *Nuclear Physics B - Proceedings Supplements*, 106107(0):195 – 196, 2002. LATTICE 2001 Proceedings of the XIXth International Symposium on Lattice Field Theory.

[63] Chulwoo Jung. Status of dynamical ensemble generation. *PoS Lattice 2009*, 002, 2010. arXiv:1001.0941.

[64] Heinz J. Rothe. *Lattice gauge theories an introduction.* World Scientific Publishing Co., 1992.

[65] Kenneth G. Wilson. *New Phenomena In Subnuclear Physics.* World Scientific Publishing Co., 1975.

[66] Leonard Susskind. Lattice fermions. *Phys. Rev. D*, 16:3031–3039, Nov 1977.

[67] H.B. Nielsen and M. Ninomiya. A no-go theorem for regularizing chiral fermions. *Physics Letters B*, 105(23):219 – 223, 1981.

[68] John Kogut and Leonard Susskind. Hamiltonian formulation of Wilson's lattice gauge theories. *Phys. Rev. D*, 11:395–408, Jan 1975.

[69] A. Bazavov, D. Toussaint, C. Bernard, et al. Nonperturbative QCD simulations with $2 + 1$ flavors of improved staggered quarks. *Rev. Mod. Phys.*, 82:1349–1417, May 2010.

[70] David B. Kaplan. A method for simulating chiral fermions on the lattice. *Physics Letters B*, 288(34):342 – 347, 1992.

[71] Stephen R. Sharpe. Future of chiral extrapolations with domain wall fermions. 2007. arXiv:0706.0218.

[72] L. Lellouch, R. Sommer, B. Svetitsky, A. Vladikas, and L. F. Cugliandolo. *Moder perspectives in lattice QCD: quantum field theory ad high performance computing*. Oxford University Press, 2011.

[73] G Munster and M Walzl. Lattice gauge theory a short primer. 2000. arXiv:hep-ph/0012005.

[74] Rajan Gupta. Introduction to Lattice QCD. 1998. arXiv:hep-lat/9807028.

[75] Jiunn-Wei Chen. Connecting the quenched and unquenched worlds via the large N_c world. *Physics Letters B*, 543(34):183 – 188, 2002.

[76] S. Aoki, M. Fukugita, S. Hashimoto, et al. Analysis of hadron propagators with one thousand configurations on a 243 64 lattice at = 6.0. *Nuclear Physics B - Proceedings Supplements*, 47(13):354 – 357, 1996.

[77] C. Alexandrou, M. Brinet, J. Carbonell, et al. Axial nucleon form factors from lattice QCD. *Phys. Rev. D*, 83:045010, Feb 2011.

[78] Walter Wilcox and Bruce Lindsay. Disconnected loop noise methods in lattice QCD. *Nuclear Physics B - Proceedings Supplements*, 63(13):973 – 975, 1998. Proceedings of the XVth International Symposium on Lattice Field Theory.

[79] R. Sommer. A new way to set the energy scale in lattice gauge theories and its application to the static force and αs in SU(2) Yang-Mills theory. *Nuclear Physics B*, 411(23):839 – 854, 1994.

[80] K. Symanzik. Continuum limit and improved action in lattice theories: (I). Principles and ϕ^4 theory. *Nuclear Physics B*, 226(1):187 – 204, 1983.

[81] M. Lüscher. Volume dependence of the energy spectrum in massive quantum field theories. *Communications in Mathematical Physics*, 104(2):177–206, 1986.

[82] N. L. Hall, A. W. Thomas, R. D. Young, and J. M Zanotti. Volume dependence of the axial charge of the nucleon. 2012. arXiv:1205.1608v1.

[83] J. Gasser and H. Leutwyler. Light quarks at low temperatures. *Physics Letters B*, 184(1):83 – 88, 1987.

[84] J. Gasser and H. Leutwyler. Thermodynamics of chiral symmetry. *Physics Letters B*, 188(4):477 – 481, 1987.

[85] J. Gasser and H. Leutwyler. Spontaneously broken symmetries: Effective lagrangians at finite volume. *Nuclear Physics B*, 307(4):763 – 778, 1988.

[86] R. Horsley, Y. Nakamura, A. Nobile, et al. Nucleon axial charge and pion decay constant from two-flavor lattice QCD. *Physics Letters B*, 732(0):41 – 48, 2014.

[87] A. Ali Khan, M. Göckeler, Ph. Hägler, et al. Axial coupling constant of the nucleon for two flavors of dynamical quarks in finite and infinite volume. *Phys. Rev. D*, 74:094508, Nov 2006.

[88] Claude Bernard, Norman Christ, Steven Gottlieb, et al. Panel discussion on the cost of dynamical quark simulations. *Nuclear Physics B - Proceedings*

Supplements, 106107(0):199 – 205, 2002. LATTICE 2001 Proceedings of the XIXth International Symposium on Lattice Field Theory.

[89] Martin Hasenbusch. Speeding up the hybrid Monte Carlo algorithm for dynamical fermions. *Physics Letters B*, 519(12):177 – 182, 2001.

[90] Martin Lüscher. Schwarz-preconditioned HMC algorithm for two-flavor lattice QCD. *Computer Physics Communications*, 165(3):199 – 220, 2005.

[91] Karl Jansen. Lattice QCD: a critical status report. *PoS Lattice 2008*, 010, 2008. arXiv:0810.5634.

[92] Remi Baron, Phillip Boucaud, Petros Dimopoulos, et al. Light meson physics from maximally twisted mass lattice QCD. *Journal of High Energy Physics*, 2010(8), 2010.

[93] J. D. Bratt, R. G. Edwards, M. Engelhardt, et al. Nucleon structure from mixed action calculations using $2 + 1$ flavors of asqtad sea and domain wall valence fermions. *Phys. Rev. D*, 82:094502, Nov 2010.

[94] Sinya Aoki, Yasumichi Aoki, Claude Bernard, et al. Review of lattice results concerning low energy particle physics. Oct 2013. arXiv:1310.8555.

[95] Joachim Kambor and Martin Mojzis. Field redefinitions and wave function renormalization to $\mathcal{O}(p^4)$ in heavy baryon chiral perturbation theory. *Journal of High Energy Physics*, 9904:31, 1999.

[96] V Bernard and Ulf G Meißner. The nucleon axial-vector coupling beyond one loop. *Physics Letters B*, 639:278–282, 2006.

[97] M R Schindler, T Fuchs, J Gegelia, and S Scherer. Axial, induced pseudoscalar, and pion-nucleon form factors in manifestly Lorentz-invariant chiral perturbation theory. *Physical Review C*, 75:025202, 2007.

[98] Véronique Bernard, Harold W. Fearing, Thomas R. Hemmert, and Ulf-G. Meiner. The form factors of the nucleon at small momentum transfer. *Nuclear Physics A*, 635(12):121 – 145, 1998.

[99] Martin J. Savage and James Walden. SU(3) breaking in neutral current axial matrix elements and the spin content of the nucleon. *Phys. Rev. D*, 55:5376–5384, May 1997.

[100] B. Borasoy. Baryon axial vector currents. *Phys. Rev. D*, 59:054021, Feb 1999.

[101] R. G. Edwards, G. T. Fleming, Ph. Hägler, et al. Nucleon axial charge in full lattice QCD. *Phys. Rev. Lett.*, 96:052001, Feb 2006.

[102] T. Yamazaki, Y. Aoki, T. Blum, et al. Nucleon axial charge in $(2 + 1)$-flavor dynamical-lattice QCD with domain-wall fermions. *Phys. Rev. Lett.*, 100:171602, Apr 2008.

[103] D Pleiter, S Collins, M Göckeler, et al. Nucleon form factors and structure functions from N_f=2 clover fermions. *PoS Lattice 2010*, 153, 2011. arXiv:1101.2326v1.

[104] S. Capitani, M. Della Morte, G. von Hippel, et al. Nucleon axial charge in lattice QCD with controlled errors. *Phys. Rev. D*, 86:074502, Oct 2012.

[105] Jeremy Green, Michael Engelhardt, Stefan Krieg, et al. Nucleon structure with pion mass down to 149 MeV. *PoS Lattice 2010*, 170, 2011.

[106] M. Procura, T.R. Hemmert, B.U. Musch, and W. Weise. Quark mass dependence of nucleon mass and axial-vector coupling constant. *Nuclear Physics B - Proceedings Supplements*, 153(1):229 – 233, 2006.

[107] Thomas R. Hemmert, Massimiliano Procura, and Wolfram Weise. Quark mass dependence of the nucleon axial-vector coupling constant. *Phys. Rev. D*, 68:075009, Oct 2003.

[108] F. Winter, M. Göckeler, Ph. Hägler, et al. Baryon axial charges and momentum fractions with $N_f = 2 + 1$ dynamical fermions. *PoS Lattice 2010*, 163, 2010. arXiv:1102.3407.

[109] Huey-Wen Lin and Konstantinos Orginos. Calculation of hyperon axial couplings from lattice QCD. *Phys. Rev. D*, 79:034507, Feb 2009.

[110] Tanmoy Bhattacharya, Saul D. Cohen, Rajan Gupta, et al. Nucleon charges and electromagnetic form factors from $2 + 1 + 1$-flavor lattice QCD. *Phys. Rev. D*, 89:094502, May 2014.

[111] Dru B Renner. Status and prospects for the calculation of hadron structure from lattice QCD. *PoS Lattice 2009*, 18, 2009. arXiv:1002.0925.

[112] B. Plaster, R. Rios, H. O. Back, et al. Measurement of the neutron β-asymmetry parameter A_0 with ultracold neutrons. *Phys. Rev. C*, 86:055501, Nov 2012.

[113] M. P. Mendenhall, R. W. Pattie, Y. Bagdasarova, et al. Precision measurement of the neutron β-decay asymmetry. *Phys. Rev. C*, 87:032501, Mar 2013.

[114] M. Bourquin, R.M. Brown, Y. Chatelus, et al. Measurements of hyperon semileptonic decays at the CERN Super Proton Synchrotron. *Zeitschrift fr Physik C Particles and Fields*, 21(1):17–26, 1983.

[115] D. Mund, B. Märkisch, M. Deissenroth, et al. Determination of the weak

axial vector coupling λ=g_A/g_V from a measurement of the β-asymmetry parameter a in neutron beta decay. *Phys. Rev. Lett.*, 110:172502, Apr 2013.

[116] M. Schumann, M. Kreuz, M. Deissenroth, et al. Measurement of the proton asymmetry parameter in neutron beta decay. *Phys. Rev. Lett.*, 100:151801, Apr 2008.

[117] Yu.A. Mostovoi, I.A. Kuznetsov, V.A. Solovei, et al. Experimental value of g_a/g_v from a measurement of both P-odd correlations in free-neutron decay. *Physics of Atomic Nuclei*, 64(11):1955–1960, 2001.

[118] P. Liaud, K. Schreckenbach, R. Kossakowski, et al. The measurement of the beta asymmetry in the decay of polarized neutrons. *Nuclear Physics A*, 612(1):53 – 81, 1997.

[119] B. Yerozolimsky, I. Kuznetsov, Yu. Mostovoy, and I. Stepanenko. Corrigendum: Corrected value of the beta-emission asymmetry in the decay of polarized neutrons measured in 1990. *Physics Letters B*, 412(34):240 – 241, 1997.

[120] P. Bopp, D. Dubbers, L. Hornig, et al. Beta-decay asymmetry of the neutron and $\frac{g_A}{g_V}$. *Phys. Rev. Lett.*, 56:919–922, Mar 1986.

[121] J. Dworkin, P. T. Cox, E. C. Dukes, et al. High-statistics measurement of $\frac{g_a}{g_v}$ in $\lambda \to p + e^- + \overline{\nu}$. *Phys. Rev. D*, 41:780–800, Feb 1990.

[122] M. Bourquin, R.M. Brown, Y. Chatelus, et al. Measurements of hyperon semileptonic decays at the CERN super proton synchrotron. *Zeitschrift fr Physik C Particles and Fields*, 21(1):1–15, 1983.

[123] J. Wise, D.A. Jensen, M.N. Kreisler, et al. Precise measurement of the ratio

of the axial vector coupling to vector coupling in $\lambda^0 \to p + e^- + \bar{\nu}$. *Physics Letters B*, 98(12):123 – 126, 1981.

[124] S. Y. Hsueh, D. Müller, J. Tang, et al. High-precision measurement of polarized-Σ^- beta decay. *Phys. Rev. D*, 38:2056–2076, Oct 1988.

[125] W. Tanenbaum, V. Hungerbuehler, R. Majka, et al. $|\frac{g_A}{g_V}|$ in the decay $\sigma^- \to ne^-\bar{\nu}$. *Phys. Rev. Lett.*, 33:175–178, Jul 1974.

[126] J.R. Batley, G.E. Kalmus, C. Lazzeroni, et al. Measurement of the branching ratio of the decay $\Xi^0 \to \Sigma^+\mu^-\bar{\nu}_\mu$. *Physics Letters B*, 720(13):105 – 110, 2013.

[127] A. Alavi-Harati, T. Alexopoulos, M. Arenton, et al. First measurement of form factors of the decay $\Xi^0 \to \Sigma^+ e^- \overline{\nu}_e$. *Phys. Rev. Lett.*, 87:132001, Sep 2001.

[128] J.R. Batley, G.E. Kalmus, C. Lazzeroni, et al. Measurement of the branching ratios of the decays $\Xi^0 \to \Sigma^+\mu^-\bar{\nu}_\mu$ and $\bar{\Xi}^0 \to \bar{\Sigma}^+ e^+ \nu_e$. *Physics Letters B*, 645(1):36 – 46, 2007.

[129] Roger F. Dashen, Elizabeth Jenkins, and Aneesh V. Manohar. Spin-flavor structure of large N_c baryons. *Phys. Rev. D*, 51:3697–3727, Apr 1995.

[130] X.-L. Ren, L.S. Geng, J.Martin Camalich, J. Meng, and H. Toki. Octet baryon masses in next-to-next-to-next-to-leading order covariant baryon chiral perturbation theory. *Journal of High Energy Physics*, 2012(12), 2012.

[131] M. F. M. Lutz and A. Semke. Large-N_c operator analysis of 2-body meson-baryon counterterms in the chiral lagrangian. *Phys. Rev. D*, 83:034008, Feb 2011.

[132] M.F.M. Lutz and E.E. Kolomeitsev. Relativistic chiral SU(3) symmetry, large-N_c sum rules and mesonbaryon scattering. *Nuclear Physics A*, 700(12):193 – 308, 2002.

[133] T. Ledwig, J. Martin Camalich, L. S. Geng, and M. J. Vicente Vacas. Octet-baryon axial-vector charges and $SU(3)$-breaking effects in the semileptonic hyperon decays. *Phys. Rev. D*, 90:054502, Sep 2014.

[134] J.A. McGovern, D.R. Phillips, and H.W. Grießhammer. Compton scattering from the proton in an effective field theory with explicit Delta degrees of freedom. *The European Physical Journal A*, 49(1), 2013.

[135] M.R. Schindler and D.R. Phillips. Bayesian methods for parameter estimation in effective field theories. *Annals of Physics*, 324(3):682 – 708, 2009.

[136] J.M. Alarcón, J.Martin Camalich, and J.A. Oller. Low energy analysis of πN scattering and the pion-nucleon sigma term with covariant baryon chiral perturbation theory. *PoS Confinement X*, 2013. arXiv:1301.3067.

[137] H. Nishino et al. Search for nucleon decay into charged antilepton plus meson in Super-Kamiokande I and II. *Phys. Rev. D*, 85:112001, Jun 2012.

[138] K.S. Babu, E. Kearns, et al. Baryon number violation. 2013. arXiv:1311.5285.

[139] Howard Georgi and S. L. Glashow. Unity of all elementary-particle forces. *Phys. Rev. Lett.*, 32:438–441, Feb 1974.

[140] Steven Weinberg. Baryon- and lepton-nonconserving processes. *Phys. Rev. Lett.*, 43:1566–1570, Nov 1979.

[141] Frank Wilczek and A. Zee. Operator analysis of nucleon decay. *Phys. Rev. Lett.*, 43:1571–1573, Nov 1979.

[142] Mark Claudson, Mark B. Wise, and Lawrence J. Hall. Chiral Lagrangian for deep mine physics. *Nuclear Physics B*, 195(2):297 – 307, 1982.

[143] K. Kobayashi, M. Earl, Y. Ashie, et al. Search for nucleon decay via modes favored by supersymmetric grand unification models in Super-Kamiokande-I. *Phys. Rev. D*, 72:052007, Sep 2005.

[144] T. Akiri, D. Allspach, M. Andrews, et al. The 2010 interim report of the Long-Baseline Neutrino Experiment collaboration physics working groups. 2010. arXiv:1110.6249.

[145] Michael Wurm, John F. Beacom, Leonid B. Bezrukov, et al. The next-generation liquid-scintillator neutrino observatory LENA. 2011. arXiv:1104.5620.

[146] W De Boer. Grand unified theories and supersymmetry in particle physics and cosmology. *Progress in Particle and Nuclear Physics*, 33(0):201 – 301, 1994.

[147] Ugo Amaldi, Wim de Boer, and Hermann Frstenau. Comparison of grand unified theories with electroweak and strong coupling constants measured at LEP. *Physics Letters B*, 260(34):447 – 455, 1991.

[148] Savas Dimopoulos and Howard Georgi. Softly broken supersymmetry and SU(5). *Nuclear Physics B*, 193(1):150 – 162, 1981.

[149] S. Dimopoulos, S. Raby, and Frank Wilczek. Supersymmetry and the scale of unification. *Phys. Rev. D*, 24:1681–1683, Sep 1981.

[150] L. F. Abbott and Mark B. Wise. Effective Hamiltonian for nucleon decay. *Phys. Rev. D*, 22:2208–2212, Nov 1980.

[151] Jose F. Nieves and Palash B. Pal. Generalized Fierz identities. *American Journal of Physics*, 72(8):1100–1108, 2004.

[152] Y. Aoki, C. Dawson, J. Noaki, and A. Soni. Proton decay matrix elements with domain-wall fermions. *Phys. Rev. D*, 75:014507, Jan 2007.

[153] S. Aoki et al. Nucleon decay matrix elements from lattice QCD. *Phys. Rev. D*, 62:014506, Jun 2000.

[154] Nobuhiro Maekawa and Yu Muramatsu. Nucleon decay via dimension-6 operators in anomalous $U(1)_A$ supersymmetric GUT. *Phys. Rev. D*, 88:095008, Nov 2013.

[155] Borut Bajc, Stephane Lavignac, and Timon Mede. Challenging the minimal supersymmetric SU(5) model. *PPC 2013*, 2013.

[156] Y. Aoki, E. Shintani, and A. Soni. Proton decay matrix elements on the lattice. *Phys. Rev. D*, 89:014505, Jan 2014.

[157] Y. Aoki, P. Boyle, P. Cooney, et al. Proton lifetime bounds from chirally symmetric lattice QCD. *Phys. Rev. D*, 78:054505, Sep 2008.

[158] N. Tsutsui, S. Aoki, M. Fukugita, et al. Lattice QCD calculation of the proton decay matrix element in the continuum limit. *Phys. Rev. D*, 70:111501, Dec 2004.

[159] G. 't Hooft and M. Veltman. Scalar one-loop integrals. *Nuclear Physics B*, 153(0):365 – 401, 1979.

[160] G. Passarino and M. Veltman. One-loop corrections for e^+e^- annihilation into $\mu^+\mu^-$ in the weinberg model. *Nuclear Physics B*, 160(1):151 – 207, 1979.

[161] A. Denner. Techniques for the calculation of electroweak radiative corrections at the one-loop level and results for W-physics at LEP 200. *Fortschritte der Physik/Progress of Physics*, 41(4):307–420, 1993.